DESY 94-241
December 1994

ISSN 0418-9833

Gutzwiller's Octagon and the Triangular Billiard $T^*(2,3,8)$ as Models for the Quantization of Chaotic Systems by Selberg's Trace Formula [1]

Holger Ninnemann

II. Institut für Theoretische Physik
Universität Hamburg
Luruper Chaussee 149, 22761 Hamburg
Federal Republic of Germany

[1] Supported by Deutsche Forschungsgemeinschaft under Contract No. DFG-Ste 241/7-1

Abstract

Two strongly chaotic systems are investigated with respect to quantization rules based on Selberg's trace formula. One of them results from the action of a particular strictly hyperbolic Fuchsian group on the Poincaré disk, leading to a compact Riemann surface of genus $g = 2$. This Fuchsian group is denoted as Gutzwiller's group. The other one is a billiard inside a hyperbolic triangle, which is generated by the operation of a reflection group denoted as $T^*(2,3,8)$. Since both groups belong to the class of arithmetical groups, their elements can be characterized explicitly as 2×2 matrices containing entries, which are algebraic numbers subject to a particular set of restrictions. In the case of Gutzwiller's group this property can be used to determine the geodesic length spectrum of the associated dynamical system completely up to some cutoff length. For the triangular billiard $T^*(2,3,8)$ the geodesic length spectrum is calculated by building group elements as products of a suitable set of generators and separating a unique representative for each conjugacy class.

The presence of reflections in $T^*(2,3,8)$ introduces additional classes of group elements besides the hyperbolic ones, which correspond to periodic orbits of the dynamical system. Due to different choices of boundary conditions along the edges of the fundamental domain of $T^*(2,3,8)$, several quantum mechanical systems are associated to *one* classical system. It has been observed, that these quantum mechanical systems can be divided into two classes according to the behavior of their spectral statistics. This peculiarity is examined from the point of view of classical quantities entering quantization rules. It can be traced back to a subtle influence of the boundary conditions, which introduces contributions from non-periodic orbits for one of the two classes.

Contents

1 Introduction

Since the development of Gutzwiller's periodic-orbit theory [30], investigating the relation between periodic orbits of a classical dynamical system and the energy spectrum of the associated quantum mechanical system has gained some attention. In this context, the diversity of dynamical systems can be classified on a scale between two extreme cases.

Considering Hamiltonian systems with a finite number n of degrees of freedom, one end of the scale is given by *integrable* systems. For this kind of dynamical systems there exist n independent constants of motion, restricting the time evolution in phase space to a n-dimensional torus. The equations of motion can be integrated, and the motion is characterized by the property, that initially neighboring trajectories diverge at most like a power t^{α} of the time.

On the other end of the scale *ergodic* systems can be found, which share the property, that almost all of their trajectories fill the $(2n-1)$-dimensional hypersurface of constant energy in phase space densely. Since for ergodic systems a trajectory will visit all regions of phase space with uniform probability, the motion can be viewed to be very irregular. Ergodicity is the weakest property of a hierarchy of increasing irregularity: mixing, Anosov property, and Bernoulli property. The common definition of "chaoticity" refers to the Anosov property, stating, that initially neighbored trajectories exponentially diverge according to $e^{\lambda t}$ under the evolution of time.

Turning to quantum mechanical systems, however, an exponential sensibility on initial conditions, as observed for classical chaotic systems, cannot occur. This can be understood as follows. Due to the exponential divergence of neighbored trajectories in classical chaotic systems, calculating a trajectory within a given accuracy requires the knowledge of the initial conditions up to an exponentially small error. Whereas for classical systems the differences in the initial conditions of neighboring trajectories can be chosen to be arbitrarily small, quantum mechanical systems are subject to the uncertainty principle. Therefore Planck's constant $\hbar$ sets a lower bound on differences in initial conditions, which can be of significance for the quantum mechanical time evolution. Mathematically speaking, this behavior is a consequence of the fact, that generally the semiclassical limit $\hbar \to 0$ and the time limit $t \to \infty$ do not commute.

Nevertheless, since classical mechanics is contained in quantum mechanics as the limit of vanishing Planck's constant $\hbar \to 0$, the question may arise, how the irregularity of a classical chaotic system is reflected in the associated quantum mechanical system. One of that fingerprints of classical chaoticity is the behavior of the quantum mechanical energy spectrum. For generic chaotic systems the statistics of energy eigenvalues can be described by investigating the eigenvalues of large random matrices [27, 46, 23], leading to so-called level repulsion. Classical integrable systems, on the other hand, result in a different statistics, yielding level clustering [21]. A particular class of chaotic systems, so-called arithmetical systems, were later shown to possess quantum spectral statistics, which are comparable to those of integrable systems [24].

Another difference between the extremes of integrable and ergodic systems is a consequence of the phase space structure described above. The latter has a profound influence on the construction of semiclassical quantization rules, which may offer an analytical tool to investigate the semiclassical limit $\hbar \to 0$. In the case of integrable systems, these rules are the WKB method, or its generalization to multi-dimensional systems, the EBK method. Both methods, however, rely upon the existence of n independent constants of motion and, thus cannot be applied to chaotic systems.

However, Gutzwiller's periodic-orbit theory establishes a semiclassical quantization rule by expressing the trace of the Green function, which has poles at the quantal energy eigenvalues, as a sum over an infinite number of periodic orbits of the classical dynamical system. As compared to the EBK method describing the integrable case, the relation between quantum mechanical side and classical side of Gutzwiller's trace formula is much more involved. Each energy eigenvalue is based on a subtle interference of terms depending on the periodic orbits. Thus a large number of periodic orbits is needed to unravel the fine structure of the quantal energy spectrum. Unfortunately chaotic systems share the property that the number of periodic orbits proliferates exponentially with their lengths. Thus in order to calculate higher and higher energy levels within a given accuracy, the computational effort rapidly increases, as opposed to the integrable case, where it is independent of the energy.

For practical considerations, the trace formula for the Green function has to be smoothed appropriately, rising the question of the actual accuracy of the semiclassical approximations for the quantal energies. Errors may arise for two reasons. On the one hand, Gutzwiller's trace formula can be considered as a first order expansion in Planck's constant $\hbar$. Not much is known so far about the higher order corrections. On the other hand, using a finite number of periodic orbits as input data may strongly affect the oscillating terms on the classical side of Gutzwiller's trace formula. It seems, however, difficult to give analytical estimates for the accuracy, which has been reached.

One of these sources of inaccuracy can be eliminated by specializing to a particular class of systems. Due to Gutzwiller [31], his trace formula becomes an exact identity for the free motion of a particle on a surface of constant negative curvature. This identity has been derived long before by Selberg [50] in order to investigate the Riemann hypothesis.

In this work quantization rules based on Selberg's trace formula will be examined by considering two particular hyperbolic surfaces. Both of them result from the action of a discrete group on the complex upper half-plane, leading to the possibility to reduce the determination of periodic orbits to a group-theoretical problem. The first system is a particular compact Riemann surface of genus $g = 2$, which is generated by an arithmetical Fuchsian group, denoted as Gutzwiller's group. Due to the arithmeticity the geodesic length spectrum can be determined up to some cutoff-length completely. This has been accomplished only for two hyperbolic surfaces before [6, 49]. One of them is the (unique) compact Riemann surface of genus $g = 2$ with highest possible degree of symmetry [17, 11, 5], being generated by the operation of the regular octagon group. The other system is known as Artin's billiard [3], defined as the free motion inside the (non-compact) fundamental domain of $\mathrm{SL}(2, \mathbb{Z})$.

The second dynamical system treated in this work is the free motion inside a hyperbolic triangle with angles $\frac{\pi}{2}$, $\frac{\pi}{3}$, and $\frac{\pi}{8}$, which results from the operation of the reflection group $T^*(2,3,8)$ on the complex upper half-plane. In contrast to a compact Riemann surface, the domain of motion then possesses a boundary and vertices, which introduce additional contributions to Selberg's trace formula. According to different boundary conditions, several quantum mechanical systems may arise from the classical dynamical system under consideration. Since the fundamental domain of $T^*(2,3,8)$ can be viewed as resulting from a desymmetrization of the compact Riemann surface of genus $g = 2$ with highest possible degree of symmetry, the quantal energy spectra of these systems have been studied before in the context of the regular octagon group by numerically solving Schrödinger's equation [5]. There the observation has been made, that the quantized systems associated to $T^*(2,3,8)$ can be divided into two classes according to the spectral statistics of their energy eigenvalues. One class, showing level clustering, yields energy spectra, which are subspectra of the dynamical system associated to the regular octagon group. Although the hyperbolic triangle group $T^*(2,3,8)$ turns out to be arithmetical, the quantal energy spectra of the other class show level repulsion, i.e., their behavior agree with the behavior expected for generic chaotic systems.

In detail the outline of this paper is as follows. Chapter 2 reviews the basic ideas of hyperbolic geometry and discrete groups acting on the pseudosphere. The latter give rise to hyperbolic surfaces, which will be used as models for chaotic systems in the main body of this work. Subsequently, the relation between the geodesic length spectrum of a given hyperbolic surface and its generating group will be discussed. After mentioning some properties used to classify chaotic dynamical systems in general, a few remarks about quantized systems associated to hyperbolic surfaces will be given.

Chapter 3 then deals with the Riemann surface of genus $g = 2$, which is generated by Gutzwiller's group Γ_{GW}. Taking advantage of arithmetical properties of Gutzwiller's group, an explicit representation of the group elements will be derived. The latter turns out to be useful in order to determine the spectrum of geodesic lengths up to a cutoff length $\mathcal{L}$ completely. Due to the exponential proliferation of periodic orbits, a typical property of chaotic systems, a cutoff length of $\mathcal{L} \simeq 18$ is chosen for numerical purposes, which amounts to the calculation of more than 4 million periodic orbits. Using the geodesic length spectrum as input data, two quantization rules derived from Selberg's trace formula will be studied. The first relies on investigating the spectral staircase $\mathcal{N}(E)$, whereas the second is based on Selberg's zeta function, whose zeroes on the so-called critical line correspond to the energy eigenvalues of the dynamical system under consideration. Chapter 3 closes by using Selberg's trace formula in "reverse" direction, i.e., the energy spectrum will be used to extract information about the geodesic length spectrum. This usage is often referred to as "inverse quantum chaology".

Chapter 4 is devoted to the study of the dynamical system associated to the hyperbolic triangle group $T^*(2,3,8)$. Since $T^*(2,3,8)$ also belongs to the class of arithmetical groups, the group elements can be characterized explicitly in analogy to the case of Γ_{GW}. The geodesic length spectrum will then be determined by building group elements as products of a convenient set of generators. Subsequently, Selberg's trace formula is extended to apply to polygonal hyperbolic billiards with mixed boundary conditions along the edges. It will be found, however, that only those billiards, whose boundary conditions are compatible with one-dimensional unitary representations of their generating group, are subject to Selberg's trace formula. For the special case of the triangular group $T^*(2,3,8)$ these turn out to be those systems, whose quantal energy spectra are subspectra of the the dynamical system generated by the regular octagon group. These will be referred to as "arithmetical" triangles, whereas the remaining ones will be denoted as "pseudoarithmetical" ones. Numerically, geodesic lengths covering the range $0 < l \leq 18$ will be used for the arithmetical case to study quantization rules based on Selberg's trace formula along the same lines as for Gutzwiller's group. Finally the pseudoarithmetical case will be investigated, by interpreting Selberg's trace formula as part of a more general Gutzwiller trace formula. Whereas the boundary and corner contributions of the fundamental domain of $T^*(2,3,8)$ can be properly adjusted in Selberg's trace formula to apply for pseudoarithmetical triangles, too, a further contribution arising from non-periodic orbits will be studied mainly by using the trace of the cosine-modulated heat kernel.

Chapter 5 summarizes the results of this paper.

2 Dynamical Systems Associated to Hyperbolic Surfaces

Both dynamical systems to be considered in this work result from the free motion of a point-particle on a surface of constant negative Gaussian curvature. Therefore the first section of this chapter reviews the main results of hyperbolic geometry on the complex upper half-plane, or equivalently the Poincaré disk. In this setting chaotic properties arise from imposing particular boundary conditions on the domain of motion, which can be related to the action of some discrete group on the upper half-plane. Having introduced the necessary notions in the second section, it will be shown, that the classical dynamics of a given system can be reduced to a group-theoretical problem. This fact turns out to be a powerful means for the examination of geodesic length spectra of hyperbolic surfaces, which are discussed in the third section of this chapter. Geodesic length spectra however are of major importance in the context of quantum chaos, since they provide the input to the classical side of periodic-orbit sum rules. After mentioning some notions useful for classifying chaoticity in classical dynamics, the chapter closes by introducing the Laplace-Beltrami operator, which will be used for the quantization procedure on hyperbolic surfaces. A more extensive review of the topics discussed in this chapter can be found in [17] and [19].

2.1 Hyperbolic Geometry

The classical motion of a point-particle of mass m sliding freely on a two-dimensional curved manifold M is governed by the Lagrangian

$$L(\vec{q},\dot{\vec{q}}) = \frac{m}{2}\, g_{ij} \frac{\mathrm{d}q^i}{\mathrm{d}t} \frac{\mathrm{d}q^j}{\mathrm{d}t}, \qquad i,j = 1,2. \tag{2.1}$$

Obviously the classical trajectories in this setting are given by the geodesics in the metric $\mathrm{d}s^2 = g_{ij}\mathrm{d}q^i\mathrm{d}q^j$. The corresponding classical Hamiltonian can be determined to be

$$H(\vec{p},\vec{q}) = \frac{1}{2m}\, p_i\, g^{ij} p_j, \quad p_i = m\, g_{ij} \frac{\mathrm{d}q^j}{\mathrm{d}t}, \tag{2.2}$$

where g^{ij} denotes the inverse of the metric tensor g_{ij}.

The simplest M of constant negative Gaussian curvature, which is simply connected, is called the *pseudosphere*. Two conformally equivalent models of the pseudosphere will be discussed in the following, each of which having its own virtues depending on the problem to be described.

The first model is the *complex upper half-plane*

$$\mathcal{H} := \{z = x + iy;\ y > 0\}\,. \tag{2.3}$$

A metric is introduced on $\mathcal{H}$ by choosing the metric tensor to be

$$g_{ij} = \frac{R^2}{y^2}\,\delta_{ij}, \tag{2.4}$$

where R is related to the Gaussian curvature K by

$$K = -\frac{1}{R^2}. \tag{2.5}$$

It is convenient to measure all distances on $\mathcal{H}$ in units of R, i.e., making all coordinates dimensionless. Therefore usually the choice $R = 1$ is made, resulting in a constant negative Gaussian curvature $K = -1$ everywhere on the complex upper half-plane. The metric constructed in this way is called *Poincaré metric* (or *hyperbolic metric*) and its line element is given by

$$\mathrm{d}s^2 = \frac{1}{y^2}\left(\mathrm{d}x^2 + \mathrm{d}y^2\right). \tag{2.6}$$

The *hyperbolic distance* $d(z, w)$ between two points $z, w \in \mathcal{H}$ is the infimum of lengths of curves connecting z and w, measured with the Poincaré metric $\mathrm{d}s^2$. It is attained for the geodesic segment connecting z and w and turns out to be

$$\cosh d(z, w) = 1 + \frac{|z - w|^2}{2 \operatorname{Im} z \operatorname{Im} w}. \tag{2.7}$$

The holomorphic automorphisms of the complex upper half-plane can be represented by the operation of the projective special linear group $\mathrm{PSL}(2, \mathbb{R}) = \mathrm{SL}(2, \mathbb{R})/\{\pm\mathbf{1}\}$ on $\mathcal{H}$. Elements $\gamma := \left(\begin{smallmatrix} a & b \\ c & d \end{smallmatrix}\right) \in \mathrm{SL}(2, \mathbb{R})$ act as fractional linear transformations on points $z \in \mathcal{H}$

$$\gamma z = \frac{az + b}{cz + d}. \tag{2.8}$$

Since both matrices γ and $-\gamma$ in $\mathrm{SL}(2, \mathbb{R})$ map a $z \in \mathcal{H}$ to identical image points, the holomorphic automorphisms of $\mathcal{H}$ are actually described by equivalence classes $[\gamma] \in \mathrm{PSL}(2, \mathbb{R})$ in the projective group. It is however convenient to deal with matrices $\gamma \in \mathrm{SL}(2, \mathbb{R})$ and choose the trace to be $\operatorname{tr} \gamma \geq 0$. The identification of γ and $-\gamma$ yielding equivalence classes $[\gamma] \in \mathrm{PSL}(2, \mathbb{R})$ will be furtheron understood implicitly.

The Poincaré metric (2.6) is invariant under the operation of $\mathrm{PSL}(2, \mathbb{R})$ on $\mathcal{H}$, therefore the holomorphic automorphisms are, spoken in geometrical terms, the *orientation-preserving isometries* of $(\mathcal{H}, \mathrm{d}s^2)$.

Transformations $\gamma \in \mathrm{PSL}(2, \mathbb{R})$, $\gamma \neq \mathbf{1}$ can be classified in three different cases according to their traces:

(i) *Elliptic* elements γ are characterized by the condition $0 \leq \operatorname{tr} \gamma < 2$. They are conjugate within $\mathrm{SL}(2, \mathbb{R})$ to a rotation and have one fixed point in the interior of $\mathcal{H}$.

(ii) *Parabolic* elements γ are characterized by the condition $\operatorname{tr} \gamma = 2$. They are conjugate within $\mathrm{SL}(2, \mathbb{R})$ to a translation $z \mapsto z + x$, $x \in \mathbb{R}$ and have one fixed point on the boundary $\partial\mathcal{H} := \mathbb{R} \cup \{\infty\}$ of the upper half-plane.

(iii) *Hyperbolic* elements γ are characterized by the condition $\operatorname{tr} \gamma > 2$. They are conjugate within $\mathrm{SL}(2, \mathbb{R})$ to a boost $z \mapsto Nz$, $N > 1$ and have two fixed point on $\partial\mathcal{H}$. N is denoted as the norm of γ.

Geodesics on the complex upper half-plane $\mathcal{H}$ equipped with the Poincaré metric are either the circular arcs or the vertical half-lines perpendicular to the real axis. The two fixed points of a hyperbolic element $\gamma \in \mathrm{PSL}(2, \mathbb{R})$ are connected by a uniquely determined geodesic. This geodesic is mapped onto itself by γ and is therefore called the *invariant geodesic of* γ.

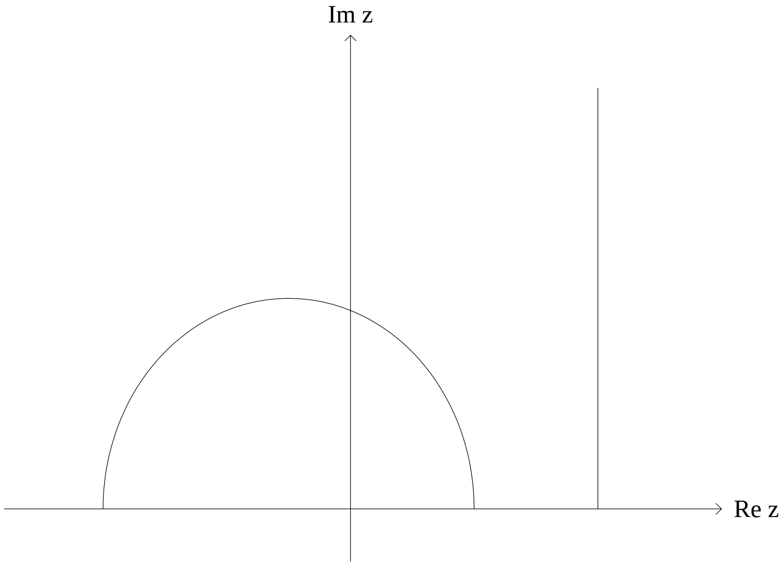

Figure 1: Geodesics on the complex upper half-plane

In the case of hyperbolic billiards, besides of the above mentioned three classes of isometries of $(\mathcal{H}, \mathrm{d}s^2)$, also the *orientation-reversing isometries* have to be taken into account due to the presence of reflections. They can be described by the operation of antiholomorphic automorphisms $\rho := \left(\begin{smallmatrix} a & b \\ c & d \end{smallmatrix}\right) \in \mathrm{GL}(2, \mathbb{R})$, $\det \rho = -1$ acting on a point $z \in \mathcal{H}$ as

$$\rho z = \frac{a\bar{z} + b}{c\bar{z} + d}. \tag{2.9}$$

As above $-\rho$ and ρ will be identified implicitly, since they map a $z \in \mathcal{H}$ to the same image point. The representative will be chosen such that $\mathrm{tr}\,\rho \geq 0$.

An orientation-reversing isometry ρ fulfilling the involution property $\rho^2 = \mathbf{1}$ geometrically describes a *pure reflection*. A ρ is called *inverse hyperbolic*, if ρ^2 is of hyperbolic type. The condition for ρ^2 to be hyperbolic $\mathrm{tr}\,\rho^2 > 2$ can easily be shown to be equivalent to $\mathrm{tr}\,\rho > 0$.

The other model of the pseudosphere to be mentioned here is the *Poincaré disk*

$$\mathcal{D} := \{z = x + iy;\ |z| < 1\}. \tag{2.10}$$

It can be mapped conformally onto the complex upper half-plane $\mathcal{H}$ by the so-called Cayley transformation

$$c : \mathcal{D} \to \mathcal{H},\ z \mapsto Cz; \qquad C = \frac{1}{\sqrt{2}} \begin{pmatrix} 1 & i \\ i & 1 \end{pmatrix}. \tag{2.11}$$

The Poincaré metric on $\mathcal{D}$ takes the form

$$\mathrm{d}s^2 = \frac{4\,(\mathrm{d}x^2 + \mathrm{d}y^2)}{(1 - x^2 - y^2)^2}, \tag{2.12}$$

leading to the hyperbolic distance between two points $z, w \in \mathcal{D}$

$$\cosh d(z, w) = 1 + \frac{2|z - w|^2}{(1 - |z|^2)(1 - |w|^2)}. \tag{2.13}$$

The orientation-preserving isometries of the Poincaré disk are represented by the operation of the projective special unitary group $\mathrm{PSU}(1,1) = \mathrm{SU}(1,1)/\{\pm\mathbf{1}\}$ on $\mathcal{D}$. Explicitly they act on a point $z \in \mathcal{D}$ as fractional linear transformations with complex coefficients $\gamma := \left(\begin{smallmatrix} u & v \\ \bar{v} & \bar{u} \end{smallmatrix}\right) \in \mathrm{SU}(1,1)$

$$\gamma z = \frac{uz + v}{\bar{v}z + \bar{u}}. \tag{2.14}$$

Geodesics of $(\mathcal{D}, \mathrm{d}s^2)$ are circular arcs or diameters orthogonal to the boundary of the Poincaré disk $\partial\mathcal{D} = \{z \in \mathbb{C};\ |z| = 1\}$. The two fixed points of hyperbolic elements in $\mathrm{PSU}(1,1)$ are placed on $\partial\mathcal{D}$.

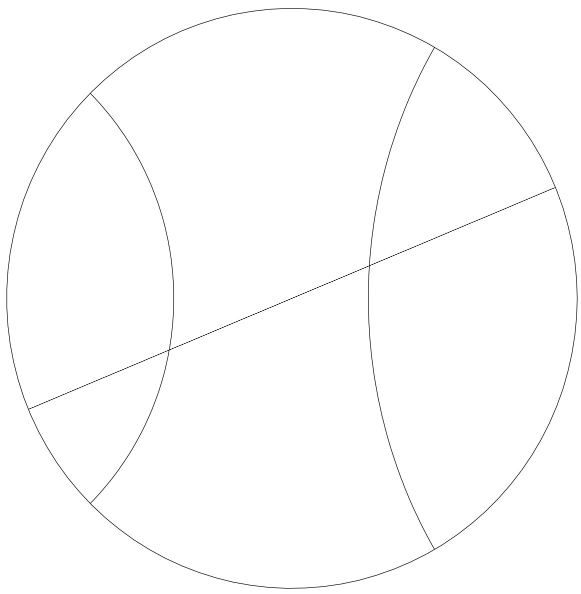

Figure 2: Geodesics on the Poincaré disk

Since matrix elements of $\gamma \in \mathrm{SU}(1,1)$ are complex numbers, it is *not* possible to characterize the orientation-reversing isometries of $(\mathcal{D}, \mathrm{d}s^2)$ by simply choosing the determinant of a transformation matrix to be -1. In order to represent concatenation of antiholomorphic automorphisms of $\mathcal{D}$ as matrix multiplication, however, the operator

$$K : \mathcal{D} \to \mathcal{D},\ z \mapsto \bar{z} \tag{2.15}$$

of complex conjugation is introduced. Then an orientation-reversing isometry ρ can be written as

$$\rho = \begin{pmatrix} u & v \\ \bar{v} & \bar{u} \end{pmatrix} K, \qquad |u|^2 - |v|^2 = 1, \tag{2.16}$$

acting on a point $z \in \mathcal{D}$ as

$$\rho z = \frac{u\bar{z} + v}{\bar{v}\bar{z} + \bar{u}}. \tag{2.17}$$

The condition for an orientation-reversing isometry $\rho : \mathcal{D} \to \mathcal{D}$ to be of inverse hyperbolic type turns out to be $|\mathrm{Re}\, v| > 0$.

2.2 Fuchsian and Reflection Groups

Let $\Gamma \subset \mathrm{PSL}(2,\mathbb{R})$ be a *discrete* subgroup of the automorphisms of the complex upper half-plane, i.e., there exists a neighborhood $U \subset \mathrm{PSL}(2,\mathbb{R})$ of the unit element $\mathbf{1} \in U$, such that $U \cap \Gamma = \{\mathbf{1}\}$. The set of all Γ-images of a point $z \in \mathcal{H}$

$$\Gamma z = \{\gamma z;\, \gamma \in \Gamma\} \tag{2.18}$$

is called the *orbit* of z. Grouping together the orbits of all $z \in \mathcal{H}$ leads to the *orbit space*

$$\Gamma\backslash\mathcal{H} = \{\Gamma z;\, z \in \mathcal{H}\}. \tag{2.19}$$

If Γ contains no elliptic elements, i.e., all $\gamma \in \Gamma$, $\gamma \neq 1$ have their fixed points on the boundary $\partial\mathcal{H}$ of the complex upper half-plane, the orbit space $\Gamma\backslash\mathcal{H}$ turns out to be a regular two-dimensional manifold. Elliptic elements in Γ however have their fixed points in the interior of $\mathcal{H}$ and therefore destroy the manifold structure of $\Gamma\backslash\mathcal{H}$ at exceptional points. In this case $\Gamma\backslash\mathcal{H}$ will be called an *orbifold*.

Since the Poincaré metric (2.6) is invariant under the action of the group Γ on $\mathcal{H}$, it induces a well-defined metric on the orbit space $\Gamma\backslash\mathcal{H}$. According to the area of $\Gamma\backslash\mathcal{H}$ being finite or infinite, Γ is called a *Fuchsian group of first kind* or *Fuchsian group of second kind*, respectively. A Fuchsian group of first kind containing no parabolic elements is called *cocompact*, since its orbit space $\Gamma\backslash\mathcal{H}$ is compact.

It is often more convenient to use the *fundamental domain* $\mathcal{F}$ of the group Γ on $\mathcal{H}$ as a concrete realization of the orbit space $\Gamma\backslash\mathcal{H}$. This can be accomplished by choosing for each orbit Γz a representative $z \in \mathcal{H}$, such that the union of all representatives is a simply connected region $\mathcal{F} \subset \mathcal{H}$. Obviously no two points in the interior of $\mathcal{F}$ are equivalent under the action of Γ. The union of all Γ-images of $\mathcal{F}$ tessellates the upper half-plane $\mathcal{H}$ without gaps and overlappings. Identifying pairwise Γ-equivalent portions of the boundary $\partial\mathcal{F}$ of the fundamental domain turns $\mathcal{F}$ into a model of the manifold $\Gamma\backslash\mathcal{H}$.

A Fuchsian group Γ consisting besides the identity $\mathbf{1} \in \Gamma$ of hyperbolic elements only, is called *strictly hyperbolic*. The resulting orbit space $\Gamma\backslash\mathcal{H}$ is a compact Riemann surface of genus $g \geq 2$, whereas the corresponding fundamental domain $\mathcal{F}$ can be realized as a polygon, bordered by $4g$ geodesic segments. According to the Gauß-Bonnet theorem, the area of the Riemann surface $\Gamma\backslash\mathcal{H}$ is determined by its genus only

$$\mathrm{area}(\Gamma\backslash\mathcal{H}) = 4\pi(g-1), \tag{2.20}$$

where the Gaussian curvature is assumed to be fixed as $K = -1$.

For a point-particle moving on the Riemann surface $\Gamma\backslash\mathcal{H}$, glueing Γ-equivalent portions of the boundary $\partial\mathcal{F}$ of the fundamental domain $\mathcal{F}$ in the case of strictly hyperbolic Fuchsian groups Γ effectively means the introduction of periodic boundary conditions. However, the case of assuming the geodesic boundary segments of the fundamental domain to be hard walls, causing an elastic reflection of the point-particle, will be of interest, too. This leads to the notion of *polygonal hyperbolic billiards*. The corresponding discrete group Γ then also have to contain orientation-reversing isometries of $\mathcal{H}$, representing the reflections as inversions across the boundary segments. Groups Γ having this property are denoted as *reflection groups*. Since the product of two inversions across adjacent boundary portions of the fundamental domain $\mathcal{F}$

of a reflection group Γ results in a rotation, groups Γ of this type will always contain elliptic elements.

Fuchsian or reflection groups Γ can be conveniently characterized by giving a set of generators and relations among them. In the case of strictly hyperbolic Fuchsian groups, i.e., groups having as fundamental domain $\mathcal{F}$ a polygon with a boundary $\partial\mathcal{F}$ consisting of $4g$ geodesic arcs, one usually chooses the transformations identifying the pairwise Γ-equivalent portions of $\partial\mathcal{F}$ together with their inverses as generators. Denoting the $4g$ generators of Γ constructed in this way as $a_1, b_1, \cdots, a_g, b_g, a_1^{-1}, b_1^{-1}, \cdots, a_g^{-1}, b_g^{-1}$, one single group relation

$$a_1 b_1 a_1^{-1} b_1^{-1} \cdots a_g b_g a_g^{-1} b_g^{-1} = \mathbf{1} \tag{2.21}$$

is fulfilled. It has to be stressed, however, that the generators as well as the order of factors in (2.21) are *not* determined by intrinsic properties of the group Γ only, but depend on the concrete choice of the fundamental domain and subtleties about the identifications of the boundary portions of $\mathcal{F}$ to be discussed in the following chapter.

Among the reflection groups, only those having as fundamental domain a hyperbolic triangle $\mathcal{T}$ will be considered in this work. It can be seen, that the sum of the inner angles of a hyperbolic triangle obeys the relation $\alpha + \beta + \gamma < \pi$. However, only hyperbolic triangles with inner angles $\frac{\pi}{l}, \frac{\pi}{m}, \frac{\pi}{n}$, where l, m, n are positive integers, tessellate the complex upper half-plane without gaps and overlappings. The corresponding reflection groups are called *hyperbolic triangle groups* and will be denoted as $T^*(l,m,n)$. A hyperbolic triangle group $T^*(l,m,n)$ is generated by the inversions L, M, N across the edges of its fundamental domain $\mathcal{T}$. The generators L, M, N obey the group relations

$$L^2 = M^2 = N^2 = \mathbf{1}, \qquad (LM)^l = (MN)^m = (NL)^n = \mathbf{1}. \tag{2.22}$$

The group elements LM, MN, NL of finite order turn out to be elliptic elements of the hyperbolic triangle group $T^*(l,m,n)$ representing rotations around the corner of the fundamental domain $\mathcal{T}$. For a detailed proof of these facts see, e.g., [42].

As has been demonstrated in the previous section, the elements $\gamma \in \Gamma$ of Fuchsian or reflection groups acting on the complex upper half-plane can be represented by real 2×2 matrices obeying the restriction $|\det\gamma| = 1$. The whole group Γ corresponding to a given fundamental domain $\mathcal{F}$ can be obtained explicitly by forming all possible products (or *words*) of the generator matrices of Γ, which have been constructed as described above. In general this procedure will lead to matrices with seemingly "random" entries. The same is true for the traces of these matrices $\gamma \in \Gamma$, which are closely connected to the lengths of periodic geodesics on $\Gamma\backslash\mathcal{H}$. The spectrum of lengths of periodic geodesics on $\Gamma\backslash\mathcal{H}$, however, is the crucial ingredient of the classical side of periodic-orbit sum rules used in the context of quantum chaos.

Calculating the length spectra of such "generic" Fuchsian or reflection groups numerically, one usually is limited to forming all products of group generators up to a given number of factors. Unfortunately this method does not give any information about the limiting length up to which the spectrum is complete. For a certain class of groups it is however possible to find an enumeration scheme for the group elements, allowing the length spectrum of $\Gamma\backslash\mathcal{H}$ to be determined completely up to some given limiting length. These so-called *arithmetic Fuchsian* or *reflection groups* consist, roughly speaking, of 2×2 matrices with entries contained in some algebraic number field. Since both groups to be treated in this work, the Fuchsian group Γ_{GW} of Gutzwiller's octagon and the hyperbolic triangle group $T^*(2,3,8)$, belong to this class, the basic facts about arithmetic Fuchsian groups will be reviewed shortly in the rest of this section. However, only crude definitions will be given; for a much more thorough discussion about arithmetic Fuchsian groups and their length spectra see e.g., [24].

An *extension* K of finite degree n of the field of rational numbers $\mathbb{Q}$ is a field that contains $\mathbb{Q}$ as a subfield and is of finite dimension n, if interpreted as a vector space over $\mathbb{Q}$. An element $\alpha \in K$ is called *algebraic*, if it is the root of a polynomial in one variable with rational coefficients

$$a_n\alpha^n + \cdots + a_1\alpha + a_0 = 0, \qquad a_n \neq 0, \qquad a_0, \cdots, a_n \in \mathbb{Q}. \tag{2.23}$$

There exists a unique polynomial with rational coefficients having a leading coefficient $a_n = 1$ and being of lowest degree, that has α as a root, the so-called *minimal polynomial* of α. If every $\alpha \in K$ is algebraic, K itself is denoted as an *algebraic number field.* Every extension K of $\mathbb{Q}$ of finite degree is known to be an algebraic number field. Moreover, every algebraic number field K of finite degree over $\mathbb{Q}$ can be generated by adding a single algebraic number $\alpha \in K$ and all its (finitely many) powers to $\mathbb{Q}$, a fact usually written as $K = \mathbb{Q}(\alpha)$.

According to (2.23), $\{1, \alpha, \cdots, \alpha^{n-1}\}$ may be used as a basis for K, viewed as a vector field of dimension n over $\mathbb{Q}$. Therefore any $x \in K$ can be written as linear combination

$$x = b_{n-1}\alpha^{n-1} + \cdots + b_1\alpha + b_0, \qquad b_k \in \mathbb{Q}. \tag{2.24}$$

The set of all algebraic numbers in K having minimal polynomials with integer coefficients forms a ring $\mathcal{R}_{\mathrm{K}}$, denoted as the *ring of integers of* K. Elements $x \in \mathcal{R}_{\mathrm{K}}$ are called *algebraic integers.*

Having at hand these notions, an *arithmetic Fuchsian group* Γ can be characterized as, roughly speaking, being an ordinary Fuchsian group consisting of matrices of the form

$$\gamma = \begin{pmatrix} x_0 + x_1\sqrt{a} & x_2\sqrt{b} + x_3\sqrt{ab} \\ x_2\sqrt{b} - x_3\sqrt{ab} & x_0 - x_1\sqrt{a} \end{pmatrix}, \tag{2.25}$$

where $a, b \in K\backslash\{0\}$ and $x_0, \cdots, x_3 \in \mathcal{R}_{\mathrm{K}}$. However, besides being algebraic integers, the coefficients x_k obey additional restrictions depending on the particular group Γ under consideration.

The most prominent example of an arithmetic Fuchsian group is the *modular group* $\mathrm{SL}(2, \mathbb{Z})$, containing 2×2 matrices with unit determinant and integer entries. In the setting described above, this is accomplished by choosing $K = \mathbb{Q}$, and hence $n = 1$, leading to $\mathcal{R}_{\mathrm{K}} = \mathbb{Z}$. Furthermore the two parameters a, b are set to be $a = 1 = b$, and the coefficients x_k have to obey no further conditions than being integer numbers.

2.3 The Geodesic Length Spectrum

Among the trajectories described by a point-particle moving freely on a Riemann surface of genus $g \geq 2$ or inside a hyperbolic billiard, the periodic ones are, as already mentioned, of major interest for the investigation of the particular model. Starting with a Fuchsian group Γ, it can be shown, that the set of closed geodesics on the Riemann surface $\Gamma\backslash\mathcal{H}$ is in one-to-one correspondence to the conjugacy classes of hyperbolic elements of Γ. Namely, to any hyperbolic $\gamma \in \Gamma$, a unique invariant geodesic $\tilde{c}_\gamma$ on $\mathcal{H}$ is associated, which is mapped onto itself by γ. Since any point z on $\tilde{c}_\gamma$ is identified with its image γz by the definition of the orbit space $\Gamma\backslash\mathcal{H}$, the invariant geodesic $\tilde{c}_\gamma$ on $\mathcal{H}$ projects down to a closed geodesic c_γ on $\Gamma\backslash\mathcal{H}$. Moreover, the invariant geodesic $\tilde{c}_{\gamma'}$ of any $\gamma' := \sigma\gamma\sigma^{-1}$, $\sigma \in \Gamma$, belonging to the same Γ-conjugacy class as γ, projects down to the same closed geodesic c_γ on $\Gamma\backslash\mathcal{H}$, since $\tilde{c}_\gamma$ is mapped isomorphically onto $\tilde{c}_{\gamma'}$ by the transformation $\sigma \in \Gamma$. On the other hand, all closed geodesics on the Riemann surface $\Gamma\backslash\mathcal{H}$ are generated in this manner, since no closed geodesics exist on the complex upper half-plane.

In order to calculate the hyperbolic length l of a given closed geodesic c_γ on $\Gamma\backslash\mathcal{H}$ in terms of its associated hyperbolic conjugacy class $[\gamma] = \{\sigma\gamma\sigma^{-1}; \sigma \in \Gamma\}$, consider the lift $\tilde{c}_{\gamma'}$ of c_γ on $\mathcal{H}$, which is the invariant geodesic of some $\gamma' \in \Gamma$ belonging to the conjugacy class $[\gamma]$. When tiling the complex upper half-plane by copies of the fundamental domain $\mathcal{F}$ of Γ, the geodesic $\tilde{c}_{\gamma'}$ is divided into segments of finite length. Denoting the endpoints of one of these segments as z and w, the length of c_γ on $\Gamma\backslash\mathcal{H}$ can be determined to be $l = d(z, w)$, since moving from z to w along the segment projects down onto exactly one traversal of c_γ on $\Gamma\backslash\mathcal{H}$. This procedure is, however, independent of the choice made about which of the (infinitely many) segments of $\tilde{c}_{\gamma'}$ is used to represent the closed geodesic c_γ on $\Gamma\backslash\mathcal{H}$.

According to their definition, the two endpoints z and w on $\mathcal{H}$ can be mapped onto each other by an hyperbolic element $\rho \in \Gamma$. Since under a continuous variation of z along $\tilde{c}_{\gamma'}$ the image point $w = \rho z$ remains to be located on the geodesic $\tilde{c}_{\gamma'}$, a fact, which cannot be accomplished by a change of the discrete transformation ρ, the points z and w must be related by the element $\gamma' \in \Gamma$ itself, which is associated to the invariant geodesic $\tilde{c}_{\gamma'}$, i.e., $\rho = \gamma'$. Hence, the length of c_γ can be determined to be $l = d(z, w) = d(z, \gamma' z)$. Since $\gamma' \in \Gamma$ is a hyperbolic transformation, it can be conjugated within $\mathrm{PSL}(2, \mathbb{R})$ to yield a diagonal matrix

$$\xi = \begin{pmatrix} N^{\frac{1}{2}} & 0 \\ 0 & N^{-\frac{1}{2}} \end{pmatrix} = q\gamma' q^{-1}, \quad q \in \mathrm{SL}(2, \mathbb{R}), \quad N > 1, \tag{2.26}$$

having the imaginary axis as invariant geodesic on $\mathcal{H}$. Now

$$l = d(z, \gamma' z) = d(z, q^{-1}\xi q z) = d(qz, \xi q z), \tag{2.27}$$

thus it is convenient to adjust qz to be purely imaginary, in order to use the hyperbolic distance formula (2.7) yielding $\cosh l = 1 + \frac{1}{2N}(N-1)^2$. This relation, at last, can be rewritten to obtain

$$2\,\cosh\frac{l}{2} = \mathrm{tr}\,\xi = \mathrm{tr}\,\gamma' = \mathrm{tr}\,\gamma. \tag{2.28}$$

In the following the length of a closed geodesic c_γ on the Riemann surface $\Gamma\backslash\mathcal{H}$ will be denoted as $l = l(\gamma)$, where γ is an arbitrary representative of the hyperbolic conjugacy class $[\gamma]$ associated to c_γ.

Considering reflection groups Γ on the other hand, the set of closed geodesics on $\Gamma\backslash\mathcal{H}$ is divided into two classes. One class of geodesics corresponds to conjugacy classes of hyperbolic elements $\gamma \in \Gamma$, and thus the above discussion carries over exactly. The other class of geodesics, however, is in one-to-one correspondence to conjugacy classes of inverse hyperbolic elements $\rho \in \Gamma$. Since for any inverse hyperbolic $\rho \in \Gamma$ the transformation ρ^2 is of hyperbolic type, and ρ^2 describes a double traversal of the closed geodesic c_ρ on $\Gamma\backslash\mathcal{H}$, the length of c_ρ can be determined to be half of the length of c_{ρ^2}, i.e., $l(\rho) = \frac{1}{2}l(\rho^2)$. Using $\det\rho = -1$ one is led to

$$2\,\sinh\frac{l}{2} = \mathrm{tr}\,\rho \tag{2.29}$$

for inverse hyperbolic $\rho \in \Gamma$.

The distinction of the set of geodesics on $\Gamma\backslash\mathcal{H}$ into two classes in the case of reflection groups has a simple geometric interpretation, as can be seen as follows. Since the generators of a reflection group Γ, which describe the inversions across the edges of the fundamental domain of Γ, belong to the orientation-reversing isometries of $\mathcal{H}$, which have a determinant of -1, any hyperbolic $\gamma \in \Gamma$ must be the product of an *even* number of generators, whereas any inverse hyperbolic $\rho \in \Gamma$ is the product of an *odd* number of generators. From the tessellation property of Γ it follows thus, that a particle moving along a closed geodesic on $\Gamma\backslash\mathcal{H}$ corresponding to a hyperbolic conjugacy class $[\gamma]$ is reflected an even number of times at the boundary of $\Gamma\backslash\mathcal{H}$, whereas on a closed geodesic associated to an inverse hyperbolic conjugacy class $[\rho]$ an odd number of reflections do occur at the boundary.

The set of lengths of closed geodesics on $\Gamma\backslash\mathcal{H}$ will be referred to as the *geodesic length spectrum* of the Fuchsian or reflection group Γ. Arranging the length spectrum in ascending order $0 < l_1 < l_2 < \cdots$, the counting function for the spectrum of distinct geodesic lengths will be defined to be

$$\hat{N}_m(l) := \#\{n; l_n \leq l\}, \tag{2.30}$$

where the index m indicates, that also multiple traversals of closed geodesics will be accounted for. Generally on $\Gamma\backslash\mathcal{H}$ several closed geodesics can be found sharing identical lengths. In the case of strictly hyperbolic Fuchsian groups for example, no $\gamma \in \Gamma$, $\gamma \neq \mathbf{1}$ is conjugate to its inverse, i.e., $[\gamma] \neq [\gamma^{-1}]$, but obviously the relation $l(\gamma) = l(\gamma^{-1})$ holds, since

$$l(\gamma) = d(z, \gamma z) = d(\gamma z, z) = d(\gamma^{-1}\gamma z, \gamma^{-1} z) = l(\gamma^{-1}) \tag{2.31}$$

for any $z \in \mathcal{H}$ located on the invariant geodesic of γ. Thus any length l of a geodesic length spectrum is accompanied by a multiplicity $g_m(l)$, counting the number of closed geodesics of length l on $\Gamma\backslash\mathcal{H}$. The *multiplicity* $g_m(l)$ can be used to introduce the counting function of periodic orbits on $\Gamma\backslash\mathcal{H}$, i.e., the lengths including multiplicities, also denoted as the *classical staircase function*

$$N_m(l) := \sum_{l_n \leq l} g_m(l_n). \tag{2.32}$$

For the case of Fuchsian groups it has been shown in [39], that the asymptotic behavior of $N_m(l)$ obeys *Huber's law*

$$N_m(l) \sim \mathrm{Ei}(l) \sim \frac{e^l}{l}, \qquad l \to \infty, \tag{2.33}$$

where $\mathrm{Ei}(l)$ denotes the exponential integral

$$\mathrm{Ei}(l) := \mathcal{P}\int_{-\infty}^{l} \mathrm{d}t\, \frac{e^t}{t}, \qquad l > 0. \tag{2.34}$$

Since Huber's law can be derived quite generally from Selberg's trace formula [17], relation (2.33) still holds in the case of polygonal hyperbolic billiards.

A closed geodesic on $\Gamma\backslash\mathcal{H}$ being not a multiple traversal of some other closed geodesic, is called *primitive*. Any representative of its associated hyperbolic or inverse hyperbolic conjugacy class $\gamma \in [\gamma]$ is also primitive, i.e., there exists no $\sigma \in \Gamma$ yielding $\gamma = \sigma^k$ for some $k \geq 2$. The set of lengths of primitive closed geodesics on $\Gamma\backslash\mathcal{H}$ will be denoted as the *primitive geodesic length spectrum* of Γ. Introducing the counting functions $\hat{N}(l)$, $N(l)$ and the multiplicities $g(l)$ of the primitive geodesic length spectrum in an analogous manner as for the full length spectrum, one finds

$$N_m(l) = \sum_{\substack{[\gamma] \\ l(\gamma)\leq l}} 1 = \sum_{k=1}^{[l/l_1]} \sum_{\substack{[\gamma]_{\rm prim} \\ kl(\gamma)\leq l}} 1 = \sum_{k=1}^{[l/l_1]} N(l/k). \tag{2.35}$$

Since $N(l)$ is a positive and monotonically increasing function, Huber's law remains true for $N(l)$, if it holds for $N_m(l)$, i.e., the exponential proliferation of primitive closed geodesics on $\Gamma\backslash\mathcal{H}$ overwhelms by far the contribution brought by multiple traversals of shorter geodesics.

Due to the fact, that $N(l)$ and $\hat{N}(l)$ are staircase functions of step-height $g(l_n)$ and 1 at $l = l_n$, respectively, an average multiplicity $< g(l) >$ can be defined by relating the slopes of $N(l)$ and $\hat{N}(l)$ in the asymptotic regime $l \to \infty$ according to

$$\frac{\mathrm{d}N}{\mathrm{d}l} \sim < g(l) > \frac{\mathrm{d}\hat{N}}{\mathrm{d}l}, \qquad l \to \infty. \tag{2.36}$$

The average multiplicity $< g(l) >$ of lengths of primitive closed geodesics on $\Gamma\backslash\mathcal{H}$ offers an example for a quantity allowing to distinguish the above mentioned arithmetic Fuchsian or reflection groups from non-arithmetic ones. While for arithmetic groups it has been shown in [24], that the mean multiplicity asymptotically behaves as

$$< g(l) > \sim c_\Gamma \frac{e^{l/2}}{l}, \qquad l \to \infty, \tag{2.37}$$

where c_Γ denotes a constant depending on the particular group Γ under consideration, it is generally believed, that in the non-arithmetic case $< g(l) >$ does not grow exponentially.

In some sense the free motion of a point-particle on a compact Riemann surface $\Gamma\backslash\mathcal{H}$ of genus $g \geq 2$ can be considered to be the simplest prototype of the strongest possible classical chaos. Namely this model exhibits a set of properties used to classify the chaoticity of classical dynamical systems in general [17, 26].

At first it should be noticed, that the model possesses no constant of motion besides the energy. Thus a trajectory in the phase space corresponding to the (two-dimensional) Riemann surface is contained on a three-dimensional hypersurface of constant energy. Moreover, the trajectories of the model are uniformly distributed on this hypersurface. Since periodic geodesics are dense on the hypersurface of constant energy, any non-periodic geodesic can be approximated arbitrarily closely by some periodic orbit, suggesting the possibility to describe the dynamical properties of the motion on $\Gamma\backslash\mathcal{H}$ by periodic orbits only. These characteristics qualify the model under consideration to be an *ergodic system*.

A further property shared by the motion on $\Gamma\backslash\mathcal{H}$ is the rapid decay of time correlations, i.e., in the limit $t \to \infty$ all observables tend to equilibrium values. This phenomenon will be referred to as *mixing*.

The geodesic flow on $\Gamma\backslash\mathcal{H}$ also exhibits the *Anosov property*, meaning that initially neighboring trajectories typically diverge at rate $e^{\lambda t}$ in the limit $t \to \infty$. The characteristic quantity $\lambda > 0$ is denoted as the *Liapunov exponent*. Anosov systems are not only known to be ergodic and mixing [2], but also share the *Bernoulli property*, indicating, roughly speaking, the strongest possible chaos for a classical dynamical system [17]. Generally the periodic orbits of Anosov systems are known to proliferate exponentially. For the class of dynamical systems to be discussed in this work the asymptotic behavior of the classical staircase function is described by

$$N(l) \sim \frac{e^{\tau l}}{\tau l}, \qquad l \to \infty, \tag{2.38}$$

where $\tau > 0$ denotes the so-called *topological entropy.* In the case of strictly hyperbolic Fuchsian groups Γ the topological entropy can be related to the Liapunov exponent by Pesin's theorem, finally leading to Huber's law (2.33), i.e., $\tau = 1$.

The triangular billiard $T^*(2,3,8)$ to be discussed in chapter 4 will be seen to result from the desymmetrisation of a particular Riemann surface $\Gamma\backslash\mathcal{H}$ of genus $g = 2$ possessing the highest possible degree of symmetry. Thus any periodic geodesic in the fundamental domain of $T^*(2,3,8)$ can be obtained by a folding procedure from a corresponding closed geodesic in the octagon $\mathcal{F}$, which represents the Riemann surface $\Gamma\backslash\mathcal{H}$. This operation will not diminish the mixing property of the geodesic flow on $\Gamma\backslash\mathcal{H}$. It is moreover believed that any polygonal hyperbolic billiard is a mixing system [17].

2.4 Quantum Mechanics on Hyperbolic Surfaces

Concluding this chapter, a few remarks about the quantization of the dynamical systems resulting from the operation of Fuchsian or reflection groups Γ on the pseudosphere will be made. The quantum mechanics on $\Gamma\backslash\mathcal{H}$ is governed by the stationary Schrödinger equation

$$-\hat{\Delta}_{LB}\psi(z) = E\psi(z), \qquad z \in \mathcal{H}, \tag{2.39}$$

where the convention $\hbar = 1 = 2m$ has been used. Here Δ_{LB} denotes the (Γ-invariant) Laplace-Beltrami operator given by

$$\Delta_{LB} = \frac{1}{\sqrt{g}}\partial_i\sqrt{g}g^{ik}\partial_k, \qquad g := \det g_{ik}. \tag{2.40}$$

The wave functions ψ obeying the Schrödinger equation will be demanded to be Γ-invariant

$$\psi(\gamma z) = \chi(\gamma)\psi(z), \qquad \forall\gamma \in \Gamma, \tag{2.41}$$

where the *character* $\chi(\gamma)$ depends on the particular choice of boundary conditions of the fundamental domain $\mathcal{F}$ of Γ. In the case of strictly hyperbolic Fuchsian groups these are always periodic ones, leading to $\chi(\gamma) = +1$, $\forall\gamma \in \Gamma$, whereas reflection groups will also allow negative values $\chi(\gamma) = \pm 1$, corresponding to Neumann or Dirichlet boundary conditions of the fundamental domain. A more detailed investigation of the characters $\chi(\gamma)$ will be postponed to the discussion of the hyperbolic triangle group $T^*(2,3,8)$ in chapter 4.

In all dynamical systems considered in this work, i.e., $\Gamma\backslash\mathcal{H}$ being a compact Riemann surface or a compact hyperbolic triangle, the quantum Hamiltonian $\hat{H} = -\hat{\Delta}_{LB}$ possesses a purely discrete spectrum $0 \le E_1 \le E_2 \le \cdots$, and the growing behavior of the $E_n = p_n^2 + \frac{1}{4}$ is described by *Weyl's law* for the asymptotic behavior of the number $\mathcal{N}(E)$ of energy eigenvalues not exceeding E

$$\mathcal{N}(E) \sim \frac{\text{area}(\Gamma\backslash\mathcal{H})}{4\pi}E, \qquad E \to \infty. \tag{2.42}$$

3 Gutzwiller's Octagon

The first example of classical chaotic dynamical systems to be investigated in this work results from the operation of a particular Fuchsian group of first kind, denoted as Gutzwiller's group Γ_{GW}, on the Poincaré disk [32]. The associated orbit space $\Gamma_{\text{GW}}\backslash\mathcal{D}$ is a compact Riemann surface of genus $g = 2$, and Γ_{GW} belongs to the class of arithmetic Fuchsian groups. Taking advantage of the arithmetical properties of Γ_{GW}, an explicit representation of the group elements can be found, which in turn allows to determine the geodesic length spectrum of Γ_{GW} up to some cutoff-length $\mathcal{L}$ completely. Subsequently the geodesic length spectrum will be used as the input data of quantization rules based on Selberg's trace formula [50], and the resulting energy eigenvalues of the dynamical system under consideration are compared with those obtained from a numerical solution of the Schrödinger equation by the method of finite elements [4]. Finally, the reverse direction will be discussed ("inverse quantum chaology"), i.e., the energy spectrum will be used to extract the geodesic lengths via Selberg's trace formula.

3.1 Properties of the Group Γ_{GW}

Remember the notion of a *symmetry* of a manifold $\Gamma\backslash\mathcal{H}$ associated to a Fuchsian group Γ. A symmetry s isometrically maps $\Gamma\backslash\mathcal{H}$ onto itself, thus symmetry transformations are a subset of the isometries of the complex upper half-plane $\mathcal{H}$, i.e., $s \in \text{GL}(2,\mathbb{R})$, $\det s = \pm 1$. An element s of the symmetry group $\mathcal{S} := \{\mathbf{1}, s_1 \cdots, s_{n-1}\}$ of the orbit space $\Gamma\backslash\mathcal{H}$ commutes with the Fuchsian group Γ, i.e., $s^{-1}\Gamma s = \Gamma$. Thus Γ can be interpreted as a normal subgroup of a reflection group $\Gamma' := \Gamma \cup s_1\Gamma \cup \cdots \cup s_{n-1}\Gamma$, such that $\mathcal{S} \cong \Gamma'/\Gamma$. The orbit space $\Gamma'\backslash\mathcal{H}$ of the reflection group Γ' can be viewed as the result of a desymmetrisation procedure of the original surface $\Gamma\backslash\mathcal{H}$, and tessellates the latter by the operation of $\mathcal{S}$.

Among all compact Riemann surfaces of genus $g = 2$, there exists exactly one, allowing a maximum number of symmetry operations. The corresponding (strictly hyperbolic) Fuchsian group will be denoted as Γ_{reg}, since the fundamental domain of $\Gamma_{\text{reg}}\backslash\mathcal{D}$ turns out to be a regular (hyperbolic) octagon $\mathcal{F}$ in the Poincaré disk (cf. fig. 3). The dynamical system associated to the regular octagon group Γ_{reg}, also denoted as the *Hadamard-Gutzwiller model*, has been investigated in a number of works, which can be dated back even to the last century [34, 3, 17, 11, 6]. In the following, a few facts about Γ_{reg}, which are necessary for the investigation of Gutzwiller's octagon, will be reviewed.

Since $\Gamma_{\text{reg}}\backslash\mathcal{D}$ is a compact Riemann surface of genus $g = 2$, the Fuchsian group Γ_{reg} can be generated by 4 generators g_0, g_1, g_2, g_3 and their inverses. The generators g_k, g_k^{-1} acting as isometry transformations of $\mathcal{D}$ map geodesic boundary segments of the regular octagon $\mathcal{F}$ onto each other, thereby identifying opposite edges as indicated in fig. 3. From the geometrical setting it can be easily seen, that the group relation the generators of Γ_{reg} have to obey to, is uniquely fixed by the choice of identifying opposite edges of the fundamental domain $\mathcal{F}$

$$g_0\, g_1^{-1} g_2\, g_3^{-1} g_0^{-1} g_1\, g_2^{-1} g_3 = \mathbf{1}. \tag{3.1}$$

Namely, the corner P of the regular octagon is mapped onto itself by the action of the left-hand side of (3.1). Since, however, Γ_{reg} is a strictly hyperbolic Fuchsian group and hyperbolic elements $\gamma \in \Gamma_{\text{reg}}$ always have their fixed points on $\partial\mathcal{D}$, the transformation (3.1) must be the identity.

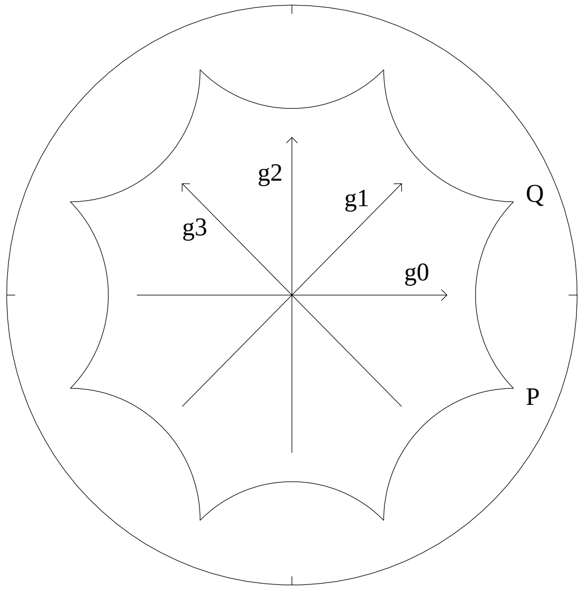

Figure 3: Fundamental domain of $\Gamma_{\rm reg}$ (opposite edges identified).

Given the corners of the regular octagon

$$p_k = 2^{-\frac{1}{4}} e^{i(\frac{\pi}{8}+k\frac{\pi}{4})}, \qquad k = 0, \cdots, 7, \tag{3.2}$$

the generators g_k of $\Gamma_{\rm reg}$ can be determined to be ($k = 0, \cdots, 3$)

$$g_k = \begin{pmatrix} 1+\sqrt{2} & (2+\sqrt{2})\,\alpha e^{i\frac{k\pi}{4}} \\ (2+\sqrt{2})\,\alpha e^{-i\frac{k\pi}{4}} & 1+\sqrt{2} \end{pmatrix}, \quad \alpha := \sqrt{\sqrt{2}-1}, \tag{3.3}$$

whereas their inverses are

$$g_k^{-1} = R_\pi g_k R_\pi^{-1}, \quad R_\varphi := \begin{pmatrix} e^{i\frac{\varphi}{2}} & 0 \\ 0 & e^{-i\frac{\varphi}{2}} \end{pmatrix}. \tag{3.4}$$

On the other hand, for any Fuchsian group Γ corresponding to an *arbitrary* compact Riemann surface of genus $g = 2$ it is always possible to construct a fundamental domain with opposite edges identified, once a set of generators obeying (3.1) is known. Consider e.g., the corners P and Q of the regular octagon. Due to the knowledge of the identification of the edges of the octagon, one finds

$$z_Q = g_1\, g_2^{-1} g_3\, z_P, \tag{3.5}$$

whereas the corners of the other edges (counter-clockwise) are connected by the transformations $g_2\, g_3^{-1} g_0^{-1}$, $g_3\, g_0\, g_1^{-1}$, $g_0^{-1} g_1\, g_2^{-1}$, $g_1^{-1} g_2\, g_3^{-1}$, $g_2^{-1} g_3\, g_0$, $g_3^{-1} g_0^{-1} g_1$, $g_0\, g_1^{-1} g_2$, respectively. The product of these 8 transformations maps the corner point P onto itself, by "shifting P once around the boundary of the octagon". Thus it must be the identity map, as can be verified by using relation (3.1). This procedure, however, does not depend on the particular shape of the *regular* octagon, but can also be applied to an arbitrary *asymmetric* octagon. Thus given the 8 generators g_k, g_k^{-1} of a Fuchsian group Γ, one can choose an arbitrary point $z \in \mathcal{D}$

as the "starting corner" of a fundamental domain $\mathcal{F}$ of Γ, and then determine the remaining corners by successively applying the transformations (3.5sqq) to $z \in \mathcal{D}$. Connecting the corners by geodesic segments yields the boundary $\partial\mathcal{F}$ of the fundamental domain. For practical calculations it is, however, convenient to start by constructing the invariant geodesics of the transformations (3.5sqq), which directly yield the boundary segments of $\mathcal{F}$. The corners of $\mathcal{F}$ are then obtained as the points of intersection of the invariant geodesics.

It should be mentioned, that for a generic Fuchsian group Γ associated to a Riemann surface of genus $g = 2$ the fundamental domain $\mathcal{F}$ obtained by the procedure described above is *not* centered around the origin. $\mathcal{F}$ can, however, always be centered by applying a conjugation in $\mathrm{SU}(1,1)$ to Γ. From the point of view of algebraic geometry, this can be understood by the fact, that a Riemann surface $\Gamma\backslash\mathcal{D}$ of genus $g = 2$ is completely determined by a set of three (complex) moduli corresponding to three corners of the fundamental domain $\mathcal{F}$. The fourth corner has to be used in order to adjust the area of the fundamental domain to be $\mathrm{area}(\mathcal{F}) = 4\pi$, according to the Gauß-Bonnet theorem (2.20). Applying inversions across the origin to these four corners yield the remaining four corners of the fundamental domain, which will then be centered around the origin by construction.

The Riemann surface $\Gamma_{\mathrm{reg}}\backslash\mathcal{D}$ of the regular octagon group allows 96 symmetry operations, which map $\Gamma_{\mathrm{reg}}\backslash\mathcal{D}$ onto itself. Due to the fact, that any Riemann surface of genus $g = 2$ is hyperelliptic, one of these symmetry transformations, the *hyperelliptic involution*, is always contained in the symmetry groups $\mathcal{S}$ of Fuchsian groups Γ having a hyperbolic octagon as fundamental domain. The regular octagon group Γ_{reg} is a normal subgroup of index 96 in a reflection group Γ', which turns out to be the hyperbolic triangle group $\Gamma' = T^*(2,3,8)$ to be discussed in chapter 4. Thus the complete desymmetrisation of the regular octagon yields a hyperbolic triangle with inner angles $\frac{\pi}{2}, \frac{\pi}{3}, \frac{\pi}{8}$.

It has been shown [11, 6, 47], that any element $\gamma \in \Gamma_{\mathrm{reg}}$ can be represented by a 2×2 matrix

$$\gamma = \begin{pmatrix} u_R + iu_I & (v_R + iv_I)\alpha \\ (v_R - iv_I)\alpha & u_R - iu_I \end{pmatrix}, \tag{3.6}$$

where u_R, u_I, v_R, v_I are *algebraic numbers* of the form

$$m + n\sqrt{2}, \qquad m, n \in \mathbb{N} \cup \{0\}. \tag{3.7}$$

Defining the algebraic conjugation

$$c = m + n\sqrt{2} \quad \rightarrow \quad \tilde{c} := m - n\sqrt{2}, \tag{3.8}$$

one finds

$$\begin{array}{ll} |\tilde{u}_R| < 1, & |\tilde{u}_I| < 1, \\ |\tilde{v}_R| < \alpha, & |\tilde{v}_I| < \alpha, \end{array} \tag{3.9}$$

by using the relation $\det\gamma = 1$. Denoting the algebraic components of the matrix entries as

$$\begin{array}{ll} u_R = m_R + n_R\sqrt{2}, & u_I = m_I + n_I\sqrt{2}, \\ v_R = p_R + q_R\sqrt{2}, & v_I = p_I + q_I\sqrt{2}, \end{array} \tag{3.10}$$

and introducing the notation

$$\pi(m) := m \bmod 2 \tag{3.11}$$

for the parity of an integer number m, a set of parity restrictions on the algebraic components of γ can be derived. These are on the one hand

$$\pi(m_R) = 1,\ \pi(m_I) = 0,\ \pi(p_R) = \pi(p_I), \tag{3.12}$$

and on the other hand

$$\begin{array}{lcl} \pi(n_R) = 0 & \Rightarrow & \begin{array}{l}\pi(n_I) = \pi(p_R) = \pi(p_I) = 0 \wedge \\ \pi(q_R) = \pi(q_I),\end{array} \\[2ex] \begin{array}{l}\pi(n_R) = 1 \wedge \\ \pi(p_R) = \pi(p_I) = 0\end{array} & \Rightarrow & \begin{array}{l}\pi(n_I) = 0 \wedge \\ \pi(q_R) \neq \pi(q_I),\end{array} \\[2ex] \begin{array}{l}\pi(n_R) = 1 \wedge \\ \pi(p_R) = \pi(p_I) = 1\end{array} & \Rightarrow & \begin{array}{l}\pi(n_I) = 0\ \wedge\ \pi(q_R) = \pi(q_I) \text{ or} \\ \pi(n_I) = 1\ \wedge\ \pi(q_R) \neq \pi(q_I).\end{array} \end{array} \tag{3.13}$$

It should be stressed, however, that the restrictions given above are only necessary conditions. In order to construct a valid group matrix $\gamma \in \Gamma_{\mathrm{reg}}$ one also has to fulfill the relation $\det \gamma = 1$. The latter is sometimes impossible, leading to "gaps" in the geodesic lenghth spectrum of Γ_{reg} (cf. section 3.2).

Whereas identifying opposite edges of the regular octagon leads to the Fuchsian group Γ_{reg}, an identification according to fig. 4 results in a different group, denoted as *Gutzwiller's group* Γ_{GW} in the following [32].

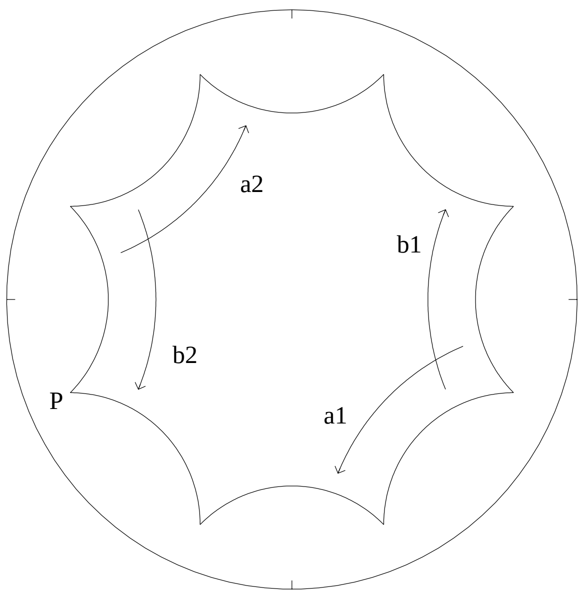

Figure 4: Fundamental domain of Γ_{GW} (genuine identification of the edges).

The generators of Gutzwiller's group $a_1, b_1, a_2, b_2 \in \Gamma_{\mathrm{GW}}$ and their inverses obey a relation different from (3.1), which can be easily deduced by constructing a word having the corner P of the octagon (fig. 4) as a fixed point

$$a_1\, b_1\, a_1^{-1} b_1^{-1} a_2\, b_2\, a_2^{-1} b_2^{-1} = \mathbf{1}. \tag{3.14}$$

In order to calculate the generators of Γ_{GW} explicitly, one observes from the geometrical setting given in fig. 4, that they are related to the generators of Γ_{reg} by some additional rotations

$$\begin{aligned} a_1 &= R_{\frac{\pi}{2}}\, g_0^{-1}, & b_1 &= g_1\, R_{-\frac{\pi}{2}}, \\ a_2 &= R_\pi\, a_1\, R_{-\pi}, & b_2 &= R_\pi\, b_1\, R_{-\pi}, \end{aligned} \tag{3.15}$$

yielding

$$\begin{aligned} a_1 &= \begin{pmatrix} \left(1+\frac{\sqrt{2}}{2}\right)(1+i) & -(1+\sqrt{2})(1+i)\,\alpha \\ -(1+\sqrt{2})(1-i)\,\alpha & \left(1+\frac{\sqrt{2}}{2}\right)(1-i) \end{pmatrix}, \\ b_1 &= \begin{pmatrix} \left(1+\frac{\sqrt{2}}{2}\right)(1-i) & (2+\sqrt{2})\,\alpha i \\ -(2+\sqrt{2})\,\alpha i & \left(1+\frac{\sqrt{2}}{2}\right)(1+i) \end{pmatrix}, \\ a_2 &= \begin{pmatrix} \left(1+\frac{\sqrt{2}}{2}\right)(1+i) & (1+\sqrt{2})(1+i)\,\alpha \\ (1+\sqrt{2})(1-i)\,\alpha & \left(1+\frac{\sqrt{2}}{2}\right)(1-i) \end{pmatrix}, \\ b_2 &= \begin{pmatrix} \left(1+\frac{\sqrt{2}}{2}\right)(1-i) & -(2+\sqrt{2})\,\alpha i \\ (2+\sqrt{2})\,\alpha i & \left(1+\frac{\sqrt{2}}{2}\right)(1+i) \end{pmatrix}. \end{aligned} \tag{3.16}$$

The group elements

$$\begin{aligned} h_0 &:= b_2^{-1} a_1\, b_1, & h_1 &:= a_2^{-1} b_2^{-1} a_1\, b_1, \\ h_2 &:= a_1, & h_3 &:= b_1^{-1} \end{aligned} \tag{3.17}$$

and their inverses offer another set of generators of Gutzwiller's group Γ_{GW}, since

$$\begin{aligned} a_1 &= h_2, & b_1 &= h_3^{-1}, \\ a_2 &= h_0\, h_1^{-1}, & b_2 &= h_2\, h_3^{-1}\, h_0^{-1}. \end{aligned} \tag{3.18}$$

As can be shown by using (3.14), the $h_0, h_1, h_2, h_3 \in \Gamma_{\mathrm{GW}}$ are subject to the relation

$$h_0\, h_1^{-1} h_2\, h_3^{-1} h_0^{-1} h_1\, h_2^{-1} h_3 = \mathbf{1}, \tag{3.19}$$

thus defining a set of generators of Γ_{GW} identifying *opposite* edges of a corresponding fundamental domain $\mathcal{F}$. The concrete shape of $\mathcal{F}$ results from the algorithm described on p. 19, i.e., by determining elements $h_1\, h_2^{-1} h_3, \cdots \in \Gamma_{\mathrm{GW}}$ having invariant geodesics containing the boundary segments of the fundamental domain $\mathcal{F}$ (fig. 5).

The structure of the 2×2 matrices representing arbitrary elements $\gamma \in \Gamma_{\mathrm{GW}}$ of Gutzwiller's group can be determined in a similar way as in the case of the regular octagon group Γ_{reg}. This is accomplished by using an induction argument for representing any $\gamma \in \Gamma_{\mathrm{GW}}$ as a product of the generators (3.16) and their inverses. Moreover, also the condition $\det \gamma = 1$ and the fact resulting from (3.15), that any $\gamma_{\mathrm{GW}} \in \Gamma_{\mathrm{GW}}$ can be written as the product of a $\gamma_{\mathrm{reg}} \in \Gamma_{\mathrm{reg}}$ and a rotation

$$\gamma_{\mathrm{GW}} = \gamma_{\mathrm{reg}}\, R_{\frac{k\pi}{2}}, \qquad k = 0, 1, 2, 3 \tag{3.20}$$

will be incorporated. Since the actual calculations are somewhat involved, only results will be presented here. For details see appendix A.

Two kinds of matrices $\gamma_1, \gamma_2 \in \Gamma_{\mathrm{GW}}$ exist in Gutzwiller's group, depending on being the product of an even or an odd number of generators $a_1, b_1, a_2, b_2 \in \Gamma_{\mathrm{GW}}$ or their inverses. Writing

$$\gamma_k = \begin{pmatrix} u_{k,R} + i u_{k,I} & (v_{k,R} + i v_{k,I})\alpha \\ (v_{k,R} - i v_{k,I})\alpha & u_{k,R} - i u_{k,I} \end{pmatrix}, \quad k = 1, 2, \tag{3.21}$$

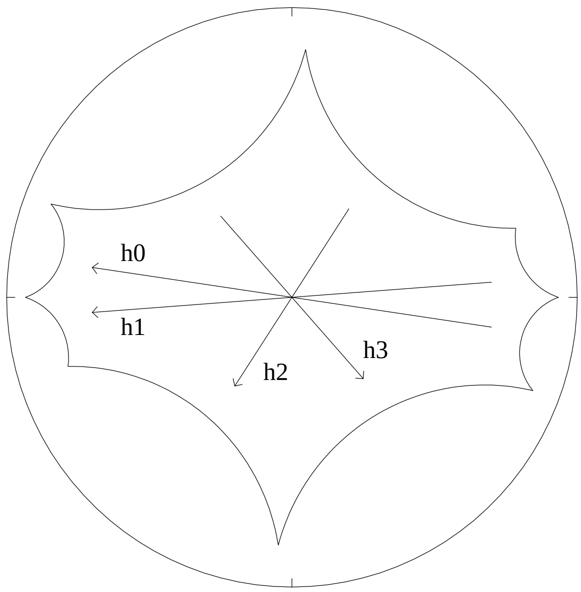

Figure 5: Fundamental domain of $\Gamma_{\rm GW}$ (opposite edges identified).

the matrix entries obey

$$\begin{array}{ll} |\tilde{u}_{k,R}| < 1, & |\tilde{u}_{k,I}| < 1, \\ |\tilde{v}_{k,R}| < \alpha, & |\tilde{v}_{k,I}| < \alpha. \end{array} \tag{3.22}$$

In the case of products of an *even* number of generators the matrix entries are algebraic numbers of the form

$$\begin{array}{ll} u_{1,R} = m_{1,R} + n_{1,R}\sqrt{2}, & u_{1,I} = m_{1,I} + n_{1,I}\sqrt{2}, \\ v_{1,R} = p_{1,R} + q_{1,R}\sqrt{2}, & v_{1,I} = p_{1,I} + q_{1,I}\sqrt{2}, \end{array} \tag{3.23}$$

obeying

$$\begin{array}{l} m_{1,R} \notin 4\mathbb{Z}, \quad \pi(m_{1,I}) \neq \pi(m_{1,R}), \\ \pi(p_{1,R}) = \pi(p_{1,I}) = \pi(n_{1,R}) = \pi(n_{1,I}), \\ \pi(p_{1,R}) = \left\{ \begin{array}{lll} 0 & \Rightarrow & \pi(q_{1,R}) = \pi(q_{1,I}) \\ 1 & \Rightarrow & \pi(q_{1,R}) \neq \pi(q_{1,I}) \end{array} \right. , \end{array} \tag{3.24}$$

whereas for products of an *odd* number of generators one finds

$$\begin{array}{ll} u_{2,R} = m_{2,R} + n_{2,R}\frac{\sqrt{2}}{2}, & u_{2,I} = m_{2,I} + n_{2,I}\frac{\sqrt{2}}{2}, \\ v_{2,R} = p_{2,R} + q_{2,R}\sqrt{2}, & v_{2,I} = p_{2,I} + q_{2,I}\sqrt{2}, \end{array} \tag{3.25}$$

subject to

$$\begin{aligned} &\pi(m_{2,R}) = \pi(m_{2,I}) = 1 = \pi(n_{2,R}) = \pi(n_{2,I}), \\ &\pi(p_{2,R}) = \pi(p_{2,I}), \\ &\pi(p_{2,R}) = \begin{cases} 0 & \Rightarrow \quad \pi(q_{2,R}) \neq \pi(q_{2,I}) \\ 1 & \Rightarrow \quad \pi(q_{2,R}) = \pi(q_{2,I}) \end{cases} . \end{aligned} \tag{3.26}$$

The parity restrictions (3.24) and (3.26) are only necessary conditions fulfilled by the elements $\gamma_k \in \Gamma_{\rm GW}$. In order to construct a valid group matrix of $\Gamma_{\rm GW}$ a method described in the next section in the context of the numerical calculation of the geodesic length spectrum will be used. Furthermore, as in the case of the regular octagon group $\Gamma_{\rm reg}$, gaps may arise by the impossibility to satisfy the parity restrictions and the determinant condition $\det \gamma_k = 1$ simultaneously. Finally it should be noted, that the relation $m_{1,R} \notin 4\mathbb{Z}$ for products being an even number of generators of $\Gamma_{\rm GW}$ is an empirical result, obtained by the numerical algorithm yielding the geodesic length spectrum.

3.2 The Length Spectrum

Having at hand the algebraic decompositions (3.21sqq) of the elements $\gamma \in \Gamma_{\rm GW}$, it is possible to derive the average multiplicity of the geodesic length spectrum of $\Gamma_{\rm GW}$. According to (2.28), the length of a closed geodesic on the Riemann surface $\Gamma_{\rm GW}\backslash\mathcal{D}$ is determined by the trace of a representative of its corresponding conjugacy class. Explicitly, for elements $\gamma_1 \in \Gamma_{\rm GW}$ being the product of an even number of generators one finds

$$\cosh \frac{l(m_{1,R}, n_{1,R})}{2} = m_{1,R} + n_{1,R}\sqrt{2}, \tag{3.27}$$

whereas in the odd case $\gamma_2 \in \Gamma_{\rm GW}$

$$\cosh \frac{l(m_{2,R}, n_{2,R})}{2} = m_{2,R} + n_{2,R}\tfrac{\sqrt{2}}{2}. \tag{3.28}$$

Using (3.22), however, unravels that in the even case $\gamma_1 \in \Gamma_{\rm GW}$ the two integer numbers on the RHS of (3.27) are not independent

$$|m_{1,R} - n_{1,R}\sqrt{2}| < 1. \tag{3.29}$$

Thus, to any $n_{1,R}$ are associated two integer numbers $m_{1,R}$, an even and an odd one. Assuming the set

$$\left\{m \in \mathbb{Z} : |m - n\sqrt{2}| < 1,\, m \equiv 0(2),\, n \in \mathbb{Z}\right\} \tag{3.30}$$

to be uniformly distributed in $2\mathbb{Z}$, leads to the counting function for different lengths corresponding to even elements $\gamma_1 \in \Gamma_{\rm GW}$

$$\hat{N}_{\rm even}(l(m_{1,R}, n_{1,R})) \sim \frac{3}{2}\, n_{1,R}, \qquad l \to \infty \tag{3.31}$$

in the limit of large lengths, since by (3.23) only $m_{1,R} \notin 4\mathbb{Z}$ are allowed. In the case of odd elements $\gamma_2 \in \Gamma_{\rm GW}$, the traces of group matrices are restricted by

$$\pi(m_{2,R}) = 1 = \pi(n_{2,R}) \tag{3.32}$$

and

$$|m_{2,R} - n_{2,R}\tfrac{\sqrt{2}}{2}| < 1. \tag{3.33}$$

Considering strictly positive $n_{2,R}$, the interval containing $m_{2,R}$ thus is

$$n_{2,R}\tfrac{\sqrt{2}}{2} - 1 < m_{2,R} < n_{2,R}\tfrac{\sqrt{2}}{2} + 1. \tag{3.34}$$

Since the width of this interval is 2, and $n_{2,R}\frac{\sqrt{2}}{2} \pm 1$ are irrational numbers, any fixed $n_{2,R}$ is accompanied by exactly one odd integer $m_{1,R}$, leading to

$$\hat{N}_{\text{odd}}(l(m_{2,R}, n_{2,R})) \sim \frac{1}{2}\, n_{2,R}, \qquad l \to \infty. \tag{3.35}$$

In order to determine the counting function $\hat{N}(l)$ of the whole geodesic length spectrum of Γ_{GW}, one observes that the condition for lengths corresponding to odd elements $\gamma_2 \in \Gamma_{\text{GW}}$ to be of the same order of magnitude as lenghts associated to even elements $\gamma_1 \in \Gamma_{\text{GW}}$ is in the limit $l \to \infty$

$$l(m_{2,R}, n_{2,R}) \overset{!}{\simeq} l(m_{1,R}, n_{1,R}) \quad \Rightarrow \quad n_{2,R} \simeq 2n_{1,R}, \tag{3.36}$$

thus

$$\hat{N}(l) \sim \frac{5}{2}\, n_{1,R}. \tag{3.37}$$

Using relation (3.27)

$$\cosh \frac{l(m_{1,R}, n_{1,R})}{2} \sim \frac{1}{2}\, e^{\frac{l(m_{1,R}, n_{1,R})}{2}} \sim 2\sqrt{2}\, n_{1,R}, \qquad l \to \infty, \tag{3.38}$$

finally reveals

$$\hat{N}(l) \sim \frac{5}{8\sqrt{2}}\, e^{\frac{l}{2}}, \qquad l \to \infty. \tag{3.39}$$

The average multiplicity of the geodesic length spectrum of Γ_{GW} is then obtained by Huber's law for the classical staircase function and (2.36)

$$< g(l) > \sim \frac{e^l}{l} \left(\frac{\mathrm{d}\hat{N}}{\mathrm{d}l}\right)^{-1} \sim \frac{16\sqrt{2}}{5}\, \frac{e^{\frac{l}{2}}}{l}, \qquad l \to \infty. \tag{3.40}$$

The estimate (3.39) for the counting function $\hat{N}(l)$ actually is an upper bound, since the relations (3.21sqq) characterizing group matrices of Γ_{GW} are only necessary conditions. It is, however, in excellent agreement with the numerical results about the geodesic length spectrum to be discussed in the following (see figures 6 and 7). The exponential growth of the multiplicities of the geodesic lengths (3.40) is a typical feature of arithmetical Fuchsian groups, and thus was to be expected for Γ_{GW} (cf. (2.37)).

The set of lengths of closed geodesics on $\Gamma_{\text{GW}}\backslash\mathcal{D}$ is, as mentioned in chapter 2, in one-to-one correspondence to the conjugacy classes of hyperbolic elements of Γ_{GW}. Using the algebraic decomposition of group matrices $\gamma_k \in \Gamma_{\text{GW}}$, these conjugacy classes will now be determined by a slight modification of the method described by Aurich, Bogomolny and Steiner [6].

Remember that the invariant geodesics of hyperbolic elements (3.21) of Γ_{GW} on the Poincaré disk $\mathcal{D}$ are either circular arcs or diameters perpendicular to the boundary $\partial\mathcal{D}$. In the first case one finds explicitly ($z = x + iy$)

$$x^2 + y^2 - \frac{2\alpha}{u_{k,I}}\,(v_{k,R}\, y - v_{k,I}\, x) + 1 = 0, \qquad (u_{k,I} \neq 0), \tag{3.41}$$

describing a circle of radius r centered at $z_M = x_M + iy_M$

$$x_M = -\frac{v_{k,I}\,\alpha}{u_{k,I}}, \quad y_M = \frac{v_{k,R}\,\alpha}{u_{k,I}}, \quad r^2 = \frac{(v_{k,R}^2 + v_{k,I}^2)\,\alpha}{u_{k,I}^2} - 1. \tag{3.42}$$

The limiting case of diameters of $\mathcal{D}$ occurs for vanishing $u_{k,I}$

$$v_{k,R}\,y = v_{k,I}\,x, \qquad (u_{k,I} = 0). \tag{3.43}$$

Any hyperbolic conjugacy class $[\gamma]$ of Γ_{GW} has at least one representative γ, which has an invariant geodesic intersecting the fundamental domain (figure 4) of Γ_{GW}. This can be seen from the tessellation property of Γ_{GW}, i.e., any invariant geodesic of a hyperbolic element $\gamma' \in \Gamma_{\mathrm{GW}}$ can be transformed under the action of Γ_{GW} to hit the fundamental domain of Γ_{GW}. This transformation, however, merely amounts to a conjugation of γ' in Γ_{GW}.

In order to find representatives having invariant geodesics, which intersect the fundamental domain of Γ_{GW}, one proceeds as follows. Since diameters of $\mathcal{D}$ always intersect the fundamental domain of Γ_{GW}, only the case of circular arcs needs to be investigated explicitly. Assume for a moment that the entries of a group matrix $\gamma_k \in \Gamma_{\mathrm{GW}}$ of the form (3.21) obey $u_{k,I} > 0$, $v_{k,R} \geq v_{k,I} \geq 0$. Then the corner of the regular octagon being next to the center of the invariant geodesic of γ_k is $p_2 = 2^{-\frac{1}{4}} e^{i\frac{5\pi}{8}}$, i.e., elements $\gamma_k \in \Gamma_{\mathrm{GW}}$ having invariant geodesics intersecting the fundamental domain of Γ_{GW} are characterized by the condition

$$|z_M - p_2| \leq r. \tag{3.44}$$

Inserting (3.42) leads to

$$u_{k,I} \leq (2 - \sqrt{2})\left(v_{k,R} + (\sqrt{2} - 1) v_{k,I}\right), \tag{3.45}$$

which can be rewritten as

$$v_{k,R}^2 + 5\,v_{k,I}^2 - 4\,v_{k,R}\,v_{k,I} \leq (1 + \sqrt{2})^3 (u_{k,R}^2 - 1) \tag{3.46}$$

by use of $\det \gamma_k = 1$. Since the restrictions $u_{k,I} > 0$, $v_{k,R} \geq v_{k,I} \geq 0$ can always be achieved by $\gamma_k \to -\gamma_k$ and rotations

$$\gamma_k \to R_{\frac{\pi}{4}}\,\gamma_k R_{-\frac{\pi}{4}}, \tag{3.47}$$

relation (3.46) can be used for arbitrary group matrices of Γ_{GW}. Thus for any conjugacy class $[\gamma]$ of Γ_{GW}, i.e., for fixed $u_{k,R}$, only a finite number of representatives exist having invariant geodesics on $\mathcal{D}$, which intersect the fundamental domain of Γ_{GW}. These group matrices will be the starting point for determining the closed geodesics on the Riemann surface $\Gamma_{\mathrm{GW}} \backslash \mathcal{D}$.

Before describing the concrete algorithm, which calculates the multiplicities of the geodesic length spectrum of Γ_{GW}, a few remarks should be made. Remember, that γ and $-\gamma$ are equivalent in $\mathrm{PSU}(1,1)$, and the convention was introduced, always to choose the representative having non-negative trace $\mathrm{tr}\,\gamma \geq 0$, thus for hyperbolic elements $\gamma_k \in \Gamma_{\mathrm{GW}}$ it is $u_{k,R} > 1$.

Furthermore in (2.31) it was shown, that the length of the closed geodesic corresponding to a conjugacy class $[\gamma]$ equals the length associated to $[\gamma^{-1}]$. In physical terms this fact reveals the time-reversal invariance of the dynamical system described by Gutzwiller's group Γ_{GW}. Explicitly one finds for the inverse of any group matrix $\gamma_k \in \Gamma_{\mathrm{GW}}$ of the form (3.21)

$$\gamma_k \to \gamma_k^{-1} \qquad \Leftrightarrow \qquad \begin{array}{ccc} u_{k,R} & \to & u_{k,R} \\ u_{k,I} & \to & -u_{k,I} \\ v_{k,R} & \to & -v_{k,R} \\ v_{k,I} & \to & -v_{k,I} \end{array}. \tag{3.48}$$

After these prerequisites, the algorithm for determining the set of primitive closed geodesics on $\Gamma_{\mathrm{GW}}\backslash\mathcal{D}$ can be described in detail now.

(i) At first, an admissible $u_{k,R}$ obeying (3.22sqq) is selected, thus the length l, for which the multiplicity $g(l)$ should be determined, is fixed.

(ii) Next, some off-diagonal entries subject to $v_{k,R} \geq v_{k,I} \geq 0$, the relation (3.46) and the parity restrictions (3.23sqq) are chosen. According to (3.46) only finitely many of such pairs exist. If furthermore a $u_{k,I} \geq 0$ of correct parity (3.23sqq) can be found, which satisfies the determinant condition $\det \gamma_k = 1$, then the matrix γ_k is a candidate for being a group element of Γ_{GW} having an invariant geodesic, which intersects the fundamental domain of Γ_{GW}. If no such $u_{k,I}$ exists, a new trial is made for another set of $v_{k,R}$ and $v_{k,I}$. If, however, in all cases no valid $u_{k,I}$ can be generated, a so-called "gap" has been found, i.e., no closed geodesic on $\Gamma_{\mathrm{GW}}\backslash\mathcal{D}$ exists, having a length corresponding to $u_{k,R}$. In this case the (non-primitive) multiplicity will be set to $g_m(l) = 0$. Since the parity restrictions (3.23sqq) are only necessary conditions on the group elements of Gutzwiller's group Γ_{GW}, the matrix γ_k may be possibly *not* contained in Γ_{GW}. These choices will be sorted out by a special treatment discussed in (v) below.

(iii) So far, only a segment of a closed geodesic on $\Gamma_{\mathrm{GW}}\backslash\mathcal{D}$ has been determined. This segment is represented by that part of the invariant geodesic of γ_k on $\mathcal{D}$, which lies inside the fundamental domain of Γ_{GW}. The full closed geodesic can be found by "following" this segment beyond the border of the fundamental domain. Explicitly this is achieved by conjugating the starting matrix γ_k by the eight generators of Γ_{GW}. For the following discussion it is convenient to denote the eight generators $a_1^{\pm 1}, b_1^{\pm 1}, a_2^{\pm 1}, b_2^{\pm 1} \in \Gamma_{\mathrm{GW}}$ of Gutzwiller's group as c_ν, $\nu = 0, \cdots 7$. Since the geodesic segment associated to γ_k hits the border of the fundamental domain of Γ_{GW} at two points, exactly two of the eight conjugates $c_\nu\, \gamma_k\, c_\nu^{-1}$ correspond to continuations of the original geodesic segment. They can be recognized by checking the condition (3.46), after possibly rotating according to (3.47). One of the two conjugates

$$\gamma_k^{(1)} := c_{\nu_1}\, \gamma_k\, c_{\nu_1}^{-1} \tag{3.49}$$

is selected arbitrarily for the following step of the algorithm, and stored together with the starting matrix γ_k in a list.

There exists, however, an exception to this rule. The geodesic segment of $\gamma_k \in \Gamma_{\mathrm{GW}}$ may – at one or both ends – intersect the border of the fundamental domain of Γ_{GW} exactly at a corner of the regular octagon. In this case the geodesic segment of γ_k can't be continued into a copy of the original fundamental domain, which is reached by a conjugation with a single generator $c_\nu \in \Gamma_{\mathrm{GW}}$. The copies touching the eight corners of the fundamental domain moreover result from conjugations with some particular group elements $d_\nu \in \Gamma_{\mathrm{GW}}$ of wordlength four, which has to be used in an analogous manner as described above.

(iv) Now, the previous step is repeated, i.e., a conjugate

$$\gamma_k^{(\mu)} := c_{\nu_\mu}\, \gamma_k^{(\mu-1)}\, c_{\nu_\mu}^{-1} \tag{3.50}$$

obeying (3.46) is selected. However, among the two conjugates fulfilling (3.46) that one is chosen, which ensures $\gamma_k^{(\mu)} \neq \gamma_k^{(\mu-2)}$. Also $\gamma_k^{(\mu)}$ is stored in the list. The "corner boosts"

$d_\nu \in \Gamma_{\rm GW}$ have to be treated as described in (iii) and will not be mentioned anymore in the following.

(v) The conjugation cycle may terminate for two reasons. For the first, assume the starting matrix was a valid group element $\gamma_k \in \Gamma_{\rm GW}$. Then after n conjugations the conjugate equals the starting matrix

$$\gamma_k^{(n)} = \gamma_k, \tag{3.51}$$

i.e., one has followed a whole traversal of a closed geodesic on $\Gamma_{\rm GW}\backslash\mathcal{D}$. If the starting matrix was a primitive hyperbolic element of Gutzwiller's group, γ_k or γ_k^{-1} (depending on the arbitrary choice in (iii)) can be obviously written as

$$\gamma_k^{\pm 1} = c_{\nu_n}\, c_{\nu_{n-1}} \cdots c_{\nu_1}. \tag{3.52}$$

If, however, the starting matrix was a power $\gamma_k = \sigma^r$, $r \geq 2$ of some primitive hyperbolic element $\sigma \in \Gamma_{\rm GW}$, then

$$\gamma_k^{\pm 1} = \left(c_{\nu_n}\, c_{\nu_{n-1}} \cdots c_{\nu_1}\right)^r, \tag{3.53}$$

thus multiple traversals of periodic orbits can be separated by checking (3.52) at the end of each conjugation cycle.

Secondly the case of starting matrices $\gamma_k \notin \Gamma_{\rm GW}$ will be considered. Since now there is no reason why the conjugation cycle should close after n steps by (3.51), another terminating condition has to be found. For this purpose, the number of conjugation steps is limited to a maximum value $n_{\max}$. Thus closed geodesics on $\Gamma_{\rm GW}\backslash\mathcal{D}$ associated to hyperbolic elements $\gamma_k \in \Gamma_{\rm GW}$ (actually representatives of hyperbolic conjugacy classes) of wordlength greater than $n_{\max}$ will be skipped by the algorithm.

(vi) If the invariant geodesic of the starting matrix γ_k was a circular arc, i.e., $u_{k,I} > 0$, a new matrix γ_k' is generated by

$$u_{k,I} \to -u_{k,I}. \tag{3.54}$$

If neither γ_k' nor $(\gamma_k')^{-1}$ is contained in the list of conjugates obtained so far, γ_k' is used as a new starting matrix in step (iii).

(vii) Since the initial starting matrix in step (i) was subject to $v_{k,R} \geq v_{k,I} \geq 0$, now seven further matrices fulfilling the parity conditions (3.23sqq) can be constructed by sign changes of $v_{k,R}$ and $v_{k,I}$, and by interchanging real and imaginary part of the off-diagonal entries $v_{k,R} \leftrightarrow v_{k,I}$. Due to (3.42) and the symmetry of the regular octagon, their corresponding invariant geodesics on $\mathcal{D}$ also intersect the fundamental domain of $\Gamma_{\rm GW}$. For each of these seven matrices it is checked, if the matrix itself or its inverse is contained in the list of conjugates. If not, it is used as a new starting matrix in step (iii).

(viii) Finally, looking for further closed geodesics of fixed length l, i.e., of fixed $u_{k,R}$, step (ii) is executed again. If in (ii) no valid matrix can be found anymore, all primitive periodic orbits of length l have been found by the procedure described above. The primitive multiplicity $g(l)$ of the length l is thus twice the number of conjugacy cycles obtained above, since according to (vi) and (vii) backward traversals are not generated explicitly.

However, four closed geodesics on $\Gamma_{\rm GW}\backslash\mathcal{D}$ have to be treated separately, since they are not recognized by the steps described above. They are of length $l = 6.11428\ldots$ and their corresponding invariant geodesics on $\mathcal{D}$ are located exactly on the boundary of the fundamental domain of $\Gamma_{\rm GW}$.

The algorithm discussed above has been used to determine the first 3815 lengths of Γ_{GW} together with their associated primitive multiplicities. The computed length spectrum covers a range from $l_1 = 2.256767\ldots$ to $l_{3815} = 18.126967\ldots$, and is based on the investigation of 4369202 different orbits (including backward traversals). The limiting wordlength in step (v) was set to $n_{\max} = 100$. Thus, if closed geodesics on $\Gamma_{\mathrm{GW}}\backslash\mathcal{D}$ corresponding to hyperbolic elements of wordlength greater than 100 were present in the considerd range of lengths, they were dropped.

For two reasons, however, there is a strong evidence, that the generated length spectrum is complete up to the cutoff length l_{3815}.

One the one hand, the terminating condition of limiting the maximum number of conjugations in step (v) occured exactly in the case of matrices of even type (3.23) having $m_{1,R} \in 4\mathbb{Z}$. In all other cases the conjugation cycles were closed by the condition (3.52). Since the maximum length of closed conjugation cycles, i.e., the maximum wordlength of hyperbolic elements $\gamma_k \in \Gamma_{\mathrm{GW}}$ corresponding to periodic orbits, was observed to be 18 in the covered range $l_1 \leq l \leq l_{3815}$, it seems to be extremly unlikely, that closed geodesics associated to elements of wordlength greater than 100 were missing. Thus afterwards the empirical rule $m_{1,R} \notin 4\mathbb{Z}$ was introduced.

On the other hand, the computed lentgh spectrum can be compared with the theoretical prediction for the counting function $\hat{N}(l)$ of different lengths (3.39). This has been done in fig. 6 for the whole investigated range of lengths, and in fig. 7 for the small interval $l \in [17.95, 18]$.

Another test is offered by the comparison of the classical staircase function with its asymptotical behavior described by Huber's law (2.33). Whereas figure 8 exhibits the exponential proliferation of the number of closed geodesics with increasing lengths, the small range plot fig. 9 also suggests, that no periodic orbits are missing in the computed length spectrum.

The first 64 different lengths of Γ_{GW}, corresponding to the range $0 \leq l \leq 10$, are given in table 1 together with their algebraic decompositions and primitive multiplicities. The numbers in parenthesis, which are sometimes contained in the column "multiplicity" describe the additional contribution arising from multiple traversals of closed geodesics, and thus have to be added to the primitive multiplicities if one is interested in the full $g_m(l)$ (see (2.31sqq)). According to (3.21), the quantity k distinguishes between lengths associated to hyperbolic elements being the product of an even number ($k = 1$) of generators, and those being the product of and odd number ($k = 2$) of generators. They are strictly separated, as can be seen from (3.27), (3.28) and the relation $\pi(n_{2,R}) = 1$.

As discussed in step (ii) above, for some lengths no periodic orbits do exist. It may, however, turn out, that for a particular length only no *primitive* closed geodesic can be found, i.e., $g(l)$=0, but multiple traversals of this length do arise. The primitive gaps contained in the computed range of lengths are listed in table 2. All except one are "true" gaps, i.e., $g_m(l) = 0$, only the length $l = 16.87369\ldots$ appears as a double traversal of $l = 8.43684\ldots$ of multiplicity $g_m(16.87369\ldots) = 48$. It should be mentioned, that all gaps in the range $0 \leq l \leq l_{3815}$ correspond to pairs $(m_{1,R}, n_{1,R})$, which are candidates for elements $\gamma_1 \in \Gamma_{\mathrm{GW}}$ being the product of an even number of generators. These pairs, moreover, even obey the restrictions (3.9sqq) describing group matrices of the regular octagon group Γ_{reg}. Thus all gaps of Γ_{GW} are also gaps of Γ_{reg}. The other direction is not true, i.e., for some gaps of Γ_{reg} closed geodesics of Γ_{GW} can be determined. For a list of gaps of the regular octagon group Γ_{reg} see, e.g., [6].

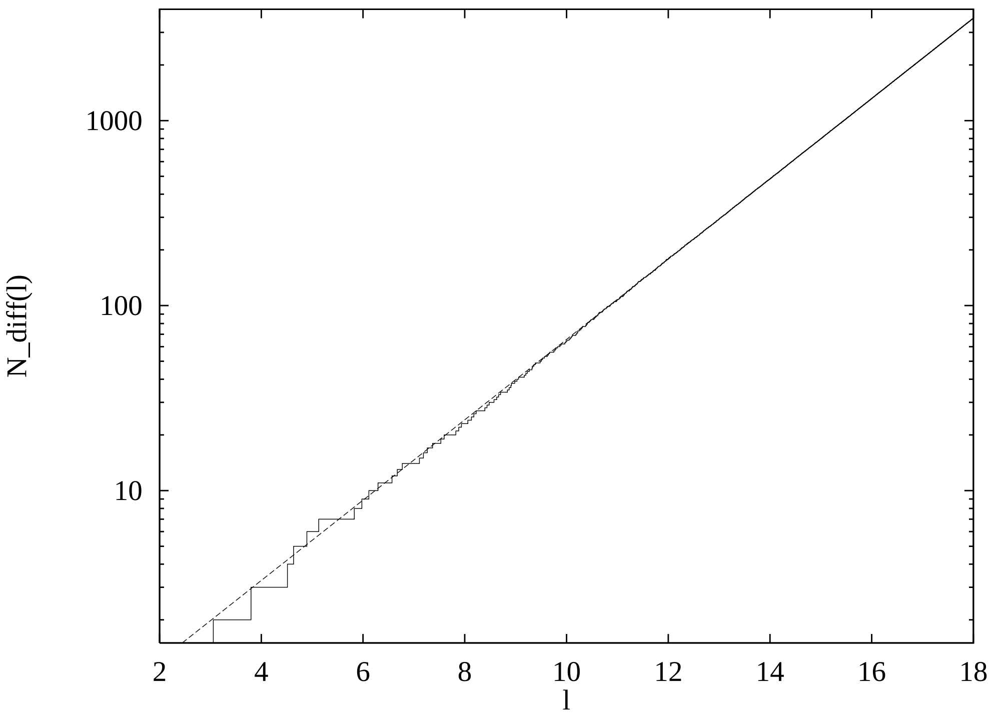

Figure 6: The counting function $\hat{N}(l)$ of Γ_{GW} in comparison with the theoretical prediction (3.39).

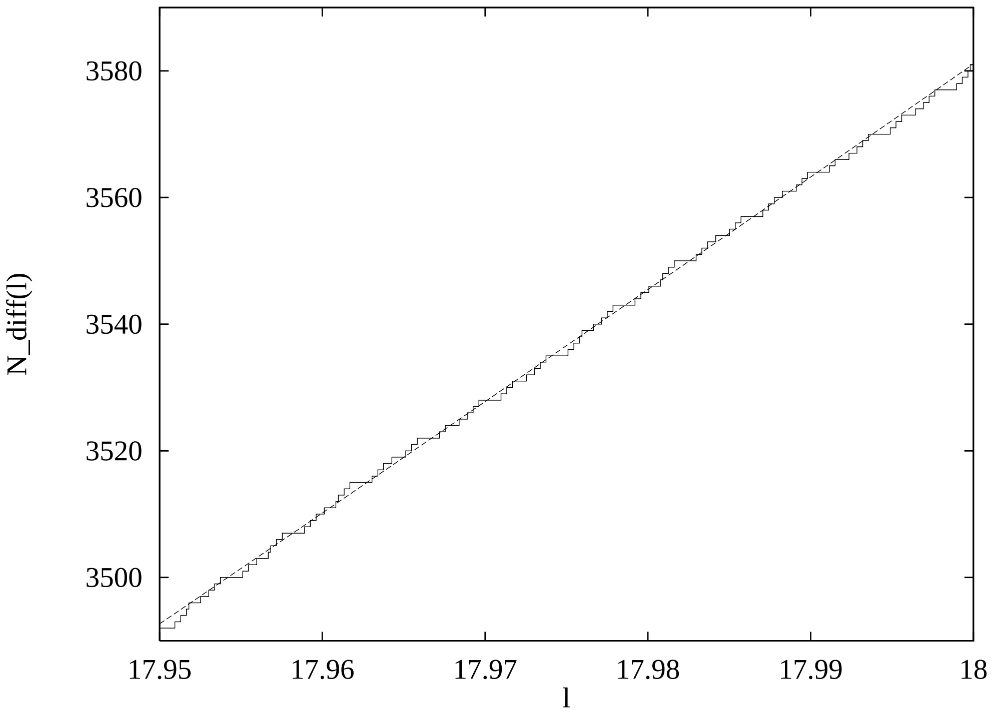

Figure 7: The same curves as in fig. 6 are shown in the small interval $l \in [17.95, 18]$.

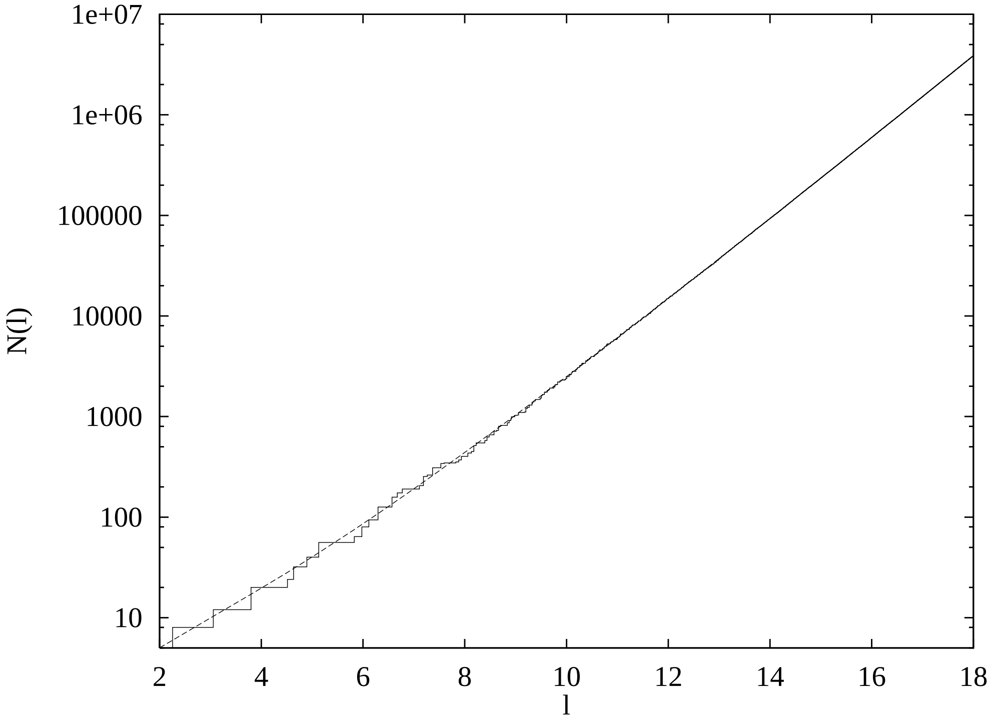

Figure 8: The classical staircase function $N(l)$ of $\Gamma_{\rm GW}$ in comparison with the asymptotic behavior described by Huber's law $N(l) \sim {\rm Ei}(l)$, $l \to \infty$.

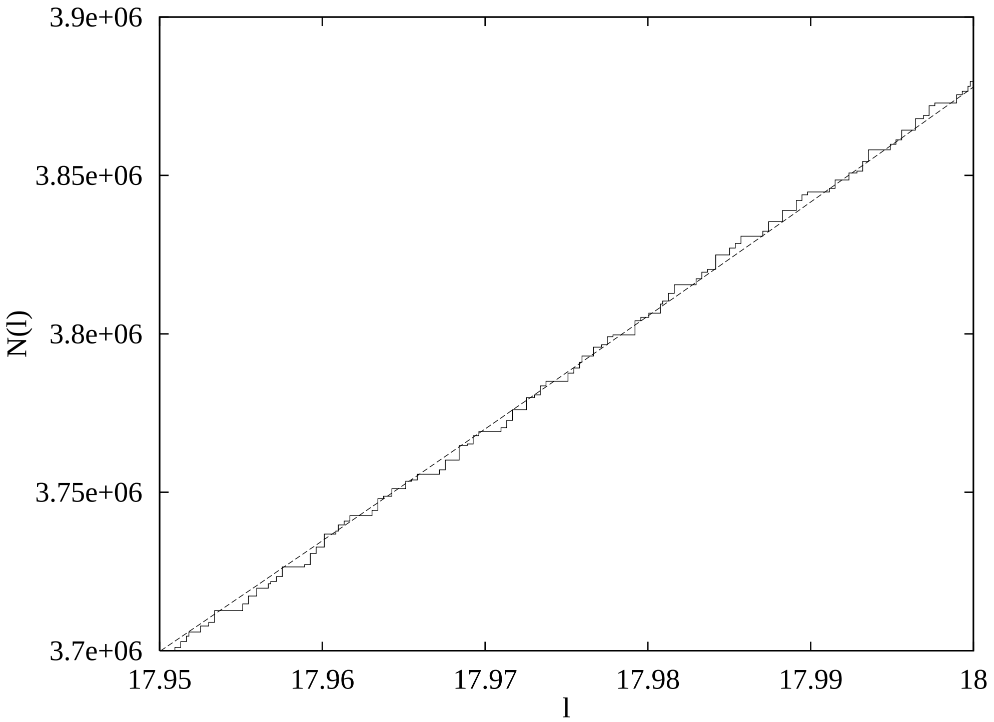

Figure 9: The same curves as in fig. 8 are shown in the small interval $l \in [17.95, 18]$.

$l_{m_{k,R},n_{k,R}}$	k	$m_{k,R}$	$n_{k,R}$	$g(l_{m_{k,R},n_{k,R}})$	$l_{m_{k,R},n_{k,R}}$	k	$m_{k,R}$	$n_{k,R}$	$g(l_{m_{k,R},n_{k,R}})$
2.256767929933	2	1	1	8	8.665952114549	2	19	27	72
3.057141838962	1	1	1	4	8.702750556432	1	19	14	16
3.797845915206	1	2	1	8	8.837684712870	2	21	29	48
4.513535859865	1	2	2	4 (8)	8.871479810735	1	21	15	48
4.633776789970	2	3	3	8	8.904713175372	2	21	31	32
4.896904895356	1	3	2	8	8.918318719921	1	22	15	48
5.128992335155	2	3	5	16	8.982740062312	1	22	16	32
5.828070775442	1	5	3	8	9.027071719731	1	23	16	8 (12)
5.976318829037	2	5	7	16	9.057836099613	2	23	33	64
6.114283677924	1	5	4	14 (4)	9.171425516886	1	25	17	8 (4)
6.294393217254	1	6	4	32	9.200062471572	2	25	35	96
6.568612058019	2	7	9	32	9.228295089636	1	25	18	32
6.672005769911	1	7	5	16	9.267553579940	1	26	18	68 (8)
6.770303789798	2	7	11	16 (8)	9.321789784434	1	26	19	48
7.107375874112	1	9	6	16	9.332840912180	2	27	37	48
7.186788450291	2	9	13	48	9.359271657904	1	27	19	32
7.263163475119	1	9	7	8	9.385357603752	2	27	39	48
7.366419207916	1	10	7	48	9.482194149272	1	29	20	48
7.531220287193	2	11	15	32	9.506734357394	2	29	41	96
7.595691830411	1	11	8	4 (8)	9.530977057139	1	29	21	32
7.824911392100	2	13	17	8	9.564767330983	1	30	21	96
7.880692288665	1	13	9	16	9.621163543210	2	31	43	72
7.934958437080	2	13	19	32	9.644065648625	1	31	22	32
8.060198615979	1	14	10	32	9.666708433895	2	31	45	64
8.130075528900	1	15	10	16	9.751099758307	1	33	23	56
8.178051862130	2	15	21	64	9.772568794520	2	33	47	96
8.224903623255	1	15	11	32	9.793809790712	1	33	24	8 (8)
8.394761067214	2	17	23	32	9.823469090622	1	34	24	128
8.436849640524	1	17	12	48	9.873105918657	2	35	49	64
8.478070345869	2	17	25	32	9.893310687773	1	35	25	32
8.574217476233	1	18	13	56	9.968829684532	2	37	51	32
8.628463656524	1	19	13	16	9.988094636657	1	37	26	64

Table 1: The geodesic length spectrum of Γ_{GW} in the range $0 < l < 10$.

$l_{m_{1,R},n_{1,R}}$	$m_{1,R}$	$n_{1,R}$	$l_{m_{1,R},n_{1,R}}$	$m_{1,R}$	$n_{1,R}$
11.195071243745	67	48	16.970634379124	1211	856
12.010953274128	101	72	17.025974987262	1245	880
13.619286275817	227	160	17.329263085353	1449	1024
13.807097226169	249	176	17.450146832648	1539	1088
13.898618903507	261	184	17.493817654885	1573	1112
14.062925092345	283	200	17.521992715807	1595	1128
14.289709009761	317	224	17.536555248372	1607	1136
14.790935353990	407	288	17.564138717984	1629	1152
15.602684527115	611	432	17.896044010303	1923	1360
15.710905146579	645	456	17.931063388417	1957	1384
15.778931208310	667	472	17.953736793196	1979	1400
15.878245974608	701	496	17.987768842919	2013	1424
16.578683372352	995	704	18.076421266499	2105	1488
16.645806049110	1029	728	18.097513602973	2127	1504
16.873699280665	1153	816	18.108444582710	2139	1512

Table 2: The (primitive) gaps of Γ_{GW} in the range $l_1 \leq l \leq l_{3815}$.

3.3 Quantization by Selberg's Trace Formula

In the previous section, the unconstrained motion of a point-particle on a particular Riemann surface of genus $g = 2$ associated to Gutzwiller's group Γ_{GW}, was investigated from the classical point of view. A quantization of the dynamical system under consideration, however, can be achieved by applying Gutzwiller's semiclassical periodic-orbit theory [30, 33], which relates the geodesic length spectrum of a classical chaotic system to the spectrum of energy eigenvalues of the corresponding quantized version. The case of Riemann surfaces of genus $g = 2$ has the advantage that the periodic-orbit theory is exact [31], since it is identical to the Selberg trace formula [50]. The latter will be used in the following to express the spectral staircase $\mathcal{N}(E)$ and the Selberg zeta function in terms of the geodesic length spectrum, finally leading to quantization rules for the dynamical system defined by Γ_{GW}.

The Selberg trace formula for Riemann surfaces of genus $g = 2$ reads [50]

$$\sum_{n=0}^{\infty} h(p_n) = \frac{A}{4\pi}\int_{-\infty}^{\infty} \mathrm{d}p\, p\, h(p) \tanh(\pi p) + \sum_{\{\gamma\}}\sum_{k=1}^{\infty} \frac{l_\gamma}{2\sinh(kl_\gamma/2)}\, \hat{h}(kl_\gamma), \qquad (3.55)$$

where p_n are the momenta corresponding to the quantum-mechanical energy eigenvalues $E_n = p_n^2 + \frac{1}{4}$, $A = \mathrm{area}(\Gamma_{\mathrm{GW}}\backslash\mathcal{D}) = 4\pi$ denotes the area of the fundamental domain of Γ_{GW}, and the sum on the right-hand side runs over primitive hyperbolic conjugacy classes $\{\gamma\}$ of Γ_{GW}. If the smearing function $h(p)$ is chosen to be even $h(p) = h(-p)$, holomorphic in the strip $|\mathrm{Im}\,(p)| \leq \frac{1}{2} + \epsilon$, $\epsilon > 0$, and furthermore to decrease asymptotically faster than $|p|^{-2}$ for

$|p| \to \infty$, all sums and integrals involved in (3.55) are absolutely convergent. The Fourier transform of $h(p)$ is denoted as

$$\hat{h}(t) = \frac{1}{2\pi} \int_{-\infty}^{\infty} \mathrm{d}p \, h(p) e^{-ipt}. \tag{3.56}$$

Whereas the left-hand side of Selberg's trace formula can be considered to be of purely quantum-mechanical nature, the right-hand side, consisting of the so-called zero-length term being proportional to the area of the fundamental domain of Γ_{GW} and a sum over the geodesic length spectrum of $\Gamma_{\mathrm{GW}} \backslash \mathcal{D}$, is completely determined by purely classical quantities.

As has been shown in [12, 14, 7], the spectral staircase $\mathcal{N}(E)$ can be obtained from Selberg's trace formula by choosing a particular smearing function

$$h(p) = \frac{1}{\epsilon\sqrt{\pi}} \left\{ e^{-\frac{(p'-p)^2}{\epsilon^2}} + e^{-\frac{(p'+p)^2}{\epsilon^2}} \right\}, \tag{3.57}$$

and integrating (3.55) over $p \in [0, \sqrt{E - \frac{1}{4}}]$ in the limit $\epsilon \to 0^+$. Since

$$\lim_{\epsilon \to 0^+} \frac{1}{\epsilon\sqrt{\pi}} \, e^{-\frac{(x-y)^2}{\epsilon^2}} = \delta(x - y), \tag{3.58}$$

the quantum-mechanical side of Selberg's trace formula yields the exact spectral staircase

$$\mathcal{N}(E) = 1 + \int_0^{\sqrt{E-\frac{1}{4}}} \mathrm{d}p \sum_{n=1}^{\infty} \left\{ \delta(p - p_n) + \delta(p + p_n) \right\}, \tag{3.59}$$

where the 1 arises from the ground state $E_0 = 0$ corresponding to the constant eigenfunction on $\Gamma_{\mathrm{GW}} \backslash \mathcal{D}$.

On the right-hand side of Selberg's trace formula, the zero-length term results in

$$\lim_{\epsilon \to 0^+} \frac{A}{4\pi} \int_0^{\sqrt{E-\frac{1}{4}}} \mathrm{d}p' \int_{-\infty}^{\infty} \mathrm{d}p \, p \, h(p) \tanh(\pi p) = \frac{A}{2\pi} \int_0^{\sqrt{E-\frac{1}{4}}} \mathrm{d}p' \, p' \tanh(\pi p'), \tag{3.60}$$

whereas the periodic-orbit sum can be determined by using

$$\int_0^p \mathrm{d}p' \, \hat{h}(t) = \frac{\sin(pt)}{\pi t} \, e^{-\frac{\epsilon^2}{4} t^2} \tag{3.61}$$

for the particular choice (3.57) of $h(p)$. Thus, the spectral staircase turns out to be ($E = p^2 + \frac{1}{4}$)

$$\mathcal{N}(E) = \frac{A}{2\pi} \int_0^p \mathrm{d}p' \, p' \tanh(\pi p') + \frac{1}{2\pi} \sum_{\{\gamma\}} \sum_{k=1}^{\infty} \frac{\sin(pkl_\gamma)}{k \sinh(kl_\gamma/2)}. \tag{3.62}$$

Since in the limit $\epsilon \to 0^+$ the smearing function $h(p)$ does not obey the restrictions mentioned above (3.55sqq), Selberg's trace formula offers no information about the convergence properties of the periodic-orbit sum. It is, however, known that (3.62) is valid in the sense of distributions [14].

For numerical calculations, relation (3.62) can be used nevertheless, if the periodic-orbit sum is regularized by the following procedure. Assume the geodesic length spectrum has been determined completely up to a cutoff length $\mathcal{L}$. Then the periodic-orbit sum can be evaluated by taking into account all closed geodesics $kl_\gamma \leq \mathcal{L}$ exactly, and approximating the remaining sum by

$$R(p,\mathcal{L}) := \frac{1}{2\pi} \sum_{\substack{\{\gamma\} \\ kl_\gamma > \mathcal{L}}} \sum_{k=1}^{\infty} \frac{\sin(pkl_\gamma)}{k \sinh(kl_\gamma/2)} \simeq \lim_{\epsilon\to 0+} \frac{1}{2\pi} \int_{\mathcal{L}}^{\infty} \mathrm{d}l \, \frac{\mathrm{d}N(l)}{\mathrm{d}l} \frac{\sin(pl_\gamma)}{\sinh(l_\gamma/2)} \, e^{-\frac{\epsilon^2}{4} l_\gamma^2}, \tag{3.63}$$

where only the asymptotically leading contribution $k = 1$ has been included, since terms associated to multiple traversals ($k \geq 2$) are exponentially suppressed. Inserting Huber's law (2.33), the remainder term can be rewritten as

$$R(p,\mathcal{L}) = \lim_{\epsilon\to 0+} \frac{1}{\pi} \int_{\mathcal{L}}^{\infty} \mathrm{d}l \, \frac{\sin(pl_\gamma)}{l} \, e^{-\frac{\epsilon^2}{4} l_\gamma^2 + \frac{1}{2} l_\gamma}, \tag{3.64}$$

The integral can be carried out [7], and after taking the limit $\epsilon \to 0^+$ one finally arrives at ($p > 0$)

$$R(p,\mathcal{L}) = \frac{1}{\pi} \operatorname{Im} \mathrm{E}_1 \left(-(\tfrac{1}{2} + ip) \, \mathcal{L} \right). \tag{3.65}$$

Here $\mathrm{E}_1(z)$ denotes the exponential integral defined by

$$\mathrm{E}_1(z) := \int_z^{\infty} \mathrm{d}t \, \frac{e^{-t}}{t}, \tag{3.66}$$

where the path of integration is assumed to exclude the origin and does not intersect the negative real axis. Thus, finally the spectral staircase can be written as

$$\mathcal{N}(E) \simeq \frac{A}{2\pi} \int_0^p \mathrm{d}p' \, p' \, \tanh(\pi p') + \frac{1}{2\pi} \sum_{\substack{\{\gamma\} \\ kl_\gamma \leq \mathcal{L}}} \sum_{k=1}^{\infty} \frac{\sin(pkl_\gamma)}{k \sinh(kl_\gamma/2)} + \frac{1}{\pi} \operatorname{Im} \mathrm{E}_1 \left(-(\tfrac{1}{2} + ip) \, \mathcal{L} \right). \tag{3.67}$$

It should be mentioned, that the expression (3.65) for the remainder term $R(p,\mathcal{L})$ does not depend on the particular group Γ_{GW} under consideration. It is, moreover, valid for all dynamical systems, for which Selberg's trace formula (3.55) and Huber's law (2.33) hold.

Decomposing the spectral staircase into a mean and an oscillatory part

$$\mathcal{N}(E) = \bar{\mathcal{N}}(E) + \mathcal{N}_{\mathrm{osc}}(E), \tag{3.68}$$

the asymptotic behavior $E \to \infty$ of the mean spectral staircase $\bar{\mathcal{N}}(E)$ can be derived from the zero-length term of (3.67). Using the geometric series expansion

$$\tanh x = 1 + \sum_{k=1}^{\infty} (-1)^k \, e^{-2kx}, \qquad x > 0, \tag{3.69}$$

one finds for Riemann surfaces of genus $g = 2$, i.e., $A = 4\pi$

$$\begin{aligned} & 2 \int_0^p \mathrm{d}x \, x \, \tanh(\pi x) \\ &= 2 \int_0^p \mathrm{d}x \, x + 4 \sum_{k=1}^{\infty} (-1)^k \int_0^p \mathrm{d}x \, x e^{-2k\pi x} \\ &= p^2 - \frac{1}{\pi^2} \sum_{k=1}^{\infty} \frac{(-1)^k}{k^2} \left\{ (2k\pi p + 1) \, e^{-2k\pi p} - 1 \right\} \\ &= p^2 - \frac{1}{\pi^2} \sum_{k=1}^{\infty} \frac{(-1)^{k+1}}{k^2} + O(pe^{-2\pi p}). \end{aligned} \tag{3.70}$$

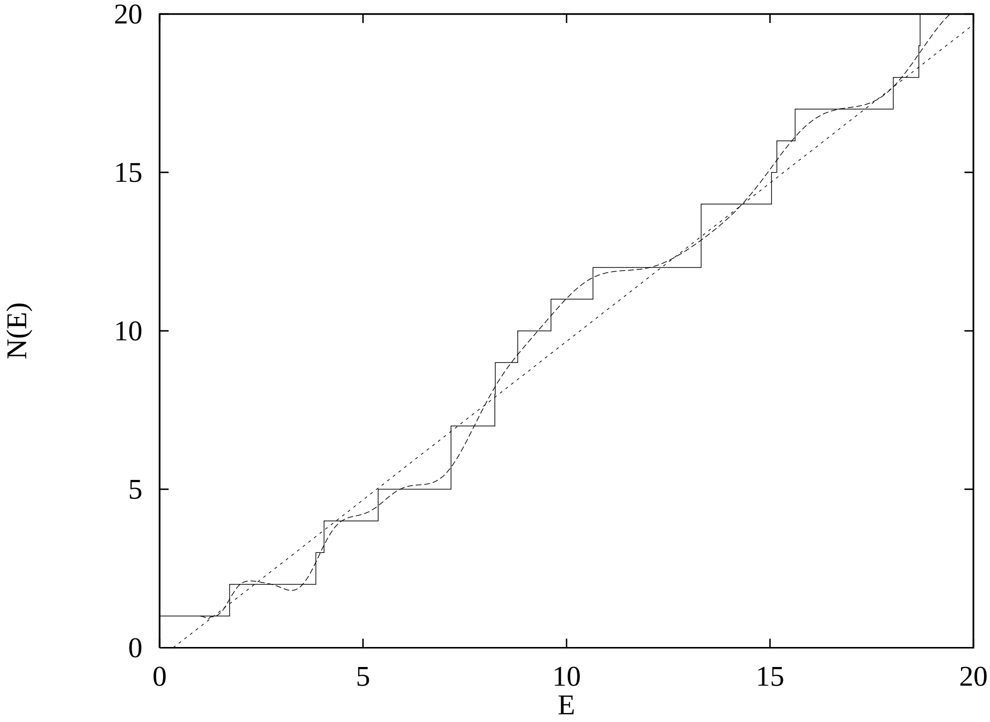

Figure 10: The spectral staircase $\mathcal{N}(E)$ of Gutzwiller's octagon (solid curve) is compared with the approximation obtained from (3.67) (dashed curve). The dotted straight line shows Weyl's law $\mathcal{N}(E) \sim E - \frac{1}{3}$.

The sum can be rearranged to yield

$$\sum_{k=1}^{\infty} \frac{(-1)^{k+1}}{k^2} = \tfrac{1}{2}\zeta(2) = \frac{\pi^2}{12}, \tag{3.71}$$

and by inserting $E = p^2 + \frac{1}{4}$ the asymptotic behavior of the mean spectral staircase turns out to be

$$\bar{\mathcal{N}}(E) = E - \tfrac{1}{3} + O(\sqrt{E}\, e^{-2\pi\sqrt{E}}), \qquad E \to \infty. \tag{3.72}$$

This relation is, apart from the exponentially small correction, identical to Weyl's law. Since the dynamical systems under consideration, i.e., Riemann surfaces of genus $g = 2$, have no boundary, the correction to the leading order term of Weyl's law (2.42) is a constant contribution.

The approximation (3.67) for the spectral staircase has been evaluated for Gutzwiller's group by using the geodesic length spectrum of Γ_{GW} discussed in the previous section ($\mathcal{L} = 18.126967\ldots$). In figs. 10 and 11 it is compared with the "true" spectral staircase $\mathcal{N}(E)$, which has been calculated by Aurich [4] by numerically solving the Schrödinger equation using the method of finite elements. Furthermore Weyl's law (3.72) is also included, which, despite being valid in the asymptotical regime $E \to \infty$, fits well even at the lowest energy eigenvalues.

The approximate energy eigenvalues E'_n of the dynamical system associated to Γ_{GW} can be derived from (3.67) by defining

$$\mathcal{N}(E'_n) = n + \frac{1}{2}, \qquad n = 1, 2, 3, \cdots . \tag{3.73}$$

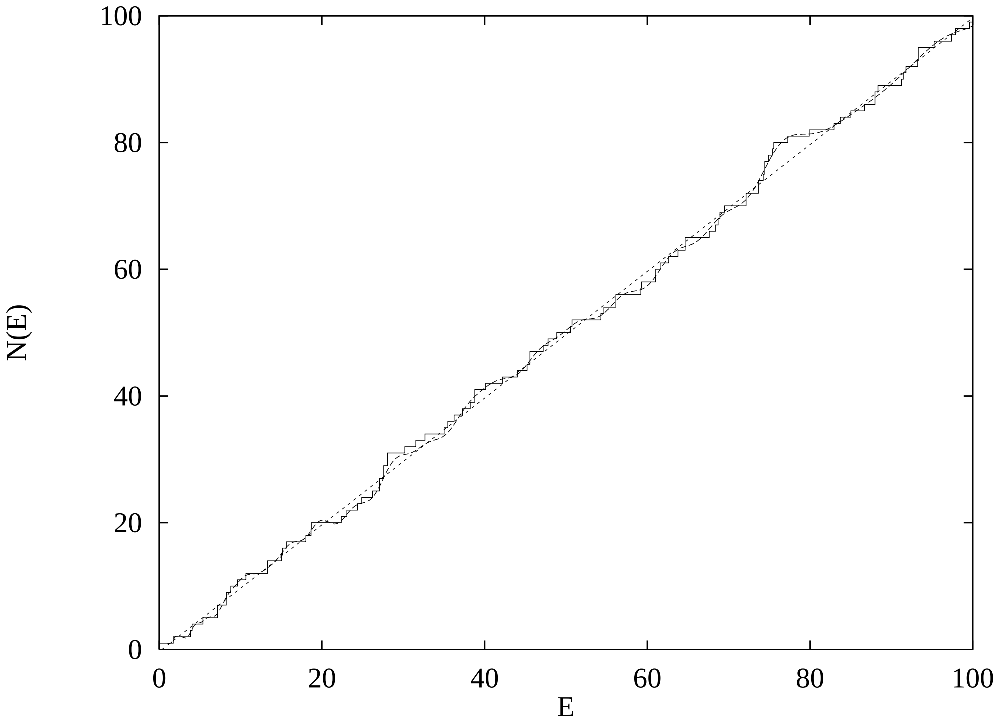

Figure 11: The same curves as in fig. 10 are shown but in the larger energy range $E \in [0, 100]$.

Here the groud state level $E_0 = 0$ has been omitted, since it leads to an imaginary momentum $p_0 = i/2$ and cannot be obtained by the method described above. For numerical purposes it is convenient to determine the energy eigenvalues as zeros of the function [14, 9]

$$\xi(E) := \cos(\pi \mathcal{N}(E)). \tag{3.74}$$

A plot of the quantization function $\xi(E)$ for Gutzwiller's group is shown in fig. 12, again in comparison with the numerical solutions of Schrödinger's equation. It can be observed, that the zeroes of $\xi(E)$ yield reasonably good approximations to the "true" energy eigenvalues E_n. Only in those cases, where the E_n are degenerated or very close to each other, relation (3.74) fails to resolve them (cf. table 3).

Theoretically, the energy resolution of the quantization rule (3.74) is restricted by the cutoff length $\mathcal{L}$. Namely the closed geodesic of largest length $\mathcal{L}$, taken into account in the periodic-orbit sum in (3.67), produces the shortest distance between two adjacent zeroes with respect to p, i.e.,

$$(\Delta p)_{\min} = \frac{\pi}{\mathcal{L}}. \tag{3.75}$$

Since the mean distance ΔE between two adjacent energy eigenvalues is determined by the mean level density $\bar{d}(E)$

$$\Delta E = \frac{1}{\bar{d}(E)} = \Delta p \frac{\mathrm{d}E}{\mathrm{d}p}, \qquad \bar{d}(E) := \frac{\mathrm{d}}{\mathrm{d}E} \bar{\mathcal{N}}(E), \tag{3.76}$$

the cutoff length $\mathcal{L}$ needed to resolve energy levels at energy $E = p^2 + \frac{1}{4}$ is given by

$$\mathcal{L} = \frac{1}{2} A\, p. \tag{3.77}$$

Thus in the case of Gutzwiller's group ($A = 4\pi$), a cutoff length of $\mathcal{L} \simeq 18$ leads to a theoretically maximal energy $E_{\max} \simeq 8.46$, above which the resolution of two adjacent energy eigenvalues starts to fail.

The numerical solutions E_n and the approximations E_n' obtained from (3.74) together with their relative errors are given in table 3 for the range $0 < E <= 20$. The maximal errors ($\sim 5\%$) occur for the degenerate energy eigenvalues at $E = 7.16$ and $E = 13.31$.

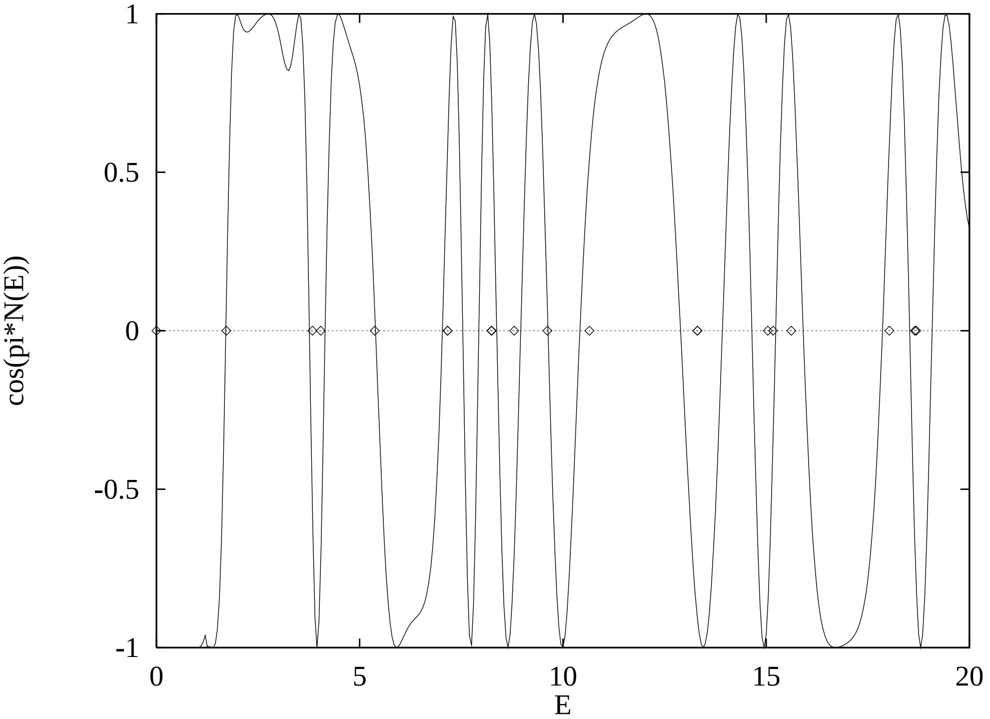

Figure 12: The quantization function $\xi(E) := \cos(\pi\mathcal{N}(E))$ of Γ_{GW} is compared with the energy eigenvalues obtained from numerically solving Schrödinger's equation by the method of finite elements.

A further method exists, based on the Selberg trace formula (3.55), which relates the geodesic length spectrum of a dynamical system to the spectrum of energy eigenvalues [8]. The starting point is the trace of the regularized resolvent

$$\sum_{n=1}^{\infty} \left\{ \frac{1}{E_n - s(s-1)} - \frac{1}{E_n} \right\} = \phi(s) + \frac{1}{2s-1} \frac{Z'(s)}{Z(s)}, \tag{3.78}$$

which can be derived from Selberg's trace formula [53]. Here the complex variable $s := \frac{1}{2} - ip$ has been introduced, thus $s(s-1) = p^2 + \frac{1}{4} = E$. It can be shown, that the pole structure of the left-hand side of (3.78) is not affected by the function $\phi(s)$, and therefore is completely determined by the term containing the logarithmic derivative of *Selberg's zeta function* [50, 37], which is defined by the Euler product

$$Z(s) := \prod_{\{\gamma\}} \prod_{n=0}^{\infty} \left(1 - e^{-(s+n)\, l_\gamma}\right), \qquad \mathrm{Re}\, s > \tau, \tag{3.79}$$

E_n	E'_n	Relative error [%]
1.72	1.70	-1.2
3.84	3.76	-2.1
4.04	4.15	2.7
5.37	5.39	0.4
7.16	7.03	-1.8
7.16	7.54	5.3
8.24	7.93	-3.8
8.25	8.37	1.5
8.80	8.96	1.8
9.62	9.63	0.1
10.65	10.42	-2.2
13.31	12.89	-3.2
13.31	13.92	4.6
15.04	14.65	-2.6
15.17	15.23	0.4
15.62	15.91	1.9
18.03	17.86	-0.9
18.66	18.53	-0.7
18.69	19.08	2.1

Table 3: The energy eigenvalues E_n of Gutzwiller's octagon in comparison with the zeroes E'_n of the quantization function $\xi(E)$, obtained from the approximation (3.67) of the spectral staircase $\mathcal{N}(E)$.

where τ denotes the topological entropy. In the case of Riemann surfaces of genus $g = 2$, i.e., in particular for Γ_{GW}, the topological entropy is known to be $\tau = 1$ (see also (2.38sqq)). As suggested by relation (3.78), the so-called non-trivial zeroes of $Z(s)$, which correspond to the energy eigenvalues of the dynamical system under consideration, are located on the *critical line*

$$s = \frac{1}{2} - ip, \qquad p \in \mathbb{R}. \tag{3.80}$$

Omitting all factors $n \geq 1$ in (3.79) leads to a simpler function, which contains the same information on the non-trivial zeroes as $Z(s)$. It is denoted as *Ruelle-type zeta function*

$$R(s) := \prod_{\{\gamma\}} \left(1 - e^{-sl_\gamma}\right), \qquad \mathrm{Re}\, s > \tau. \tag{3.81}$$

The Euler products (3.79) and (3.81) converge absolutely for $\mathrm{Re}\, s > \tau$, i.e., to the right of the so-called "entropy-barrier". Since in the case of Γ_{GW} the topological entropy is $\tau = 1$, the Euler product representations of $Z(s)$ and $R(s)$ seem to be of no use to calculate the non-trivial zeroes located on the critical line $\mathrm{Re}\, s = 1/2$. Moreover, a convergence of the Euler products on the critical line cannot be expected, since in an absolutely convergent product a zero only occurs if at least one of the factors vanishes, which in turn would determine a quantum-mechanical energy eigenvalue E_n in terms of a single length l_γ.

In order to investigate the convergence properties of the Ruelle-type zeta function $R(s)$, the product in (3.81) is expanded, which turns the Euler product into a Dirichlet series

$$R(s) = \sum_{\rho} (-1)^{|L_\rho|} \, e^{-sL_\rho}, \qquad \mathrm{Re}\, s > \tau. \tag{3.82}$$

The sum now runs over all *Dirichlet-orbits*, henceforth called *D-orbits*, which are defined as formal combinations of primitive closed geodesics of *D-lengths* $L_\rho := l_{\gamma_1} + \cdots + l_{\gamma_n}$. The number of primitive closed geodesics constituting a D-orbit is denoted as $|L_\rho|$. As the Euler product (3.81), the Dirichlet series (3.82) converges absolutely to the right of the entropy barrier. Generally it is known, that Dirichlet series of the form (3.82) converge conditionally in right half-planes $\mathrm{Re}\, s > \sigma_c$, and converge absolutely in right half-planes $\mathrm{Re}\, s > \sigma_a$, $\sigma_a \geq \sigma_c$. Thus if the critical line $\mathrm{Re}\, s = 1/2$ is contained in the strip $\sigma_c < \mathrm{Re}\, s \leq \sigma_a$, the Dirichlet series representation of the Ruelle-type zeta function can be used to determine the non-trivial zeroes of $R(s)$.

Arranging the D-orbits in ascending order $L_1 \leq L_2 \leq L_3 \leq \cdots$, the *abscissae of convergence* are obtained by the relations

$$\begin{aligned} \sigma_a &= \limsup_{N\to\infty} \frac{1}{L_N} \, \log \sum_{n=1}^{N} \left|(-1)^{|L_n|}\right|, \\ \sigma_c &= \limsup_{N\to\infty} \frac{1}{L_N} \, \log \left|\sum_{n=1}^{N} (-1)^{|L_n|}\right|. \end{aligned} \tag{3.83}$$

In [8] a random walk model for the coefficients of the Dirichlet series is proposed, which allows to predict the value of σ_c. The model is based on a few reasonable assumptions. At first, it can be shown for compact Riemann surfaces of genus $g \geq 2$, that the counting function of the so-called *pseudo-orbits* [20, 41], which are formal combinations of primitive closed geodesics of *pseudo-lengths* $\tilde{L}_\rho := m_1 \, l_{\gamma_1} + \cdots + m_n \, l_{\gamma_n}$, $m_k \in \mathbb{N}$, asymptotically behaves as [15]

$$\tilde{N}(L) := \#\{\tilde{\rho}; \tilde{L}_\rho \leq L\} \sim \frac{Z(2)}{Z'(1)} \, e^{\tau L}, \quad L \to \infty, \tag{3.84}$$

with $\tau = 1$. Since the counting function $N_D(L)$ for D-orbits is restricted by $N(L) \leq N_D(L) \leq \tilde{N}(L)$, the conclusion

$$L_N \sim \frac{1}{\tau} \log N, \qquad N \to \infty \tag{3.85}$$

can be drawn. By inserting this relation into (3.83), one obviously recovers $\sigma_a = \tau$.

Secondly, it is assumed that the multiplicities $g_D(L)$ of the vast majority of D-lengths result from on the multiplicities of the primitive geodesic length spectrum, i.e.,

$$g_D(L) \simeq \prod_{i=1}^{n} g(l_i) \tag{3.86}$$

for a D-length $L = l_1 + \cdots l_n$ composed of primitive closed geodesics of different lengths. Then from (3.40) the asymptotic behavior of the average D-multiplicity can be concluded to be

$$< g_D(L) > \sim \; d e^{\alpha L}, \qquad L \to \infty, \tag{3.87}$$

for some positive parameters d and α. Using the D-multiplicities, the Dirichlet series (3.82) can be rewritten as a sum over distinct D-lengths

$$R(s) = \sum_{n=1}^{\infty} A_n \, g_D(L_n) \, e^{-sL_n}, \qquad \mathrm{Re}\, s > \tau, \tag{3.88}$$

where A_n denotes the common D-coefficient of the degenerate D-orbits of D-length L_n ($A_0 = 1 = g_D(0)$).

Finally, the Dirichlet coefficients A_n are assumed to be randomly distributed as a result of arranging the D-lengths in ascending order $L_1 \leq L_2 \leq L_3 \leq \cdots$. Thus the value of A_k is independent of A_n for $k \neq n$, allowing the application of the random walk model.

Putting all this together, the parameter α obtained from a fit of (3.87) turns out to be related to the abscissa of conditional convergence

$$\sigma_c = \frac{1}{2}(\tau + \alpha). \tag{3.89}$$

It should be emphasized, that this value of σ_c is derived for a fixed, namely ascending, order of D-lengths. The random walk model crucially depends on this ingredient. It is, however, conceivable that it is possible to find a "better" ordering of the D-lengths, which yields an even smaller σ_c. In this case the statistical model may break down and the general relation (3.83) has to be used to determine σ_c.

For the Gutzwiller group Γ_{GW} the geodesic length spectrum up to $l = l_{3815} = 18.126967\ldots$ has been used to determine the spectrum of D-lengths up to $L = l_{3815}$, resulting in 31637374 D-orbits of 12010 different D-lengths. A fit of the average D-multiplicity according to (3.87), yielding the fit parameters $d = 1.6250\ldots$ and $\alpha = 0.4324\ldots$, is shown in fig. 13. From (3.89) the prediction $\sigma_c = 0.7162\ldots$ is derived and compared in fig. 15 with a numerical evaluation of the partial sums (3.83). The prediction (3.89) of σ_c seems to be somewhat larger than the value obtained from the sequences (3.83). But since the latter grow very slowly, i.e., logarithmically, the numerically used range $1 \leq N \leq 12010$ may be too small to draw a conclusion for the limit $N \to \infty$. However, the deviation may be also caused by a slight violation of the assumption, that the Dirichlet coefficients in (3.82) are randomly distributed (see fig. 14). A similar observation has been made in the case of Artin's billiard, obtained from the action of $\mathrm{SL}(2,\mathbb{Z})$ on $\mathcal{H}$, where the deviation between the prediction (3.89) and the value for σ_c obtained from (3.83) is even larger than for Gutzwiller's group Γ_{GW} [8].

The value of σ_c derived from (3.83) and (3.89) forbids to evaluate the Dirichlet series representation (3.82) of the Ruelle-type zeta function $R(s)$ on the critical line in the case of Gutzwiller's octagon. However, in the context of the triangular group $T^*(2,3,8)$ to be discussed in the next chapter, the method described above will turn out to be of some use, since then the strip of conditional convergence of (3.82) includes the critical line.

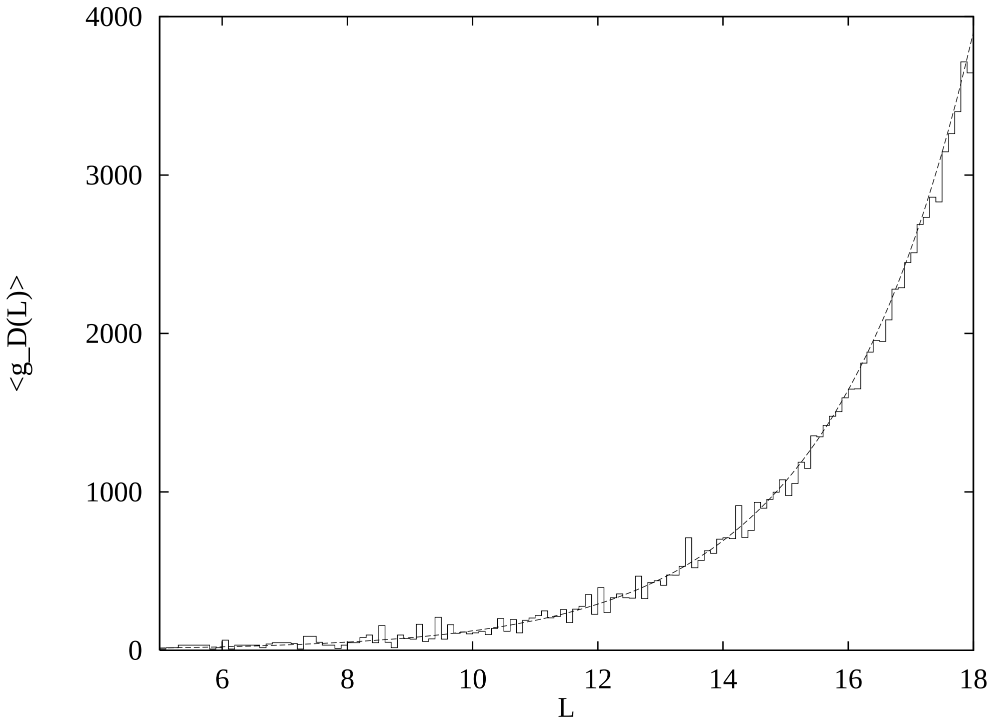

Figure 13: The average D-multiplicity $< g_D(L) >$ of Gutzwiller's group Γ_{GW} is shown together with the fit curve $de^{\alpha L}$.

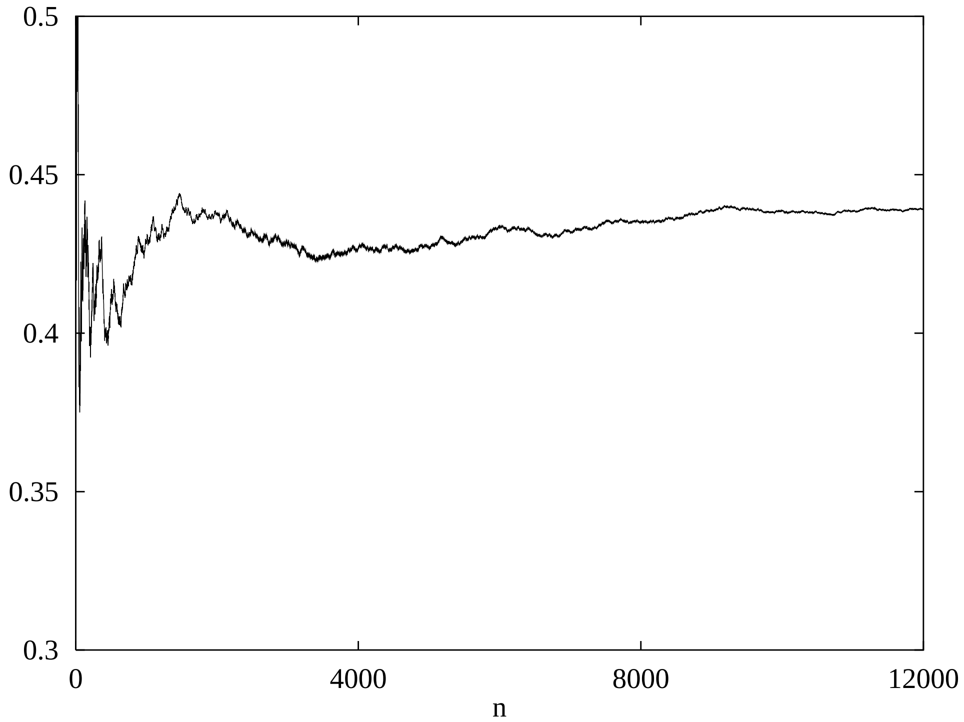

Figure 14: The probability for the coefficient A_{n+1} to have the same sign as A_n in the Dirichlet series representation (3.88) of $R(s)$.

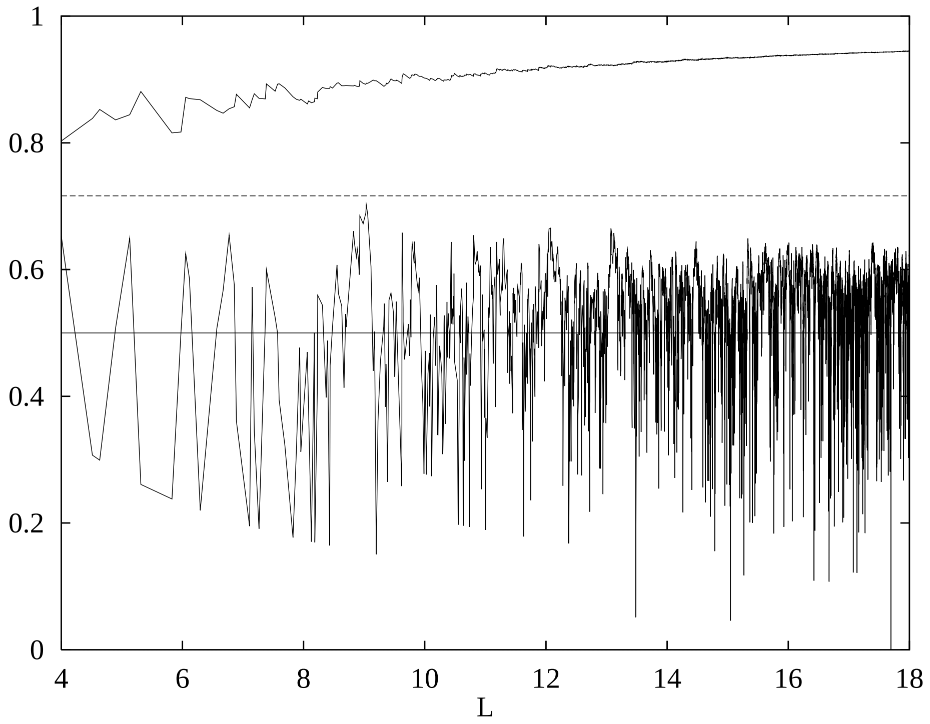

Figure 15: The numerical evaluations of the partial sums (3.83) are plotted as functions of the D-length L_N. The upper curve corresponds to σ_a, the lower one to σ_c. The critical line is indicated by the full horizontal line at $s = \frac{1}{2}$, whereas the prediction (3.89) from the statistical model is shown as a dashed line at $\sigma_c = 0.7162\ldots$.

3.4 Inverse Quantum Chaology

So far, the Selberg trace formula has been used to derive the energy eigenvalues of the dynamical system associated to Γ_{GW} from the geodesic length spectrum. Now the reverse direction will be attacked, i.e., the energy spectrum will be used as input, and a suitable choice of the smearing function $h(p)$ unravels (the lower part of) the spectrum of geodesic lengths. Since a much more effective method exists, which allows to determine the geodesic length spectrum (cf. section 3.2), the results of this section mainly serve as a cross check to unmask possibly missing lengths or wrong multiplicities.

For this purpose the smearing function to be inserted in Selberg's trace formula is chosen to be

$$h(p) = \cos(pL)\, e^{-\left(p^2+\frac{1}{4}\right)t}, \qquad t > 0, \quad L \in \mathbb{R}, \tag{3.90}$$

resulting in the Fourier transform

$$\hat{h}(q) = \frac{e^{-\frac{t}{4}}}{4\sqrt{\pi t}} \left\{ e^{-\frac{(L-q)^2}{4t}} + e^{-\frac{(L+q)^2}{4t}} \right\}. \tag{3.91}$$

Inserting into (3.55) yields the trace of the *cosine-modulated heat kernel*

$$\begin{aligned} &\cosh\frac{L}{2} + \sum_{n=1}^{\infty} \cos(p_n\, L)\, e^{-\left(p_n^2+\frac{1}{4}\right)t} \\ =\; &\frac{A}{2\pi}\, e^{-\frac{t}{4}} \int_0^\infty \mathrm{d}p\, p\, \tanh(\pi p) \cos(pL)\, e^{-p^2 t} \\ &+ \frac{e^{-\frac{t}{4}}}{8\sqrt{\pi t}} \sum_{\{\gamma\}} \sum_{k=1}^{\infty} \frac{l_\gamma}{2\sinh(k l_\gamma/2)} \left\{ e^{-\frac{(L-kl_\gamma)^2}{4t}} + e^{-\frac{(L+kl_\gamma)^2}{4t}} \right\}, \end{aligned} \tag{3.92}$$

where the ground state energy level $E_0 = 0$ has been separated on the left-hand side. The periodic-orbit sum of the trace of the cosine-modulated heat kernel produces Gaussian peaks of width $\Delta L \sim 2\sqrt{2t}$ at the lengths l_γ of the closed geodesics on $\Gamma_{\mathrm{GW}}\backslash\mathcal{D}$, if the parameter L is varied for a fixed but small value of t. For any $t > 0$ the sums of (3.92) are absolutely convergent.

For numerical purposes, usually only a finite number of energy eigenvalues $0 \le E_n \le E_N$ is available, which can be used to evaluate the left-hand side of (3.92). The remaining part of the sum over energy eigenvalues can, however, be approximated by the following method. Remember that according to (3.68sqq) the average behavior of the spectral staircase $\mathcal{N}(E)$ is described by ($E = p^2 + \frac{1}{4}$)

$$\bar{\mathcal{N}}(E) = \frac{A}{2\pi} \int_0^p \mathrm{d}p'\, p'\, \bar{d}(p') = \frac{A}{2\pi} \int_0^p \mathrm{d}p'\, p' \tanh(\pi p'), \tag{3.93}$$

and therefore ($A = 4\pi$)

$$\sum_{n=N+1}^{\infty} \cos(p_n\, L)\, e^{-\left(p_n^2+\frac{1}{4}\right)t} \simeq \frac{A}{2\pi}\, e^{-\frac{t}{4}} \int_{p_N}^{\infty} \mathrm{d}p\, p\, \tanh(\pi p) \cos(pL)\, e^{-p^2 t}. \tag{3.94}$$

Thus, if on the left-hand side of the trace of the cosine-modulated heat kernel energy eigenvalues up to E_N are used, the upper limit of the zero-length term on the right-hand side will be set to p_N.

In fig. 16 the periodic-orbit sum of the trace of the cosine-modulated heat kernel of Gutzwiller's group Γ_{GW} is compared with the difference between the energy sum and the zero-length term of (3.92) for $t = 0.01$. Whereas the geodesic length spectrum was used up to $l_{\max} = l_{3815}$, the energy sum was evaluated from the first 200 quantal energies [4]. The value of the parameter t yields $\Delta L \simeq 0.28$, and as a result only the first three peaks correspond to single lengths of closed geodesics (compare table 1). The pronounced minima near 5.5 and 6.9 originate from exceptionally large intervals containing no lenghts of periodic orbits, whereas the minimum near 7.7 is produced by very low multiplicities of the corresponding lengths. For larger L the geodesic length spectrum becomes exponentially dense according to (3.39), and the trace of the cosine-modulated heat kernel shows a smooth behavior. In principle the resolution can be improved by a smaller choice of the parameter t, but since only a limited number of energy eigenvalues serves as input for the left-hand side of (3.92), oscillations of the trace of the cosine-modulated heat kernel arise, making it impossible to identify the Gaussian peaks of the periodic-orbit sum.

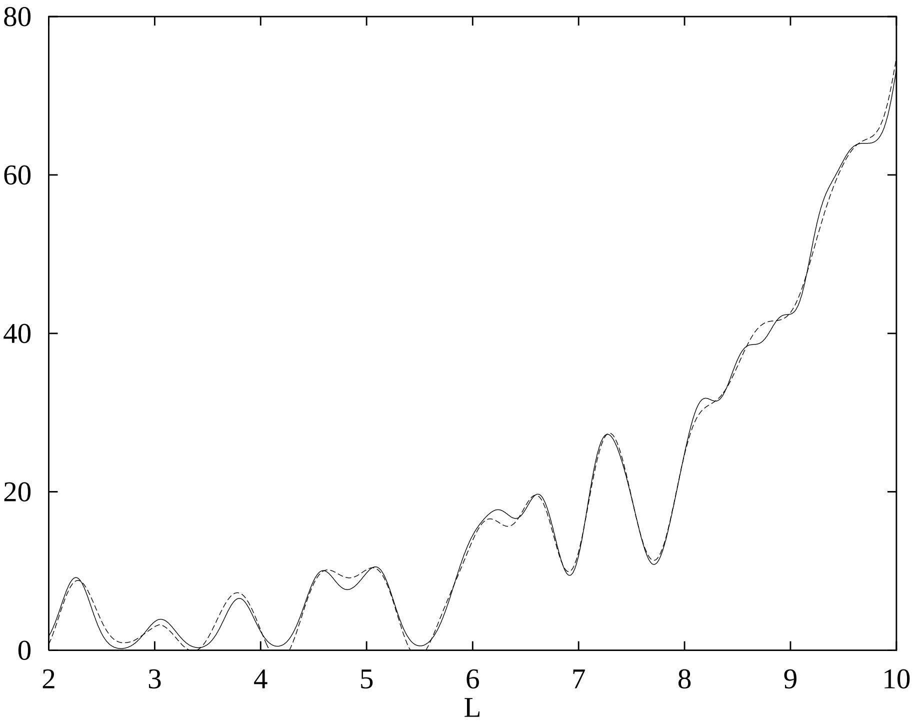

Figure 16: The periodic-orbit sum of the trace of the cosine-modulated heat kernel for Γ_{GW}, calculated by using the geodesic length spectrum (solid curve) and the energy spectrum (dashed curve). The parameter t has been chosen as $t = 0.01$.

The classical staircase function $N(l)$ can be derived from the trace of the cosine-modulated heat kernel by an integration of (3.92) [14]. For this purpose the operation

$$\int_{l_0}^{l} \mathrm{d}L \, \frac{4}{L} \sinh\left(\frac{L}{2}\right), \qquad 0 < l_0 < l_1 \leq l \tag{3.95}$$

is applied on both sides of (3.92). Here the lower limit of the integral has to be smaller than the length l_1 of the shortest closed geodesic on $\Gamma_{\mathrm{GW}} \backslash \mathcal{D}$. Performing the limit $t \to 0^+$ turns the

Gaussian peaks of the periodic-orbit sum into Dirac δ-functions (see (3.58)). Explicitly

$$\sum_{k=1}^{\kappa(l)} \frac{1}{k} \sum_{\{\gamma\}} \int_{l_0}^{l} \mathrm{d}L \, \frac{k l_\gamma}{L} \, \frac{\sinh \frac{L}{2}}{\sinh \frac{k l_\gamma}{2}} \, \delta(L - k l_\gamma) = \int_{l_0}^{l} \mathrm{d}L \, \frac{4 \sinh \frac{L}{2} \cosh \frac{L}{2}}{L}$$

$$+ \sum_{n=1}^{\infty} \int_{l_0}^{l} \mathrm{d}L \, \frac{4 \sinh \frac{L}{2} \cos(p_n L)}{L} + \int_{l_0}^{l} \mathrm{d}L \, \frac{4 \sinh \frac{L}{2}}{L} \, \frac{\cosh \frac{L}{2}}{2 \sinh^2 \frac{L}{2}}, \tag{3.96}$$

where $\kappa(l) := \left[\frac{l}{l_1}\right]$ is the maximum upper limit occuring in the sum over multiple traversals for closed geodesics of lengths shorter than l. The periodic-orbit sum can be related to the classical staircase function $N(l)$

$$\sum_{k=1}^{\kappa(l)} \frac{1}{k} \sum_{\{\gamma\}} \int_{l_0}^{l} \mathrm{d}L \, \delta(L - k l_\gamma) = \sum_{k=1}^{\kappa(l)} \frac{1}{k} \sum_{\{\gamma\}} \Theta\left(\frac{l}{k} - l_\gamma\right) = \sum_{k=1}^{\kappa(l)} \frac{1}{k} N\left(\frac{l}{k}\right), \tag{3.97}$$

whereas the right-hand side of (3.96), denoted as $F(l)$, yields

$$F(l) := \int_{l_0}^{l} \frac{\mathrm{d}L}{L} \left(e^{L} - e^{-L}\right) + 4 \sum_{n=1}^{\infty} \int_{l_0}^{l} \frac{\mathrm{d}L}{L} \sinh \frac{L}{2} \cos(p_n L) + 2 \int_{l_0}^{l} \frac{\mathrm{d}L}{L} \coth \frac{L}{2}, \tag{3.98}$$

thus

$$\sum_{k=1}^{\kappa(l)} \frac{1}{k} N\left(\frac{l}{k}\right) \; = \; F(l). \tag{3.99}$$

Using the Möbius inversion formula [36], equation (3.99) can be solved for $N(l)$

$$N(l) \; = \; \sum_{k=1}^{\kappa(l)} \frac{\mu(k)}{k} F\left(\frac{l}{k}\right), \tag{3.100}$$

where $\mu(k)$ denotes the Möbius function, defined to be $(-1)^n$ if k can be written as a product of n different primes, and zero if at least one prime number occurs twice ($\mu(1) := 1$).

Inserting the definition (2.34) of the exponential integral $\mathrm{Ei}(l)$ into (3.98) unravels the asymptotic behavior of the function $F(l)$

$$F(l) = \mathrm{Ei}(l) + \sum_{\{s_n\}} \mathrm{Ei}(s_n \, l) + 2 \log l + O(1), \tag{3.101}$$

where the sum over energy eigenvalues has been rewritten to run over all pairs $s_n = \frac{1}{2} \pm i p_n$, $p_n > 0$ of non-trivial zeros of Selberg's zeta function (3.79).

If the Ei-function in the sum over $\{s_n\}$ is approximated by its leading term

$$\mathrm{Ei}(l) \sim \frac{e^{l}}{l}, \qquad l \to \infty, \tag{3.102}$$

relation (3.100) finally leads to

$$N(l) = \mathrm{Ei}(l) - \frac{e^{\frac{l}{2}}}{l} + 2 \, \frac{e^{\frac{l}{2}}}{l} \sum_{n=1}^{\infty} \frac{\cos(\, p_n \, l - \arctan(2 p_n)\,)}{\sqrt{E_n}} + \cdots. \tag{3.103}$$

Evaluating (3.103) by using the first 200 energy eigenvalues of the dynamical system associated to Γ_{GW} only smoothly approximates the classical staircase function $N(l)$. The general growing behavior of $N(l)$, however, is reproduced, again suggesting the completeness of the geodesic length spectrum calculated in section 3.2.

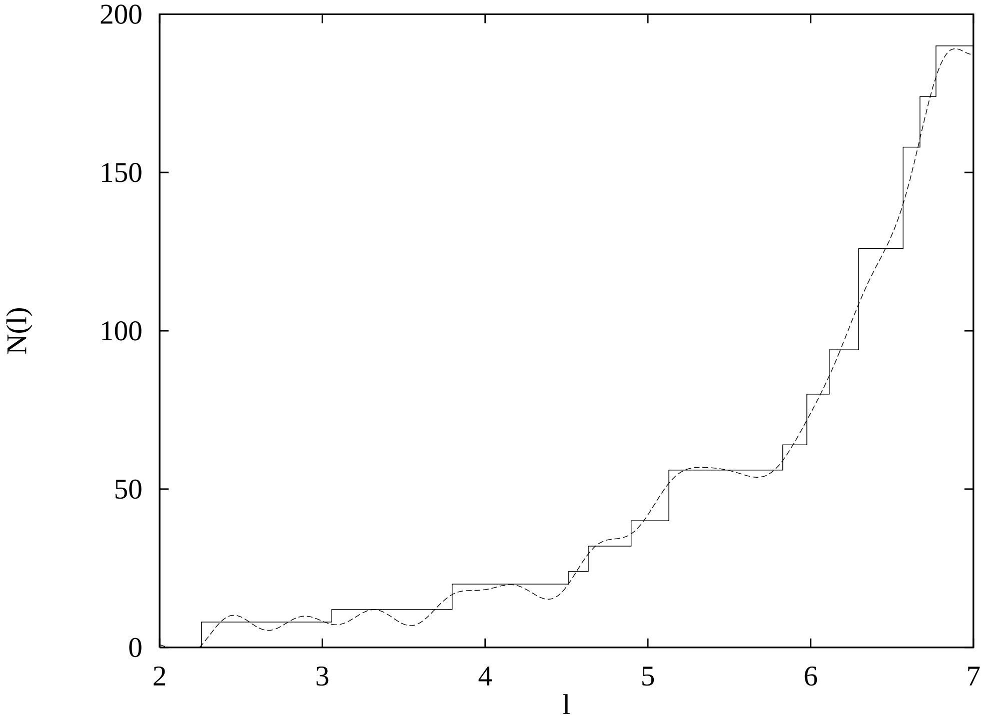

Figure 17: The classical staircase function $N(l)$ of $\Gamma_{\rm GW}$ (solid curve) is compared with the approximation (3.103) obtained from the first 200 energy eigenvalues (dashed curve).

4 The Triangular Billiard $T^*(2,3,8)$

As already mentioned in the previous chapter, the Riemann surface $\Gamma_{\mathrm{reg}}\backslash\mathcal{D}$ can be isometrically mapped onto itself by the operation of a symmetry group $\mathcal{S}$ of order 96. The regular octagon group Γ_{reg} is thus a normal subgroup of a particular reflection group, which turns out to be the triangular group $T^*(2,3,8)$. In this chapter the dynamical system associated to $T^*(2,3,8)$, i.e., a free particle moving inside a hyperbolic triangle with inner angles $\frac{\pi}{2}, \frac{\pi}{3}$ and $\frac{\pi}{8}$, will be investigated.

In the context of the quantization of classical chaotic systems, this system possesses some interesting features.

On the one hand, due to the small area of the fundamental domain of $T^*(2,3,8)$, the efficiency of the periodic-orbit theory is improved in comparison to the investigation of Γ_{reg}. Thus the interplay between the geodesic length spectrum and the spectrum of energy eigenvalues can be observed in more detail.

On the other hand, depending on the choice of boundary conditions of the hyperbolic triangle under consideration, the energy spectrum of the quantized system shows quite different statistical properties. Remember, that the orbit space $\Gamma_{\mathrm{GW}}\backslash\mathcal{D}$ of Gutzwiller's group, as discussed in the previous chapter, has no boundary. This is a consequence of the fact, that Γ_{GW} is a strictly hyperbolic Fuchsian group, resulting in a fundamental domain with periodic boundary conditions. The dynamical system corresponding to a reflection group, however, can be seen from the physical point of view as a particle moving inside a domain bounded by hard walls. During the quantization procedure of the triangular billiard $T^*(2,3,8)$ thus eight different systems arise, according to the choice of Dirichlet or Neumann boundary conditions along the edges of the fundamental domain, each having the same spectrum of periodic geodesics.

The outline of this chapter will be as follows. After a discussion of the hyperbolic triangle group $T^*(2,3,8)$ itself, the geodesic length spectrum will be investigated. Subsequently, a Selberg trace formula, taking into account the additional kinds of group elements arising in $T^*(2,3,8)$ with mixed boundary conditions, will be derived. However, only four of the eight possible choices of boundary conditions are subject to Selberg's trace formula. The remaining four lead to the investigation of particular non-periodic orbits in the fundamental domain of $T^*(2,3,8)$. By use of Selberg's trace formula, the connection between geodesic lengths and quantal energies will be studied in analogy to the treatment described in the context of Γ_{GW}.

4.1 Properties of the Group $T^*(2,3,8)$

According to (2.22), the hyperbolic triangle group $T^*(2,3,8)$ is generated by elements L, M, N, representing inversions across the edges of the fundamental domain $\mathcal{T}$ (cf. fig. 18). They are subject to the group relations

$$L^2 = M^2 = N^2 = \mathbf{1}, \qquad (LM)^2 = (MN)^3 = (NL)^8 = \mathbf{1}. \tag{4.1}$$

It is no difficult to show, that LM, MN, NL are the only primitive elliptic elements of $T^*(2,3,8)$, having fixed points exactly on the vertices Q, P, O of the fundamental domain $\mathcal{T}$.

Some general relations exist [42], describing the coordinates of a hyperbolic triangle in the Poincaré disk with inner angles $\varphi, \frac{\pi}{2}$ and ψ obeying $\varphi + \psi < \frac{\pi}{2}$. Denoting the coordinates of

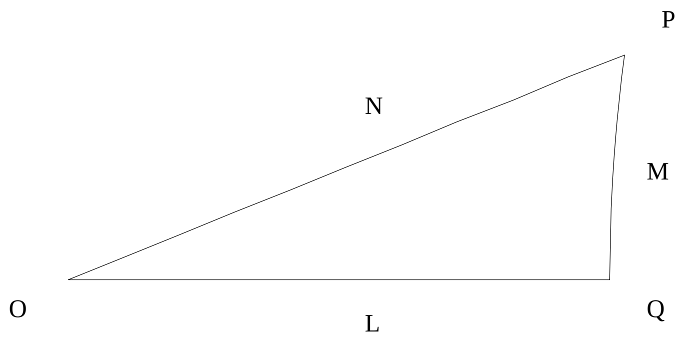

Figure 18: The fundamental domain of $T^*(2,3,8)$.

the vertices with angles φ, $\frac{\pi}{2}$ and ψ as

$$z_O = 0, \quad z_Q = x_Q, \quad z_P = x_P + iy_P, \tag{4.2}$$

respectively, one finds

$$\begin{aligned} x_Q &= \frac{\cos\psi - \sin\varphi}{\rho}, \qquad \rho := \sqrt{\cos^2\psi - \sin^2\varphi}, \\ x_P &= \frac{\cos\varphi\,\cos(\varphi+\psi)}{\rho}, \qquad y_P = \frac{\sin\varphi\,\cos(\varphi+\psi)}{\rho}. \end{aligned} \tag{4.3}$$

The side OQ is part of the real axis, whereas the side OP is the straight euclidian line joining O and P. The side QP is part of a circle with radius r, centered at $z_c = x_c$, where

$$r = \frac{\sin\varphi}{\rho}, \qquad x_c = \frac{\cos\psi}{\rho}. \tag{4.4}$$

Introducing

$$\beta := \sqrt{\sqrt{2}}, \qquad \gamma := \sqrt{2-\sqrt{2}}, \tag{4.5}$$

which will be used throughout this chapter in addition to α defined in (3.3), the particular case of $T^*(2,3,8)$ results in

$$\begin{aligned} z_Q = \frac{1-\gamma}{\alpha}, \qquad z_P = \frac{1+\sqrt{2}-\sqrt{3}}{4\alpha}\left(\sqrt{2}+i(2-\sqrt{2})\right), \\ z_c = \frac{1}{\alpha}, \qquad r = \frac{\gamma}{\alpha}. \end{aligned} \tag{4.6}$$

The hyperbolic lengths of the edges OQ, QP, OP can be determined to be $l_L = 0.7642\ldots$, $l_M = 0.3635\ldots$ and $l_N = 0.8607\ldots$, respectively. The area of the fundamental domain $\mathcal{T}$ turns out to be $\mathrm{area}(T^*(2,3,8)\backslash\mathcal{D}) = \frac{\pi}{24}$. Under the action of the generators L, M and N, the Poincaré disk is tessellated by copies of $\mathcal{T}$. Exactly 96 copies fit into the regular octagon.

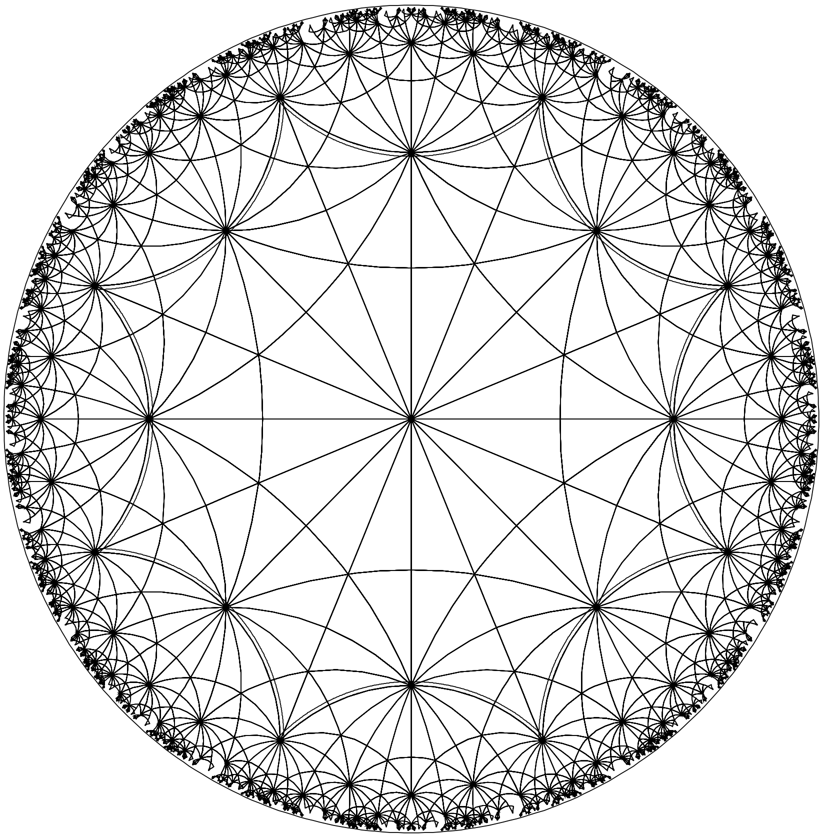

Figure 19: The fundamental domain of $T^*(2,3,8)$ tessellating the Poincaré disk. The regular octagon is indicated by the double lines.

According to (4.1) the inversions M and N belong to the same conjugacy class

$$N = (MN) \cdot M \cdot (NM) = (MN) \cdot M \cdot (MN)^{-1}. \tag{4.7}$$

Geometrically, this can be seen from the tessellation picture fig. 19. The invariant axis of M can be mapped onto the invariant axis of N by a rotation around the vertex P of the fundamental domain $\mathcal{T}$. This feature always arises for inversions across edges adjacent to a vertex with angle

$$\phi = \frac{\pi}{2n-1}, \qquad n \in \mathbb{N}, \tag{4.8}$$

since in that case the associated elliptic element is of odd order.

By this peculiarity the eight quantum-mechanical systems associated to $T^*(2,3,8)$ are divided into two classes. Namely, only if the boundary conditions along the invariant axes of M and N are chosen to be equivalent, representations of $T^*(2,3,8)$ can be found. Only the quantal energy spectra of these four triangular billiards are contained in the energy spectrum of the dynamical system associated to the regular octagon group $\Gamma_{\rm reg}$, and as has been pointed out in [5, 48, 10], their spectral statistics are in accordance with the behavior expected for arithmetically chaotic systems. The remaining four combinations, i.e., different boundary conditions along the edges M and N, lead to spectral statistics obeying random-matrix theory [27, 46]. Since the classical dynamical system is generated by an arithmetic group nevertheless, the latter are referred to as *pseudoarithmetical*.

Furthermore, Gutzwiller's semiclassical periodic-orbit theory turns out to be exact only in those cases, where representations of $T^*(2,3,8)$ can be found, because only in that case a Selberg trace formula can be derived from the properties of the group. In the pseudoarithmetical case, particular non-periodic orbits arise on the classical side of Gutzwiller's trace formula (cf. section 4.6).

Starting with the fundamental domain of $T^*(2,3,8)$ on the Poincaré disk $\mathcal{D}$, the matrix representations of the corresponding generators L, M, N can be easily determined by use of (4.6)

$$\begin{aligned} L &= \begin{pmatrix} 1 & 0 \\ 0 & 1 \end{pmatrix} K, \\ M &= \begin{pmatrix} i\left(1+\frac{\sqrt{2}}{2}\right)\gamma & -i\frac{\sqrt{2}}{2}\beta \\ i\frac{\sqrt{2}}{2}\beta & -i\left(1+\frac{\sqrt{2}}{2}\right)\gamma \end{pmatrix} K, \\ N &= \begin{pmatrix} \left(\frac{1+\sqrt{2}}{2}+\frac{i}{2}\right)\gamma & 0 \\ 0 & \left(\frac{1+\sqrt{2}}{2}-\frac{i}{2}\right)\gamma \end{pmatrix} K. \end{aligned} \tag{4.9}$$

Remember, that in contrary to Gutzwiller's group $\Gamma_{\rm GW}$, the reflection group $T^*(2,3,8)$ also contains orientation-reversing isometries of $(\mathcal{D}, {\rm d}s^2)$, which are accounted for by introducing the operator K of complex conjugation (cf. (2.9sqq)). Thus elements $\gamma \in T^*(2,3,8)$ being the product of an odd number of generators can be identified by the presence of the complex conjugation K.

For numerical purposes it is convenient to use the matrix representations of L, M, N on the complex upper half-plane $\mathcal{H}$, since they can be chosen to have real entries. The distinction between orientation-preserving and orientation-reversing isometries is then established by the choice of the determinant $\det\gamma = \pm 1$ of an element of $T^*(2,3,8)$. A possible set of matrix representations is [22]

$$\begin{aligned} L_{\mathcal{H}} &= \begin{pmatrix} 1 & 0 \\ 0 & -1 \end{pmatrix}, \\ M_{\mathcal{H}} &= \begin{pmatrix} 0 & 1 \\ 1 & 0 \end{pmatrix}, \\ N_{\mathcal{H}} &= \begin{pmatrix} -\frac{1}{2}\left(1+\sqrt{2}\right)\gamma & \frac{1}{2}(1+\alpha) \\ \frac{1}{2}(1-\alpha) & \frac{1}{2}\left(1+\sqrt{2}\right)\gamma \end{pmatrix}. \end{aligned} \tag{4.10}$$

An algorithm generating all group elements of $T^*(2,3,8)$ has to take properly into account the group relations (4.1), in order to avoid a double counting of words. Among all sequences consisting of the generators L, M, N one would thus define those containing LL, MM, NN, ML, NMN and $(LN)^4$ to be forbidden, since these words can be rewritten in terms of admissible ones by use of (4.1). Besides the "canonical" generators L, M, N obeying six relations, there exist, however, simpler choices. Namely, $T^*(2,3,8)$ can be generated by two elements only

$$U := LMN, \qquad V = LN, \tag{4.11}$$

since

$$L = UV^6U^2V^6, \qquad M = UV^7, \qquad N = V^7UV^6U^2V^6. \tag{4.12}$$

The group relations, the generators U and V have to fulfill, can be determined to be

$$V^8 = (UV^7)^2 = (U^2V^5)^2 = (U^3V^6)^2 = \mathbf{1}. \tag{4.13}$$

Unfortunately it is impossible to decide, if a given set of group relations represents the simplest possible choice [43]. For the special case of the hyperbolic triangle group $T^*(2,3,8)$ it is, however, pointed out in [22], that the elements

$$A := U, \qquad B := VU, \qquad C := V^2U, \tag{4.14}$$

subject to the only grammar rule forbidding CA, actually generate $T^*(2,3,8)$ besides some non-primitive elements corresponding to multiple traversals of the boundary orbits, running along the edges of the fundamental domain $\mathcal{T}$. Since in this work emphasis is laid on the investigation of the *primitive* geodesic length spectrum of $T^*(2,3,8)$, the generators A, B, C will be the most preferable choice in the following.

As already mentioned above, the hyperbolic triangle group $T^*(2,3,8)$ belongs to the class of arithmetic groups. It is worthwhile to mention, that only finitely many arithmetic triangle groups do exist (see [54], which also contains a complete list of these cases). The arithmetical properties of $T^*(2,3,8)$ are reflected in the possibility to characterize arbitrary elements $\gamma \in T^*(2,3,8)$ explicitly, in analogy to the case of Gutzwiller's group. Again, only results will be presented. For details see appendix B.

At first one observes, that for an arbitrary group element of $T^*(2,3,8)$, given by a 2×2 matrix possibly preceded by the operator K of complex conjugation acting on points z of the Poincaré disk, the (left-)multiplication by the generator L does not affect the arithmetical properties of the matrix entries. It merely interchanges between the classes of orientation-preserving and orientation-reversing transformations and changes the signs of the imaginary parts. Thus only the case of orientation-preserving group elements need to be discussed explicitly.

Among these, two different kinds of matrices $\gamma_1, \gamma_2 \in T^*(2,3,8)$ can be distinguished

$$\begin{aligned}
\gamma_1 &= \begin{pmatrix} \frac{1}{2}(u_{1,R} + iu_{1,I}) & \frac{1}{2}(v_{1,R} + iv_{1,I})\,\alpha \\ \frac{1}{2}(v_{1,R} - iv_{1,I})\,\alpha & \frac{1}{2}(u_{1,R} - iu_{1,I}) \end{pmatrix}, \\
\gamma_2 &= \begin{pmatrix} \frac{1}{2}(u_{2,R} + iu_{2,I})\,\gamma & \frac{1}{2}(v_{2,R} + iv_{2,I})\,\beta \\ \frac{1}{2}(v_{2,R} - iv_{2,I})\,\beta & \frac{1}{2}(u_{2,R} - iu_{2,I})\,\gamma \end{pmatrix},
\end{aligned} \tag{4.15}$$

where the matrix entries are algebraic numbers of the form $(k = 1, 2)$

$$\begin{aligned}
u_{k,R} &= m_{k,R} + n_{k,R}\sqrt{2}, \quad u_{k,I} = m_{k,I} + n_{k,I}\sqrt{2}, \\
v_{k,R} &= p_{k,R} + q_{k,R}\sqrt{2}, \quad\;\, v_{k,I} = p_{k,I} + q_{k,I}\sqrt{2}.
\end{aligned} \tag{4.16}$$

In the first case, the matrix entries are subject to

$$\begin{array}{ll} |\tilde{u}_{1,R}| < 2, & |\tilde{u}_{1,I}| < 2, \\ |\tilde{v}_{1,R}| < 2\alpha, & |\tilde{v}_{1,I}| < 2\alpha, \end{array} \tag{4.17}$$

and their parities are restricted by

$$\begin{gathered} \pi(m_{1,R}) = \pi(m_{1,I}) = \pi(p_{1,R}) = \pi(p_{1,I}), \\ \pi(m_{1,R}) = \begin{cases} 0 & \Rightarrow \quad \pi(n_{1,R}) = \pi(n_{1,I}) \\ 1 & \Rightarrow \quad \pi(n_{1,R}) \neq \pi(n_{1,I}) \end{cases}, \\ \pi(p_{1,R}) = \begin{cases} 0 & \Rightarrow \quad \pi(q_{1,R}) = \pi(q_{1,I}) \\ 1 & \Rightarrow \quad \pi(q_{1,R}) \neq \pi(q_{1,I}) \end{cases}, \end{gathered} \tag{4.18}$$

whereas the second case yields

$$\begin{array}{ll} |\tilde{u}_{2,R}| < \sqrt{2}\,\gamma, & |\tilde{u}_{2,I}| < \sqrt{2}\,\gamma, \\ |\tilde{v}_{2,R}| < \sqrt{2}\,\beta, & |\tilde{v}_{2,I}| < \sqrt{2}\,\beta, \end{array} \tag{4.19}$$

and

$$\pi(m_{1,R}) = \pi(m_{1,I}), \qquad \pi(p_{1,R}) = \pi(p_{1,I}). \tag{4.20}$$

All group elements of $T^*(2,3,8)$ obey the relations (4.15sqq). The discussion in the following section will suggest, however, that some additional rules seem to be hidden in the algebraic structure of $T^*(2,3,8)$. For the calculation of the geodesic length spectrum, therefore, a method will be chosen, which is different from the one used in the context of Gutzwiller's group Γ_{GW}. It is based on building valid products of the abstract generators (4.14) and properly choosing a single representative for each conjugacy class.

4.2 The Length Spectrum

Before calculating the geodesic length spectrum of $T^*(2,3,8)$ itself, an approximation for the average multiplicity $< g(l) >$ will be derived from the algebraic decompositions of (4.15). Remember, that the matrices (4.15) represent (possible) group elements of $T^*(2,3,8)$ acting on the Poincaré disk $\mathcal{D}$. Thus the length of a closed geodesic on $T^*(2,3,8)\backslash\mathcal{D}$, associated to a *hyperbolic* conjugacy class, is given by the same relation (2.28) as derived for matrices acting on the complex upper half-plane $\mathcal{H}$. The lengths of closed geodesics, corresponding to *inverse hyperbolic* conjugacy classes $[\rho]$, however, are determined by the sum of the off-diagonal entries of the matrix representations

$$2\,\sinh\frac{l}{2} = \operatorname{atr}\rho, \tag{4.21}$$

with a representative ρ chosen according to $\operatorname{atr}\rho > 0$.

In the hyperbolic triangle group $T^*(2,3,8)$, therefore, four different kinds of geodesic lengths arise, according to two different types of matrices $\gamma_1, \gamma_2 \in T^*(2,3,8)$ and the distinction between elements being the product of an even or an odd number of generators, i.e., hyperbolic or inverse hyperbolic elements

$$\begin{array}{ll} 2\,\cosh\dfrac{l_e^{(1)}}{2} = m_{1,R} + n_{1,R}\sqrt{2}, & 2\,\cosh\dfrac{l_e^{(2)}}{2} = (m_{2,R} + n_{2,R}\sqrt{2})\,\gamma, \\ 2\,\sinh\dfrac{l_o^{(1)}}{2} = (p_{1,R} + q_{1,R}\sqrt{2})\,\alpha, & 2\,\sinh\dfrac{l_o^{(2)}}{2} = (p_{2,R} + q_{2,R}\sqrt{2})\,\beta. \end{array} \tag{4.22}$$

The right-hand sides of these equations are subject to the restrictions (4.17) and (4.19). Assuming generally an algebraic number to be restricted by

$$|m - n\sqrt{2}| < \delta, \qquad m, n \in \mathbb{Z}, \tag{4.23}$$

then for a fixed value of $n > \frac{\delta}{\sqrt{2}}$ the integer number m is contained in the interval

$$n\sqrt{2} - \delta < m < n\sqrt{2} + \delta, \tag{4.24}$$

of width 2δ, bounded by irrational numbers. Thus one can expect, that for a large number of different values of integers n, to each n there are associated an average value of 2δ different integers m. The counting function for distinct geodesic lengths in $T^*(2,3,8)$ therefore results in

$$\hat{N}(l) \sim 4n_{1,R} + 2\sqrt{2}\gamma\, n_{2,R} + 4\alpha\, q_{1,R} + 2\sqrt{2}\beta\, q_{2,R}, \qquad l \to \infty \tag{4.25}$$

if all kinds of lengths are taken into account up to the same order of magnitude,

$$l \sim l_e^{(1)}, \quad n_{2,R} \sim \frac{n_{1,R}}{\gamma}, \quad q_{1,R} \sim \frac{n_{1,R}}{\alpha}, \quad q_{2,R} \sim \frac{n_{1,R}}{\beta}, \tag{4.26}$$

i.e.,

$$\hat{N}(l) \sim (8 + 4\sqrt{2})n_{1,R}, \qquad l \to \infty. \tag{4.27}$$

Using

$$2\,\cosh\frac{l}{2} \sim 2\,\sinh\frac{l}{2} \sim e^{\frac{l}{2}}, \qquad l \to \infty, \tag{4.28}$$

leads to

$$e^{\frac{l_e^{(1)}}{2}} \sim 2\sqrt{2}\, n_{1,R}, \qquad l \to \infty, \tag{4.29}$$

by (4.22), finally revealing

$$\hat{N}(l) \sim 2\,(1 + \sqrt{2})\, e^{\frac{l}{2}}, \qquad l \to \infty. \tag{4.30}$$

Huber's law and relation (2.36) then offer the average multiplicity of the geodesic length spectrum of $T^*(2,3,8)$ as derived from (4.15)

$$< g(l) > \sim \frac{e^l}{l}\left(\frac{\mathrm{d}\hat{N}}{\mathrm{d}l}\right)^{-1} \sim (\sqrt{2} - 1)\,\frac{e^{\frac{l}{2}}}{l}, \qquad l \to \infty. \tag{4.31}$$

The primitive geodesic length spectrum of $T^*(2,3,8)$ has been investigated numerically by building group elements as products of the generators A, B, C given in (4.14), obeying the grammar rule forbidding CA. However, closed geodesics of $T^*(2,3,8)\backslash\mathcal{D}$ correspond to conjugacy classes of hyperbolic or inverse hyperbolic elements of $T^*(2,3,8)$, thus an algorithm has to be found, which separates a unique representative for each conjugacy class. This can be accomplished as follows.

(i) At first, all words γ consisting of the letters A, B, C are constructed, which do not contain the sequence CA.

(ii) Then the word γ, consisting of n letters, is permuted cyclically. This operation corresponds to a conjugation of γ in $T^*(2,3,8)$. If among the resulting $\gamma^{(k)}$, $k = 1, \cdots n-1$ there is one, which equals the starting word, i.e., $\gamma^{(\nu)} = \gamma$, a representative of a conjugacy class associated to a multiple traversal of a closed geodesic has been found, if γ was a hyperbolic or inverse hyperbolic element. For the investigation of the primitive geodesic length spectrum, thus, γ has to be dropped.

(iii) If all of the cyclical permutations $\gamma^{(k)}$, $k = 1, \cdots n-1$ are different from γ, but one $\gamma^{(\nu)}$ contains the forbidden sequence CA, the word γ is dropped to avoid double countings. Namely, $\gamma^{(\nu)}$ represents a conjugacy class associated to a word, which can be constructed as a valid word by using the group relations.

(iv) For the next step a lexicographical ordering is introduced among the words γ in the obvious way. If none of the cyclical permutations $\gamma^{(k)}$, $k = 1, \cdots n-1$ contains the forbidden sequence CA, but one $\gamma^{(\nu)}$ is lexicographically smaller than γ, the word γ is dropped, too. The sequence $\gamma^{(\nu)}$ will in that case arise as a starting word in step (i). This step ensures, that for each conjugacy class a unique representative is selected, which is chosen to be the lexicographically smallest one.

(v) If a valid (unique) representative γ for a conjugacy class of $T^*(2,3,8)$ has been found by the above procedure, the matrix representation of γ is determined. It can then be checked, if γ represents a hyperbolic or inverse hyperbolic element. If yes, a primitive periodic geodesic on $T^*(2,3,8)\backslash\mathcal{D}$ has been found.

In a quantized version of the triangular billiard $T^*(2,3,8)$ the boundary conditions along the edges of the fundamental domain have to be taken into account. According to Neumann or Dirichlet boundary conditions along a particular edge, a wavefunction on $T^*(2,3,8)\backslash\mathcal{D}$ has to be symmetric or antisymmetric, respectively, under inversion across that edge. In the group-theoretical setting above, this can be incorporated by introducing a multiplicative character χ for automorphic forms of weight m, subject to [37]

$$\begin{aligned} &|\,\chi(\gamma)\,| = 1, \\ &\chi(\gamma_1\,\gamma_2) = \chi(\gamma_1)\,\chi(\gamma_2), \\ &\chi(-\mathbf{1}) = e^{-i\pi m}, \end{aligned} \tag{4.32}$$

where $\gamma_1, \gamma_2 \in T^*(2,3,8)$. The character χ establishes a one-dimensional unitary representation of $T^*(2,3,8)$. If, e.g., the boundary conditions of the fundamental domain of $T^*(2,3,8)$ are chosen to be Dirichlet along the edge L and Neumann along the edges M and N, which will be referred to as the "dnn-case" in the future discussion, one defines

$$\chi(L) = -1, \qquad \chi(M) = +1, \qquad \chi(N) = +1, \tag{4.33}$$

to ensure the correct transformation behavior (2.41) of the wave functions ψ. For an arbitrary group element γ, the character can be determined by its representation as a product of the generators L, M, N and the second relation of (4.32). For any γ' belonging to the same conjugacy class as γ, one obviously finds $\chi(\gamma') = \chi(\gamma)$. Thus the character χ is an invariant of a closed geodesic on $T^*(2,3,8)\backslash\mathcal{D}$.

According to (4.7) the inversions across the edges M and N of the fundamental domain of $T^*(2,3,8)$ are members of the same conjugacy class, i.e., they share the same character

$$\chi(M) = \chi(N). \tag{4.34}$$

Thus one-dimensional unitary representations of $T^*(2,3,8)$, compatible with a set of boundary conditions of the fundamental domain, can be constructed only if the boundary conditions along the edges M and N are chosen to be equivalent. Only for this case a Selberg trace formula can be derived, which relates the quantal energy spectrum to the set of primitive conjugacy classes of $T^*(2,3,8)$ (cf. section 4.3). In the pseudoarithmetical case, i.e., different boundary conditions along the edges M and N, Selberg's trace formula can be interpreted as part of a semiclassical approximation along the lines of Gutzwiller's periodic-orbit theory. However, on the one hand, additional contributions may be present on the classical side of Gutzwiller's trace formula (cf. section 4.6). On the other hand, the quantal energy spectrum is then a priori *not* related to a sum over primitive conjugacy classes of $T^*(2,3,8)$ anymore. It turns into a sum running merely over lengths of primitive closed geodesics on $T^*(2,3,8)\backslash\mathcal{D}$, besides the contribution from the area, the boundary and the vertices of the fundamental domain.

In the special case of the hyperbolic triangle group $T^*(2,3,8)$, however, for each of the eight quantum mechanical systems, the underlying classical dynamical system is the same. Thus the closed geodesics on $T^*(2,3,8)\backslash\mathcal{D}$ can be constructed by group-theoretical methods nevertheless. Only the determination of the characters entering Gutzwiller's trace formula in the pseudoarithmetical case deserves a special treatment, described in the following.

By the algorithm defined above, for each closed geodesic on $T^*(2,3,8)\backslash\mathcal{D}$ a representative γ of its associated conjugacy class $[\gamma]$ is determined. There is, however, no reason why the invariant geodesic of γ on $\mathcal{D}$ should intersect the fundamental domain $\mathcal{T}$ (4.6) of $T^*(2,3,8)$. Thus repeated conjugation of γ by the group generators L, M, N is used to find a representative γ' of $[\gamma]$, which has an invariant geodesic hitting $\mathcal{T}$. The matrix γ' then represents a segment of the closed geodesic associated to $[\gamma]$. The full closed geodesic will be constructed by "following" the segment beyond the borders of the fundamental domain $\mathcal{T}$, in the same way as discussed in the context of Gutzwiller's group Γ_{GW} (cf. p. 27). As a result, the matrix γ' can be written as a product of generators L, M, N, each representing a "physical" reflection across the corresponding edge

$$\gamma' = c_{\nu_1}\, c_{\nu_2}\, \cdots c_{\nu_n}, \qquad c_\nu \in \{L, M, N\}. \tag{4.35}$$

The character $\chi(\gamma')$, which enters Gutzwiller's trace formula, is then calculated as the product

$$\chi(\gamma') = \chi(c_{\nu_1})\, \chi(c_{\nu_2})\, \cdots \chi(c_{\nu_n}). \tag{4.36}$$

Numerically, the geodesic length spectrum of $T^*(2,3,8)$ has been determined by taking into account products of the generators A, B, C, consisting of at most 22 factors. Totally, 118976317 conjugacy classes arose, and the computed geodesic lengths covered the range from $l_1 = 0.632974\ldots$ to $l_{\mathrm{max}} = 31.269816\ldots$. Comparing with Huber's law (2.33), however, reveals that the computed length spectrum is far from being complete up to l_{max}. At $l \simeq 18$ already $\sim 3\%$ of the periodic orbits are missing (fig. 20 and fig. 21). Thus only the geodesic lengths covering the range $l_1 \leq l \leq 18$, amounting to 3746841 conjugacy classes, will be used in the discussion of the quantized system in section 3.4. The missing of conjugacy classes towards higher lengths can be understood by considering the distribution of geodesic lengths among group elements being the product of a fixed number of generators (fig. 22). The distribution shows a Gaussian shape, and long words can be observed to contribute to comparatively small geodesic lengths. The shortest length associated to a conjugacy class generated by a word consisting of 22 letters e.g., turns out to be $l_{\min}^{(22)} = 14.116210\ldots$.

The first 40 different (primitive) lengths of $T^*(2,3,8)$ are listed in table 4. Since not the characters χ itself, but merely the *effective multiplicities*

$$g_\chi(l) := \sum_{\substack{\{\gamma\}\\ l_\gamma = l}} \chi(\gamma) \tag{4.37}$$

enter Selberg's or Gutzwiller's trace formula, the latter are listed for all combinations of boundary conditions. Not contained in table 4 are the periodic orbits running exactly on the boundary of the fundamental domain $\mathcal{T}$. There are in total two of them. The first, being of length $1.528570\ldots$, runs along the edge L and is then reflected backwards. Since it is invariant under inversion by L, it is associated to a hyperbolic and an inverse hyperbolic conjugacy class, i.e., twofold degenerated. The second, being of length $2.448452\ldots$, runs along the edge N beyond the vertex of angle $\frac{\pi}{3}$, then along the edge M, and is finally reflected backwards. This boundary orbit is twofold degenerated, too. The peculiarity of passing a vertex is due to the fact, that the inversions across the adjacent edges belong to the same conjugacy class (cf. 4.7sqq).

Translating words consisting of the generators A, B, C to a representation using L, M, N by (4.14) shows, that a maximal wordlength of 22 for the set A, B, C corresponds to a maximal wordlength of 152 for the set L, M, N, since the longest word is produced by the sequence BC^{21}. Thus the periodic orbits generated above, may bounce the edges of the fundamental domain $\mathcal{T}$ at most 152 times. A few examples of closed geodesics inside $\mathcal{T}$ are given in fig. 24.

Finally, the counting function $\hat{N}(l)$ for different lengths is compared with the theoretical prediction (4.30), derived from the algebraic decomposition of matrices in $T^*(2,3,8)$ (fig. 23). Since the difference at $l \sim 18$ is larger ($\sim 5\%$) than for the counting function $N(l)$ of closed geodesics, it seems, that the theoretical prediction is somewhat too large, due to the presence of additional algebraical restrictions of the group elements. However, it may be, that the asymptotic regime for the validity of the assumption (4.23sqq) is not reached within the considered range of lengths.

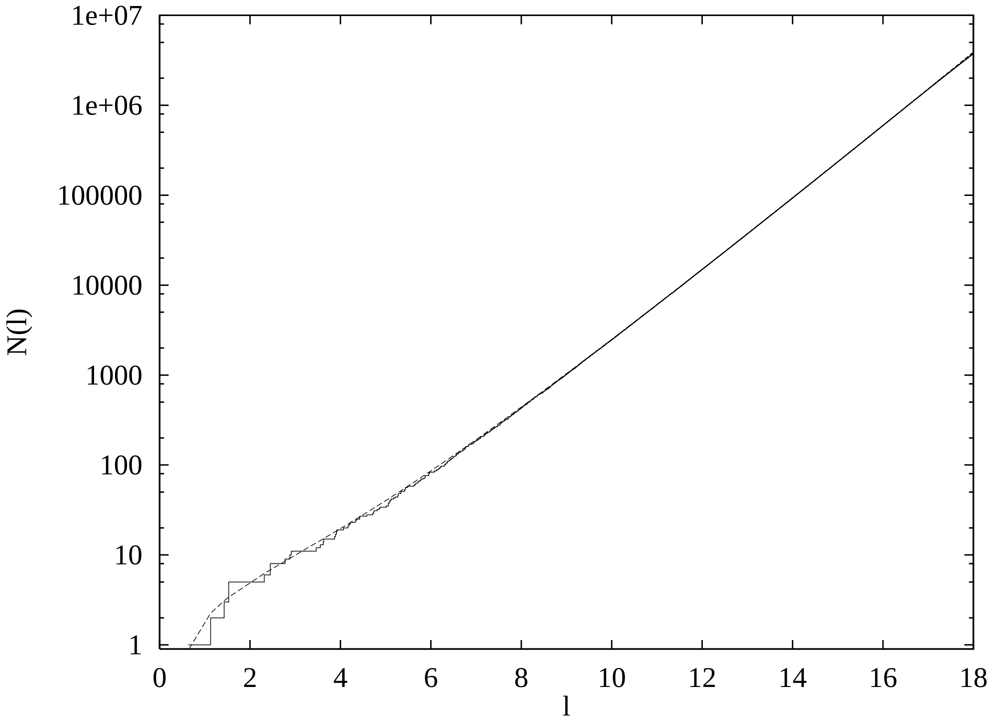

Figure 20: The classical staircase $N(l)$ of $T^*(2,3,8)$ is shown in comparison with Huber's law $N(l) \sim \mathrm{Ei}(l)$, $l \to \infty$.

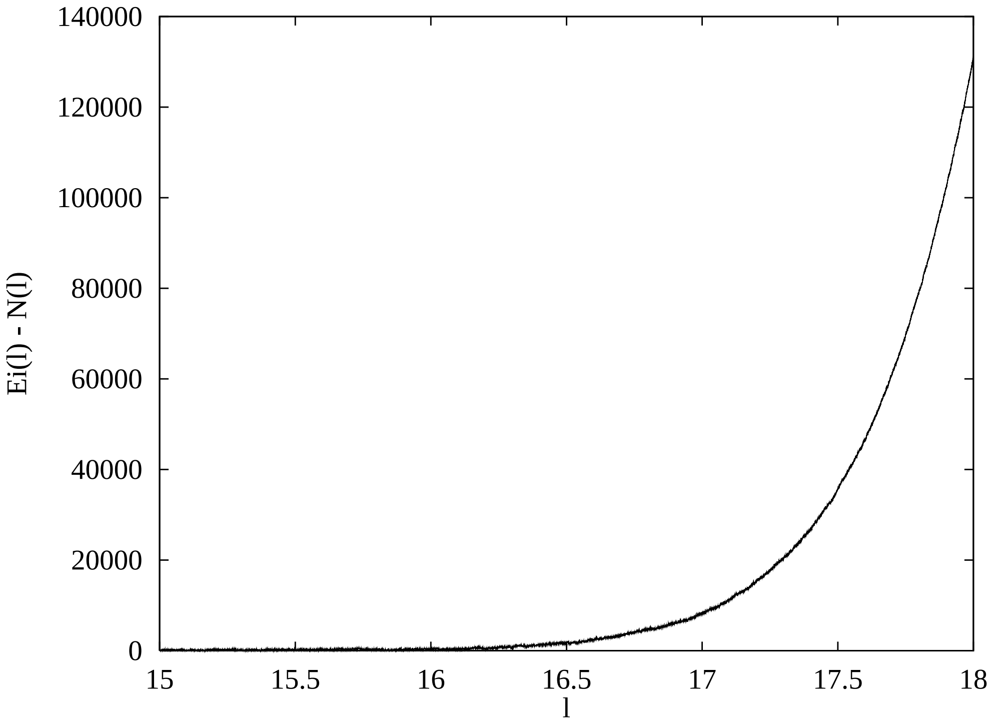

Figure 21: The difference between Huber's law and the classical staircase, i.e., $\mathrm{Ei}(l) - N(l)$ is plotted using a linear scale, revealing the missing conjugacy classes towards longer orbits.

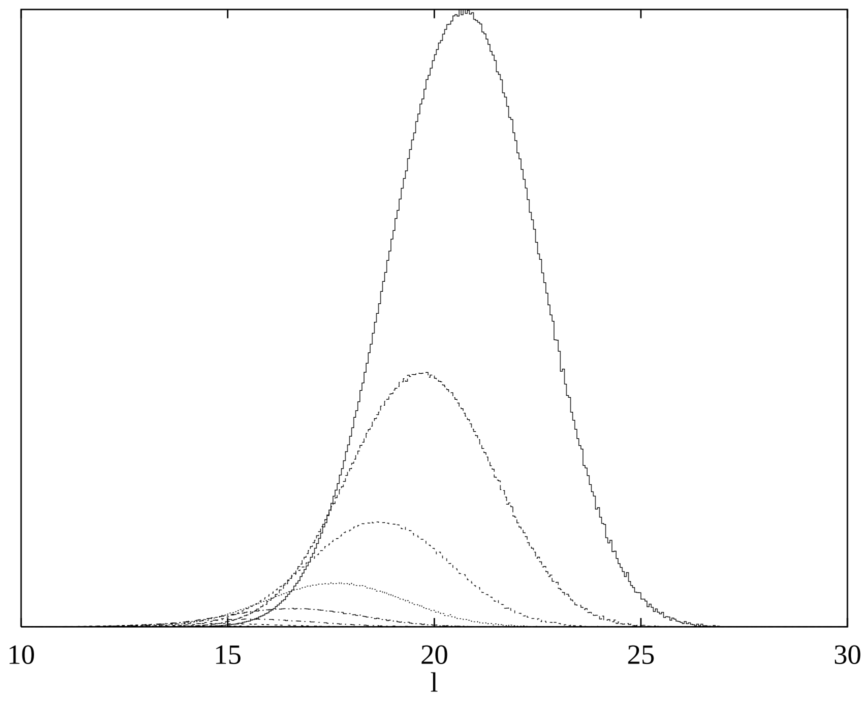

Figure 22: The distribution of geodesic lengths arising from words consisting of a fixed number of letters is shown. The highest curve corresponds to a wordlength of 20, the lower ones to $19, 18, \cdots, 13$.

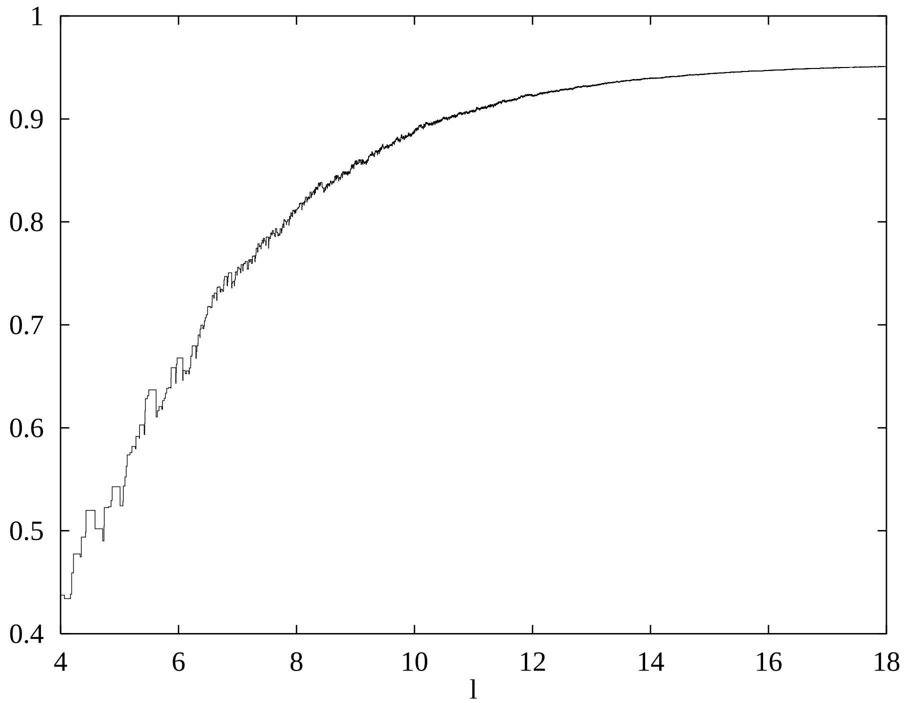

Figure 23: The counting function of distinct lengths is compared with the theoretical prediction (4.30), i.e., $\hat{N}(l)/\hat{N}_{\text{theor.}}(l)$ is plotted versus geodesic lengths.

l	par	nnn	dnn	ndn	ddn	nnd	dnd	ndd	ddd
0.632974319201	1	1	-1	-1	1	-1	1	1	-1
1.128383964966	1	1	1	-1	-1	1	1	-1	-1
1.429036246039	1	1	-1	-1	1	-1	1	1	-1
2.316888394985	1	1	1	-1	-1	1	1	-1	-1
2.773126164854	1	1	-1	1	-1	1	-1	1	-1
2.881636604457	0	1	-1	1	-1	-1	1	-1	1
2.914035387721	1	1	1	1	1	-1	-1	-1	-1
3.463835764702	0	1	1	1	1	1	1	1	1
3.553687937056	1	1	1	-1	-1	1	1	-1	-1
3.620547300604	1	1	-1	-1	1	-1	1	1	-1
3.631581737559	0	1	-1	-1	1	1	-1	-1	1
3.871634380606	0	1	-1	-1	1	1	-1	-1	1
3.892253494796	1	1	-1	1	-1	1	-1	1	-1
3.912455696050	1	1	1	-1	-1	1	1	-1	-1
3.920705543304	0	1	1	1	1	1	1	1	1
4.065037764450	1	1	-1	-1	1	-1	1	1	-1
4.166842119797	0	1	-1	1	-1	-1	1	-1	1
4.188532248096	0	1	1	-1	-1	-1	-1	1	1
4.218424820262	1	1	1	1	1	-1	-1	-1	-1
4.332976057275	1	1	1	-1	-1	1	1	-1	-1
4.351375278216	0	1	-1	-1	1	1	-1	-1	1
4.423821178548	0	1	1	-1	-1	-1	-1	1	1
4.430820234407	1	1	-1	-1	1	-1	1	1	-1
4.585712758443	1	1	1	-1	-1	1	1	-1	-1
4.714558786083	0	1	1	1	1	1	1	1	1
4.735970195373	0	1	-1	1	-1	-1	1	-1	1
4.741097074636	1	1	-1	1	-1	1	-1	1	-1
4.810581771605	1	1	1	-1	-1	1	1	-1	-1
4.856954340898	1	1	-1	-1	1	-1	1	1	-1
4.875549879154	0	1	-1	-1	1	1	-1	-1	1
5.010279562612	1	1	-1	1	-1	1	-1	1	-1
5.057452705724	0	2	-2	-2	2	2	-2	-2	2
5.063794553608	0	1	1	1	1	1	1	1	1
5.091317939403	1	2	2	2	2	-2	-2	-2	-2
5.112098403850	1	1	-1	1	-1	1	-1	1	-1
5.128992335155	0	1	1	1	1	1	1	1	1
5.176656991338	0	1	-1	1	-1	-1	1	-1	1
5.209040231773	1	1	-1	-1	1	-1	1	1	-1
5.268689627145	1	2	2	2	2	-2	-2	-2	-2
5.278062857180	0	2	2	2	2	2	2	2	2

Table 4: The effective multiplicities (4.37) of the shortest 40 geodesic lengths of $T^*(2,3,8)$ for all combinations of boundary conditions. The column "par" distinguishes between hyperbolic (0) and inverse hyperbolic (1) conjugacy classes.

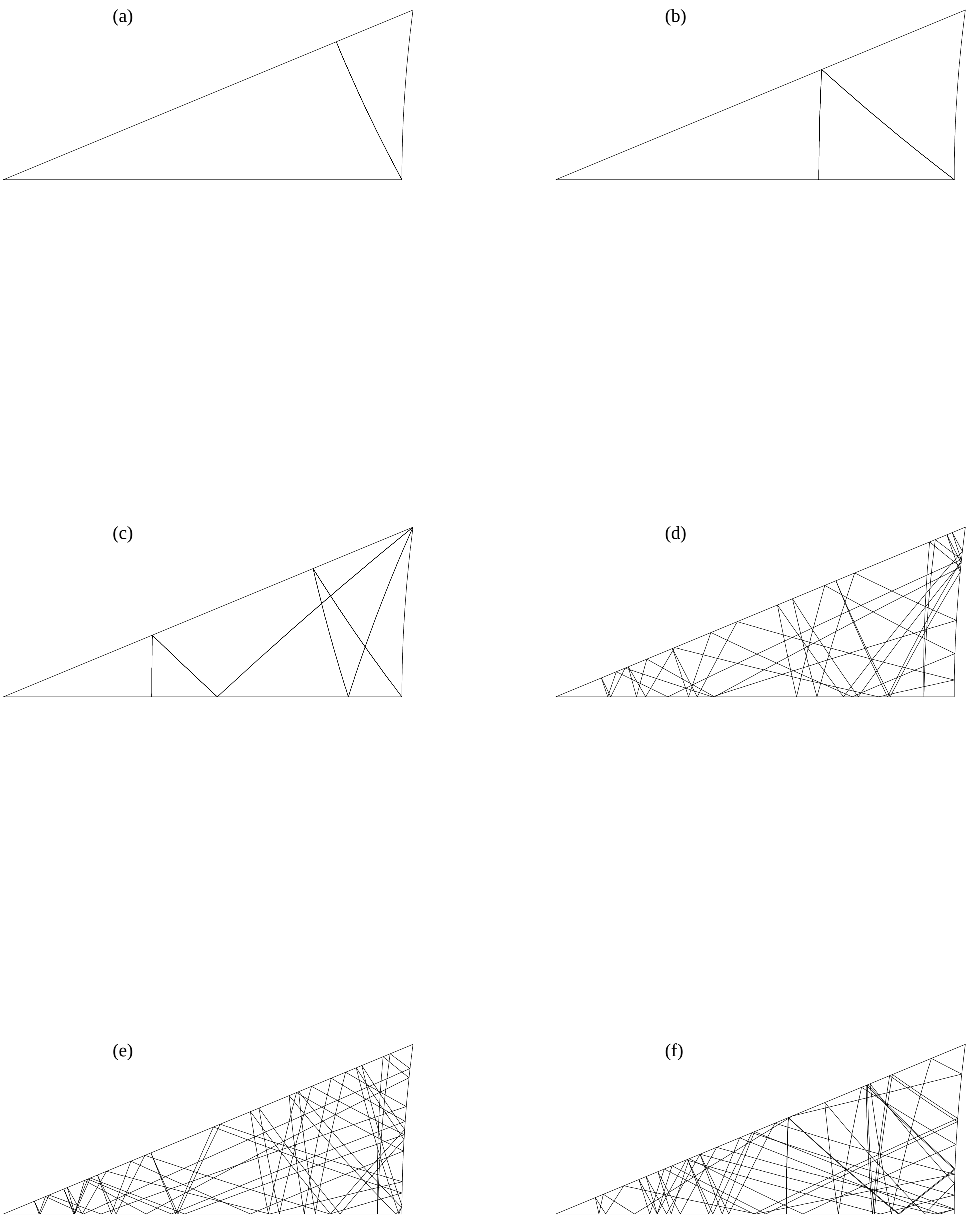

Figure 24: The two shortest geodesics inside the fundamental domain of $T^*(2,3,8)$ are drawn in (a) LMN, $l_a = 0.6329\ldots$ and (b) $LNLMN$, $l_b = 1.1283\ldots$. Figure (c) shows the shortest geodesic running through the vertex of angle $\pi/3$; $MNMLNLNLMNMLNLMNL$, $l_c = 3.5536\ldots$. The remaining orbits correspond to words consisting of 66 (d), 66 (e) and 68 (f) letters L, M, N. Their geodesic lengths are $l_d = 13.7287\ldots$, $l_e = 13.8040\ldots$ and $l_f = 14.1279\ldots$, respectively.

4.3 Selberg's Trace Formula for Hyperbolic Billiards with Mixed Boundary Conditions

Hyperbolic billiards with boundary conditions, which allow a one-dimensional unitary representation of the corresponding reflection group Γ, are subject to a generalized form of Selberg's trace formula. The latter has been derived in [17] for equal boundary conditions at all edges of billiard domain. In this section, now, the case of arbitrary mixed boundary conditions will be investigated, mainly by evaluating the trace of Green's function. Smoothing the trace formula for Green's function with suitable analytic test functions then yields the extended form of Selberg's trace formula (3.55). Since emphasis is laid on the correct treatment of the characters $\chi(\gamma)$, which incorporate the boundary conditions, the smoothing procedure is not presented explicitly. It can be taken over without changes from the case of equal boundary conditions (cf. e.g., [17], appendix L).

Starting point is the free Green function on the Poincaré disk $\mathcal{D}$ ($E =: \rho^2 + \frac{1}{4}$)

$$G_0(z, z'; E) = -\frac{1}{2\pi\sqrt{2}} \int_{d(z,z')}^{\infty} \mathrm{d}t \, \frac{e^{-i\rho t}}{\sqrt{\cosh(t) - \cosh[d(z, z')]}}, \tag{4.38}$$

which is obviously a symmetric function with respect to z and z'. The Green function is the kernel of the integral operator $(\Delta_{\mathrm{LB}} + E)^{-1}$ on $\mathcal{D}$

$$\left[(\Delta_{\mathrm{LB}} + E)^{-1}\psi\right](z) = \int_{\mathcal{D}} G_0(z, z'; E)\, \psi(z')\, \mathrm{d}s^2(z'). \tag{4.39}$$

Turning to the fundamental domain $\mathcal{F}$ of a reflection group Γ, the wave functions ψ are demanded to be automorphic functions transforming according to (2.41). The Green function on $\mathcal{F}$ can be constructed by summing the free Green function $G_0(z, z'; E)$ over all images $\gamma z'$, $\gamma \in \Gamma$ of the source point z'

$$G_{\mathcal{F}}(z, z'; E) = \sum_{\gamma\in\Gamma} \chi(\gamma)\, G_0(z, \gamma z'; E). \tag{4.40}$$

Since, however, the image points $\gamma z'$ proliferate exponentially with respect to their distances, this sum only converges in the half-plane $\mathrm{Re}\,\kappa > \frac{1}{2}$, $\kappa := i\rho$. The trace of Green's function diverges, because $G_{\mathcal{F}}(z, z'; E)$ has a logarithmic singularity at $z = z'$. Therefore a regularization is introduced by differentiating with respect to E

$$K\left[\cosh d(z, z')\right] := K_0(z, z'; E) = -\frac{\partial}{\partial E} G_0(z, z'; E), \tag{4.41}$$

which yields by summing over image points

$$K_{\mathcal{F}}(z, z'; E) = \sum_{\gamma\in\Gamma} \chi(\gamma)\, K\left[\cosh d(z, \gamma z')\right] \tag{4.42}$$

the integral kernel of the operator $(\Delta_{\mathrm{LB}} + E)^{-2}$ on $\mathcal{F}$. Evaluating the trace of this operator in the eigenfunction basis leads to a sum over eigenvalues E_n of $-\Delta_{\mathrm{LB}}$ on $\mathcal{F}$

$$\mathrm{tr}\, K_{\mathcal{F}} = \sum_{n=0}^{\infty} \frac{1}{(E - E_n)^2}. \tag{4.43}$$

Using (4.42), however, yields

$$\mathrm{tr}\, K_{\mathcal{F}} = \int_{\mathcal{F}} K_{\mathcal{F}}(z, z; E)\, \mathrm{d}s^2 = \sum_{\gamma\in\Gamma} \chi(\gamma) \int_{\mathcal{F}} K\left[\cosh d(z, \gamma z)\right]\, \mathrm{d}s^2, \tag{4.44}$$

thus relating a sum over quantal energy eigenvalues to an expression depending merely on the properties of the group Γ.

The summation over group elements in (4.44) can be rearranged to a summation of conjugacy classes of Γ. For this purpose, one observes that Γ can be decomposed into conjugacy classes according to

$$[1], \cdots, [\gamma_p^n], \cdots, \qquad n \geq 1, \tag{4.45}$$

where γ_p runs over a set $\{\gamma_p\}$ of primitive, mutually inconjugate elements of Γ. The elements within each conjugacy class $[\gamma]$ can be written as $\sigma\gamma\sigma^{-1}$, $\sigma \in \Gamma$. Since, however, any σ' being element of the *centralizer* of γ

$$C_\gamma := \{\sigma \in \Gamma;\ \sigma\gamma\sigma^{-1} = \gamma\} \tag{4.46}$$

results in $\sigma\sigma'\gamma(\sigma\sigma')^{-1} = \sigma\gamma\sigma^{-1}$, the proper enumeration of elements within the conjugacy class $[\gamma]$ turns out to be

$$\gamma' = \sigma\gamma\sigma^{-1}, \qquad \sigma \in \Gamma/C_\gamma, \tag{4.47}$$

where Γ/C_γ denotes the right coset space of C_γ in Γ. Rewriting (4.44) thus yields

$$\operatorname{tr} K_{\mathcal{F}} = \sum_{[\gamma]} \sum_{\sigma\in\Gamma/C_\gamma} \chi(\gamma) \int_{\mathcal{F}} K \left[\cosh d(z, \sigma\gamma\sigma^{-1}z)\right] \mathrm{d}s^2. \tag{4.48}$$

The symmetry property of the hyperbolic distance reveals $d(z, \sigma\gamma\sigma^{-1}z') = d(\sigma^{-1}z, \gamma\sigma^{-1}z')$, which turns (4.48) into

$$\operatorname{tr} K_{\mathcal{F}} = \sum_{[\gamma]} \sum_{\sigma\in\Gamma/C_\gamma} \chi(\gamma) \int_{\sigma^{-1}\mathcal{F}} K \left[\cosh d(z, \gamma z)\right] \mathrm{d}s^2, \tag{4.49}$$

by using $\sigma^{-1}z$ as the new integration variable. Since the integral in this expression depends on σ only by the choice of the integration domain, the disjoint copies $\sigma^{-1}\mathcal{F}$ are grouped together

$$\mathcal{F}_\gamma := \bigcup_{\sigma\in\Gamma/C_\gamma} \sigma^{-1}\mathcal{F}, \tag{4.50}$$

yielding the fundamental domain $\mathcal{F}_\gamma$ of the centralizer C_γ. Thus (4.49) can be simplified to

$$\operatorname{tr} K_{\mathcal{F}} = \sum_{[\gamma]} \chi(\gamma) \int_{\mathcal{F}_\gamma} K \left[\cosh d(z, \gamma z)\right] \mathrm{d}s^2. \tag{4.51}$$

The summation over conjugacy classes $[\gamma]$ will now be investigated according to the different kinds of elements in the reflection group Γ.

At first, the *identity* element $\mathbf{1} \in \Gamma$ yields $C_{\mathbf{1}} = \Gamma$, i.e., $\mathcal{F}_{\mathbf{1}} = \mathcal{F}$. Thus it contributes

$$\operatorname{area}(\mathcal{F})\, K(1) \tag{4.52}$$

to the trace formula. This contribution is usually denoted as "zero-length term", and can be rewritten more explicitly by inserting (4.38)

$$K(1) = -\frac{\partial\kappa}{\partial E}\frac{\partial}{\partial\kappa}\, G_0(z, z; E) = \frac{1}{4\pi\kappa}\frac{\partial}{\partial\kappa}\,\psi(\kappa + \frac{1}{2}), \tag{4.53}$$

where $\psi(z) = \frac{\partial}{\partial z}\log\Gamma(z)$.

Next, *inversions* $I \in \Gamma$ will be treated. Any inversion I is associated to an edge of the fundamental domain $\mathcal{F}$, being the invariant axis of I. The centralizer C_I contains three kinds of elements. At first, the inversion $I_\perp$ across a perpendicular axis. Secondly, any rotation R_π by π around a point of the invariant axis of I. Finally, hyperbolic or inverse hyperbolic elements having invariant geodesics, which coincide with the invariant axis of I. The set of inversions $I \in \Gamma$ can be divided into conjugacy classes as follows. Assume I and J are inversions across adjacent edges of the fundamental domain. The vertex between them, being of angle $\frac{\pi}{m_r}$, will be denoted as even or odd depending on the parity of the integer m_r. The rotation around that vertex gives rise to the group relation

$$(IJ)^{m_r} = 1. \tag{4.54}$$

If I and J belong to the same conjugacy class, i.e., $J = \gamma I \gamma^{-1}$, the invariant axis of I can be mapped onto the invariant axis of J by the operation of γ. In the case of *triangular* billiards, this can only be accomplished by a rotation $\gamma = (IJ)^k$ around the vertex under consideration. Thus

$$J = (IJ)^k I (JI)^k \qquad \Rightarrow \qquad (IJ)^k I (JI)^k J = (IJ)^{2k+1} = 1, \tag{4.55}$$

i.e., inversions adjacent to odd vertices are conjugate, whereas inversions adjacent to even vertices are not. Inside each portion of the boundary $\partial\mathcal{F}$ of the fundamental domain, which is delimited by even vertices, the edges are invariant axes of mutually conjugate inversions. Choosing for each portion a representative inversion I, yields the complete list $[I]$ of inversion conjugacy classes. The *total* length of each portion is denoted as $l_{[I]}$.

If at least one vertex of the fundamental domain is even, the centralizer C_I is generated by I and the two rotations R_π around the endpoints of the associated boundary portion. Namely, the inversion $I_\perp$ across a perpendicular axis results from $I_\perp = R_\pi I$, whereas the product of the two rotations yields the primitive hyperbolic element $\gamma_{I,p}$ corresponding to a boundary orbit of length $2l_{[I]}$ along the invariant axis of I. Finally, the associated primitive inverse hyperbolic boundary orbit can be found to be $I\gamma_{I,p}$. The boundary orbits commuting with I form an Abelian group $\{\gamma_{I,p}^k, I\gamma_{I,p}^k\}$. A coordinate transformation, which maps the invariant axis of I onto the imaginary axis, and the rotation centers onto i and $i \exp l_{[I]}$, turns the fundamental domain of the centralizer C_I into

$$\mathcal{F}_I = \{z = x + iy \in \mathcal{H};\ x \geq 0,\ 1 \leq y < \exp l_{[I]}\}, \tag{4.56}$$

yielding

$$\chi(I) \int_1^{\exp l_{[I]}} \frac{\mathrm{d}y}{y^2} \int_0^\infty \mathrm{d}x\, K\left[\cosh d(z, -\bar{z})\right] = \frac{\chi(I)\, l_{[I]}}{2\sqrt{2}} \int_1^\infty \mathrm{d}t\, \frac{K(t)}{\sqrt{t-1}} \tag{4.57}$$

as contribution of the inversion conjugacy class $[I]$. In the case where all vertices are odd, there is only one inversion conjugacy class $[I]$. The corresponding boundary orbit then runs around the whole boundary of the fundamental domain. Defining $l_{[I]} := \mathrm{length}(\partial\mathcal{F})$, also leads to (4.57).

Elliptic elements of Γ correspond to rotations around the vertices of the fundamental domain $\mathcal{F}$. A primitive rotation r can be written as the product of two inversions across adjacent edges, i.e., $r = IJ$. If its fixed point is a vertex of angle $\frac{\pi}{m_r}$, the elliptic element r rotates by $\frac{2\pi}{m_r}$, and is subject to (4.54). The centralizer of r^k, $1 \leq k < m_r$, $k \neq \frac{m_r}{2}$ is the rotation subgroup $\{r^n\}$, thus the fundamental domain $\mathcal{F}_{r^k}$ of C_{r^k} results to be a sector of opening $\frac{2\pi}{m_r}$ in the Poincaré disk $\mathcal{D}$. Using polar coordinates, the contribution of the elliptic conjugacy class $[r^k]$ can be calculated to be

$$\chi(r^k) \int_{\mathcal{F}_{r^k}} K\left[\cosh d(z, r^k z)\right] = \frac{2\pi}{m_r} \frac{\chi(r^k)}{2\sqrt{2}\,\sin\frac{\pi k}{m_r}} \int_1^\infty \mathrm{d}t\, \frac{K(t)}{\sqrt{t - \cos\left(\frac{2\pi k}{m_r}\right)}}. \tag{4.58}$$

In the case of $k = \frac{m_r}{2}$ the rotation $r^k = R_\pi$ commutes with I or J, doubling the centralizer C_{r^k} and cutting the fundamental domain $\mathcal{F}_{r^k}$ by half, thus leading to half of the contribution (4.58). In the case $k \neq \frac{m_r}{2}$, on the other hand, the rotations r^k and r^{m_r-k} are conjugated by I or J. Putting all together, the contribution of all elliptic conjugacy classes can be established by summing over all nontrivial powers of primitive rotations and multiplying with an additional factor $\frac{1}{2}$

$$\sum_{\{r\}} \sum_{k=1}^{m_r-1} \frac{2\pi}{m_r} \frac{\chi(r^k)}{4\sqrt{2}\,\sin\frac{\pi k}{m_r}} \int_1^\infty \mathrm{d}t\, \frac{K(t)}{\sqrt{t - \cos\left(\frac{2\pi k}{m_r}\right)}}. \tag{4.59}$$

Among the *hyperbolic* elements, two cases have to be distinguished. At first, assume $\gamma \in \Gamma$ is a primitive hyperbolic element corresponding to a geodesic of length l_γ running *inside* the fundamental domain $\mathcal{F}$. Its centralizer contains all integer powers of γ

$$C_\gamma = \{\gamma^k\}_{k\in\mathbb{Z}}. \tag{4.60}$$

Using half-plane coordinates, which diagonalizes γ, the fundamental domain of the centralizer can be chosen as

$$\mathcal{F}_\gamma = \{z \in \mathcal{H};\ 1 < \operatorname{Im} z < \exp l_\gamma\}, \tag{4.61}$$

leading to the contribution of the hyperbolic conjugacy class $[\gamma^k]$

$$\chi(\gamma^k) \int_1^{\exp l_\gamma} \frac{\mathrm{d}y}{y^2} \int_{-\infty}^{\infty} \mathrm{d}x\, K\left[\cosh d(z, e^{k l_\gamma} z)\right] = \frac{\chi(\gamma^k)\, l_\gamma}{\sqrt{2}\sinh\frac{k l_\gamma}{2}} \int_{\cosh(k l_\gamma)}^\infty \mathrm{d}t\, \frac{K(t)}{\sqrt{t - \cosh(k l_\gamma)}}. \tag{4.62}$$

Hyperbolic conjugacy classes associated to *boundary orbits*, however, need a slight modification. As discussed above, the centralizer then turns into

$$C_{\gamma_I} = \{\gamma_I^k, I\gamma_I^k\}_{k\in\mathbb{Z}}, \tag{4.63}$$

reducing the integration domain by a factor $\frac{1}{2}$. Thus the contribution of all hyperbolic conjugacy classes sums up to

$$\left(\sum_{\{\gamma\}} + \frac{1}{2}\sum_{\{\gamma_I\}}\right) \sum_{k=1}^{\infty} \frac{\chi(\gamma^k)\, l_\gamma}{\sqrt{2}\sinh\frac{k l_\gamma}{2}} \int_{\cosh(k l_\gamma)}^\infty \mathrm{d}t\, \frac{K(t)}{\sqrt{t - \cosh(k l_\gamma)}}. \tag{4.64}$$

Inverse hyperbolic elements can be treated along the same lines as (direct) hyperbolic elements. However, inverse hyperbolic elements act on a point $z \in \mathcal{D}$ according to

$$\gamma z = -e^{l_\gamma}\,\bar{z}, \tag{4.65}$$

in coordinates, which diagonalize γ. The contribution of an inverse hyperbolic conjugacy class $[\gamma^k]$ associated to a periodic orbit running *inside* the fundamental domain then results in

$$\frac{2\chi(\gamma^k)\, l_\gamma}{\sqrt{2}\left[\exp\left(\frac{k l_\gamma}{2}\right) - (-1)^k \exp\left(-\frac{k l_\gamma}{2}\right)\right]} \int_{\cosh(k l_\gamma)}^\infty \mathrm{d}t\, \frac{K(t)}{\sqrt{t - \cosh(k l_\gamma)}}. \tag{4.66}$$

Inverse hyperbolic conjugacy classes associated to *boundary orbits* are of the form $[I\gamma_I^k]$, and have a centralizer twice as large, in complete analogy to the hyperbolic case. Notice, that even powers of primitive inverse hyperbolic elements are of (direct) hyperbolic type, whereas multiple traversals of boundary orbits corresponding to inverse hyperbolic elements $I\gamma_I^k$ always are of inverse hyperbolic type. Thus the contribution of the conjugacy class $[I\gamma_I^k]$ is

$$\frac{1}{2}\,\frac{\chi(I\gamma_I^k)\,l_\gamma}{\sqrt{2}\cosh\frac{kl_\gamma}{2}}\int_{\cosh(kl_\gamma)}^{\infty}\mathrm{d}t\,\frac{K(t)}{\sqrt{t-\cosh(kl_\gamma)}}. \tag{4.67}$$

Due to the compactness of the fundamental domain $\mathcal{F}$, *parabolic* elements do not arise.

Rewriting all occurrences of the integral kernel $K(t)$ by the free Green function $G_0(z,z';E)$, and smoothing as pointed out in the beginning of this section, finally leads to the Selberg trace formula for a smearing function $h(p)$, subject to the restrictions listed in the context of the strictly hyperbolic case (3.55sqq)

$$\begin{aligned}
\sum_{n=0}^{\infty} h(p_n) \quad = \quad & \frac{\mathrm{area}(\mathcal{F})}{4\pi}\int_{-\infty}^{\infty}\mathrm{d}p\,p\,h(p)\tanh(\pi p) \;+\; \sum_{\{I\}}\frac{\chi(I)\,l_{[I]}}{4}\,\hat{h}(0) \\
& + \;\sum_{\{r\}}\sum_{k=1}^{m_r-1}\frac{\chi^k(r)}{4m_r\sin\frac{\pi k}{m_r}}\int_{-\infty}^{\infty}\mathrm{d}p\,h(p)\,\frac{e^{-2\pi p\frac{k}{m_r}}}{1+e^{-2\pi p}} \\
& + \;\sum_{\{\gamma_I\}}\sum_{k=1}^{\infty}\frac{\chi^k(\gamma_I)\,l_{\gamma_I}}{4}\left\{\frac{1}{\sinh\frac{kl_{\gamma_I}}{2}}+\frac{\chi(I)}{\cosh\frac{kl_{\gamma_I}}{2}}\right\}\hat{h}(kl_{\gamma_I}) \\
& + \;\sum_{\{\gamma_{\mathrm{hyp}}\}}\sum_{k=1}^{\infty}\frac{\chi^k(\gamma)\,l_\gamma}{\exp\left(\frac{kl_\gamma}{2}\right)-\sigma^k(\gamma)\,\exp\left(-\frac{kl_\gamma}{2}\right)}\,\hat{h}(kl_\gamma) \qquad ,
\end{aligned} \tag{4.68}$$

where p_n are the momenta related to the energy eigenvalues by $E_n = p_n^2 + \frac{1}{4}$. Hyperbolic and inverse hyperbolic conjugacy classes have been grouped together by introducing

$$\sigma(\gamma) = \begin{cases} +1, & \gamma \text{ direct hyperbolic,} \\ -1, & \gamma \text{ inverse hyperbolic.} \end{cases} \tag{4.69}$$

In the special case of the hyperbolic triangle group $T^*(2,3,8)$, remember that the requirement of one-dimensional unitary representations to exist, enforces the choice of boundary conditions compatible with

$$\chi(M) = \chi(N), \tag{4.70}$$

because the inversions M and N belong to the same conjugacy class. There are in total two inversion conjugacy classes, and the lengths of the associated boundary portions of the fundamental domain are given by

$$l_{[L]} = l_L, \qquad l_{[M]} = l_{[N]} = l_M + l_N. \tag{4.71}$$

The hyperbolic conjugacy classes associated to the two boundary orbits can be calculated to be

$$\gamma_L \sim LN(LMN)^2, \qquad \gamma_M \equiv \gamma_N \sim (LMNLN)^2 LN, \tag{4.72}$$

thus

$$\chi(\gamma_L) = \chi(\gamma_M) = \chi(L)\,\chi(N). \tag{4.73}$$

4.4 The Energy Spectrum

In this section Selberg's trace formula for polygonal hyperbolic billiards (4.68) will be used to derive quantization rules for the dynamical system associated to $T^*(2,3,8)$ along the same lines as described in the context of Gutzwiller's group Γ_{GW}.

Inserting the smearing function (3.57) into Selberg's trace formula and integrating over the interval $[0, \sqrt{E-\frac{1}{4}}]$ in the limit $\epsilon \to 0^+$ yields an expression for the spectral staircase $\mathcal{N}(E)$. Since the structure of the zero-length term and of the sums over hyperbolic conjugacy classes in (4.68) coincide with the corresponding terms in the strictly hyperbolic case (3.55), only the remaining contributions need to be investigated explicitly.

Using the Fourier tansform of the smearing function $h(p)$

$$\hat{h}(q) = \frac{1}{\pi} \cos(p'q)\, e^{-\frac{\epsilon^2}{4}q}, \tag{4.74}$$

the term of inversion conjugacy classes yields ($E = p^2 + \frac{1}{4}$)

$$\lim_{\epsilon\to 0^+} \int_0^p \mathrm{d}p' \sum_{\{I\}} \frac{\chi(I)\, l_{[I]}}{4\pi} = \frac{p}{4\pi} \sum_{\{I\}} \chi(I)\, l_{[I]}. \tag{4.75}$$

Elliptic conjugacy classes can be found to contribute

$$\begin{aligned} &\lim_{\epsilon\to 0^+} \int_0^p \mathrm{d}p' \sum_{\{r\}} \sum_{k=1}^{m_r-1} \frac{\chi^k(r)}{4m_r \sin\frac{\pi k}{m_r}} \int_{-\infty}^{\infty} \mathrm{d}t\, h(t)\, \frac{e^{-2\pi t \frac{k}{m_r}}}{1+e^{-2\pi t}} \\ &= \sum_{\{r\}} \sum_{k=1}^{m_r-1} \frac{\chi^k(r)}{4\pi m_r \sin\frac{\pi k}{m_r}} \int_0^{\pi p} \mathrm{d}x\, \frac{\cosh\left[\left(\frac{2k}{m_r}-1\right)\, x\right]}{\cosh x}. \end{aligned} \tag{4.76}$$

The hyperbolic triangle group $T^*(2,3,8)$ contains three primitive elliptic conjugacy classes, which will now be investigated separately.

(i) $r = LM$, $m_r = 2$: Only the term $k=1$ arises in (4.76), yielding [29]

$$\frac{\chi(LM)}{8\pi} \int_0^{\pi p} \frac{\mathrm{d}x}{\cosh x} = \frac{\chi(LM)}{8\pi} \arctan(\sinh \pi p). \tag{4.77}$$

(ii) $r = MN$, $m_r = 3$: For $k=1$ the contribution can be found to be [29]

$$\frac{\chi(MN)}{6\pi\sqrt{3}} \int_0^{\pi p} \mathrm{d}x\, \frac{\cosh\frac{x}{3}}{\cosh x} = \frac{\chi(MN)}{6\pi} \arctan(\sqrt{3}\, \tanh\frac{\pi p}{3}). \tag{4.78}$$

Since, however, equal boundary conditions along the edges M and N of the fundamental domain of $T^*(2,3,8)$ have to be chosen in order to ensure one-dimensional unitary representations χ to exist, one finds $\chi(MN) = 1$. The term $k=2$ also leads to (4.78), thus the total contribution of the elliptic conjugacy class $[MN]$ is

$$\frac{1}{3\pi} \arctan(\sqrt{3}\, \tanh\frac{\pi p}{3}). \tag{4.79}$$

(iii) $r = LN$, $m_r = 8$: Using the symmetry properties with respect to k, the sum in (4.76) can be splitted

$$\sum_{k=1}^{7} \frac{\chi^k(LN)}{32\pi \sin \frac{\pi k}{8}} \int_0^{\pi p} \mathrm{d}x \, \frac{\cosh\left[\left(\frac{k}{4}-1\right)\, x\right]}{\cosh x}$$

$$= \frac{1}{32\pi} \, \arctan(\sinh \pi p) + \sum_{k=1}^{3} \frac{\chi^k(LN)}{16\pi \sin \frac{\pi k}{8}} \int_0^{\pi p} \mathrm{d}x \, \frac{\cosh\left[\left(1-\frac{k}{4}\right)\, x\right]}{\cosh x}. \tag{4.80}$$

The integral can be solved in a number of steps. At first, a geometric series expansion of the denominator leads to

$$\begin{aligned} I := \int_0^{\pi p} \mathrm{d}x \, \frac{\cosh\left[\left(\frac{k}{4}-1\right)\, x\right]}{\cosh x} & \\ = \; & \sum_{\nu=0}^{\infty} (-1)^\nu \int_0^{\pi p} \mathrm{d}x \, \left\{ e^{-2(\nu+\frac{k}{8})x} + e^{-2(\nu+(1-\frac{k}{8}))x} \right\} \\ = \; & \tfrac{1}{2} \sum_{\nu=0}^{\infty} (-1)^\nu \left\{ \frac{1}{\nu+\frac{k}{8}} + \frac{1}{\nu+(1-\frac{k}{8})} \right\} \\ & - 4 \sum_{\nu=0}^{\infty} (-1)^\nu \left\{ z^{\frac{k}{8}} \, \frac{z^\nu}{8\nu+k} + z^{1-\frac{k}{8}} \, \frac{z^\nu}{8\nu+8-k} \right\}, \end{aligned} \tag{4.81}$$

where the notation $z := e^{-2\pi p}$ has been introduced. The first sum can be identified as a partial fraction expansion [44]

$$\frac{\pi}{2 \sin \frac{k\pi}{8}} = \tfrac{1}{2} \sum_{\nu=0}^{\infty} (-1)^\nu \left\{ \frac{1}{\nu+\frac{k}{8}} + \frac{1}{\nu+(1-\frac{k}{8})} \right\}, \tag{4.82}$$

whereas the second one can be summed up by using [35]

$$\begin{gathered} \sum_{\nu=0}^{\infty} (-1)^\nu \, \frac{z^\nu}{n\nu+m} = -\frac{1}{n} \, z^{-\frac{m}{n}} \sum_{\mu=0}^{n-1} e^{-(2\mu+1)\frac{i\pi m}{n}} \, \log\left\{ 1 - z^{\frac{1}{n}} \, e^{(2\mu+1)\frac{i\pi}{n}} \right\}, \\ m, n = 1, 2, 3, \cdots; \quad m \le n; \quad |z| < 1, \end{gathered} \tag{4.83}$$

leading to

$$I = \frac{\pi}{2 \sin \frac{k\pi}{8}} - 2 \sum_{\mu=0}^{3} \sin\left\{ (2\mu+1) \frac{k\pi}{8} \right\} \arctan\left\{ \frac{\sin[(2\mu+1)\frac{\pi}{8}]}{\exp(\frac{\pi p}{4}) - \cos[(2\mu+1)\frac{\pi}{8}]} \right\}. \tag{4.84}$$

Substituting into (4.80) finally reveals the contribution of the elliptic conjugacy class $[LN]$

$$\begin{aligned} & \frac{1}{32\pi} \, \arctan(\sinh \pi p) + \frac{1}{8\pi} \, \arctan\left(\sqrt{2} \, \sinh \frac{\pi p}{2} \right) \\ & \qquad + \frac{\chi(LN)}{4\pi} \left\{ \arctan\left(\frac{2 \sinh \frac{\pi p}{4}}{\sqrt{2-\sqrt{2}}} \right) + \arctan\left(\frac{2 \sinh \frac{\pi p}{4}}{\sqrt{2+\sqrt{2}}} \right) \right\}. \end{aligned} \tag{4.85}$$

Putting all terms together leads to the spectral staircase $\mathcal{N}(E)$ for $T^*(2,3,8)$ as derived from Selberg's trace formula

$$
\begin{aligned}
\mathcal{N}(E) \;=\;& \frac{A}{2\pi}\int_0^p \mathrm{d}p'\,p'\,\tanh(\pi p') \;+\; \frac{p}{4\pi}\sum_{\{I\}}\chi(I)\,l_{[I]} \\
&+\frac{\chi(LM)}{8\pi}\,\arctan(\sinh\pi p)+\frac{1}{3\pi}\,\arctan(\sqrt{3}\,\tanh\frac{\pi p}{3}) \\
&+\frac{1}{32\pi}\,\arctan(\sinh\pi p)+\frac{1}{8\pi}\,\arctan\left(\sqrt{2}\,\sinh\frac{\pi p}{2}\right) \\
&+\frac{\chi(LN)}{4\pi}\left\{\arctan\left(\frac{2\sinh\frac{\pi p}{4}}{\sqrt{2-\sqrt{2}}}\right)+\arctan\left(\frac{2\sinh\frac{\pi p}{4}}{\sqrt{2+\sqrt{2}}}\right)\right\} \\
+\;& \frac{1}{4\pi}\sum_{\{\gamma_I\}}\sum_{k=1}^{\infty}\chi^k(\gamma_I)\left\{\frac{1}{\sinh\frac{kl_{\gamma_I}}{2}}+\frac{\chi(I)}{\cosh\frac{kl_{\gamma_I}}{2}}\right\}\frac{\sin(pkl_{\gamma_I})}{k} \\
+\;& \frac{1}{\pi}\sum_{\{\gamma_{\text{hyp}}\}}\sum_{k=1}^{\infty}\frac{1}{k}\,\frac{\chi^k(\gamma)\,\sin(pkl_\gamma)}{\exp\left(\frac{kl_\gamma}{2}\right)-\sigma^k(\gamma)\,\exp\left(-\frac{kl_\gamma}{2}\right)}\qquad, \qquad (4.86)
\end{aligned}
$$

where $A=\frac{\pi}{24}$. The asymptotic behavior of $\mathcal{N}(E)$ in the limit $E\to\infty$, i.e., Weyl's law, is controlled by the zero-length term and the terms associated to inversions and elliptic conjugacy classes. Using the result (3.70sqq) obtained in the context of Gutzwiller's group Γ_{GW}, and noticing that $\chi(LM)=\chi(LN)$, one finds

$$
\mathcal{N}(E)=\frac{A}{4\pi}\,E+\frac{\chi(L)\,l_L+\chi(M)(l_M+l_N)}{4\pi}\,\sqrt{E}+\frac{107+180\,\chi(LM)}{576}+\cdots. \qquad (4.87)
$$

In the discussion of the strictly hyperbolic case it has been pointed out, that the sum over hyperbolic conjugacy classes needs a regularization, since in the limit $\epsilon\to 0^+$ the smearing function $h(p)$ as defined in (3.57) is not a valid test function. If all boundary conditions at the edges of the fundamental domain of $T^*(2,3,8)$ are chosen to be Neumann, the sum over hyperbolic conjugacy classes in (4.86) possesses the same structure as the corresponding sum in (3.62). Thus the remainder term $R(p,\mathcal{L})$, defined in (3.65), has to be used, if the geodesic length spectrum is taken into account up to a cutoff length $\mathcal{L}$. For all other combinations of boundary conditions, the sign changes of the characters $\chi(\gamma)$ seem to cause conditional convergence of the periodic orbit sum in (4.86), i.e., no remainder term is needed.

Based on numerically solving Schrödinger's equation by the method of finite elements, the first 200 energy eigenvalues of the dynamical system associated to $T^*(2,3,8)$ have been calculated for all combinations of boundary conditions in [5]. Later, the two special cases of Dirichlet boundary condition along edge L, and Neumann boundary conditions along edges M and N (dnn), as well as Neumann boundary conditions along edges L and M, and Dirichlet boundary condition along edge N (nnd) were studied by the more effective boundary element method [10, 48], yielding all quantal energies in the range $0\le E_n\le 100000$, which amounts to roughly 1050 energy levels for each system.

The spectral staircase $\mathcal{N}(E)$ of the dnn-case, which is subject to Selberg's trace formula (4.68) is compared in figs. 25 and 26 with the expression (4.86). The latter has been evaluated by taking into account the geodesic length spectrum of $T^*(2,3,8)$ up to a cutoff length of $\mathcal{L} \simeq 18$. The two curves agree much better than in the case of Gutzwiller' group $\Gamma_{\rm GW}$. Small fluctuations around the "true" staircase function can be observed, which are similar to the classical Gibbs phenomenon. They are due to cutting off the periodic orbit sum of (4.86) at a finite geodesic length.

The much better resolution in the case of $T^*(2,3,8)$, as compared with $\Gamma_{\rm GW}$, can be understood by relation (3.77). Due to the small area of the fundamental domain $A_{T^*(2,3,8)} = A_{\Gamma_{\rm GW}}/96$, a cutoff length of $\mathcal{L} \simeq 18$ now leads to a maximum energy $E_{\max} \simeq 75636$, above which the fluctuations of (4.86) become comparable with the step-height of $\mathcal{N}(E)$. Thus the quantization rule (3.74) is expected to yield reasonable good approximations for the first ~ 800 quantal energies. In fig. 27 the quantization function $\xi(E)$ is compared with the "true" eigenvalues of the dnn-case for different energy ranges. Even above the 1000th energy eigenvalue the quantization rule (3.74) works reasonably good. Only values of E_n, which are very close to each other cannot be resolved. But the *number* of eigenvalues can be read off, nevertheless. The relative error of the energy eigenvalues derived from $\xi(E)$ does not exceed $\sim 0.05\%$ within the whole range $0 \leq E_n \leq 100000$. For those remaining combinations of boundary conditions, which lead to systems obeying Selberg's trace formula, $\xi(E)$ is compared with the energy eigenvalues obtained by the method of finite elements in fig. 28.

Comparing the first two terms of Weyl's law (4.87) with the energy spectrum derived from Schrödinger's equation, a fit value $\sigma_{\rm fit}$ for the constant contribution $\sigma_{\rm theor} = \frac{1}{576}(107 + 180\chi(LM))$ can be calculated. The results are given in table 5. It must be pointed out, however, that the fit value obtained fo the dnn-case is the most reliable one, since it is based on five times as much energy levels than for the remaining combinations of energy levels. By the same reason, for the dnn-case a much higher energy range is reached, for which Weyl's asymptotic approximation is expected to be better.

boundary condition	ddd	nnn	dnn	ndd
$\sigma_{\rm theor.}$	+0.4982	+0.4982	-0.1267	-0.1267
$\sigma_{\rm fit}$	+0.543	+0.521	-0.125	-0.088

Table 5: The fit value $\sigma_{\rm fit}$ for the constant contribution in Weyl's law (4.87), as obtained from the numerical solutions of Schrödingers equation, is compared with the theoretical prediction.

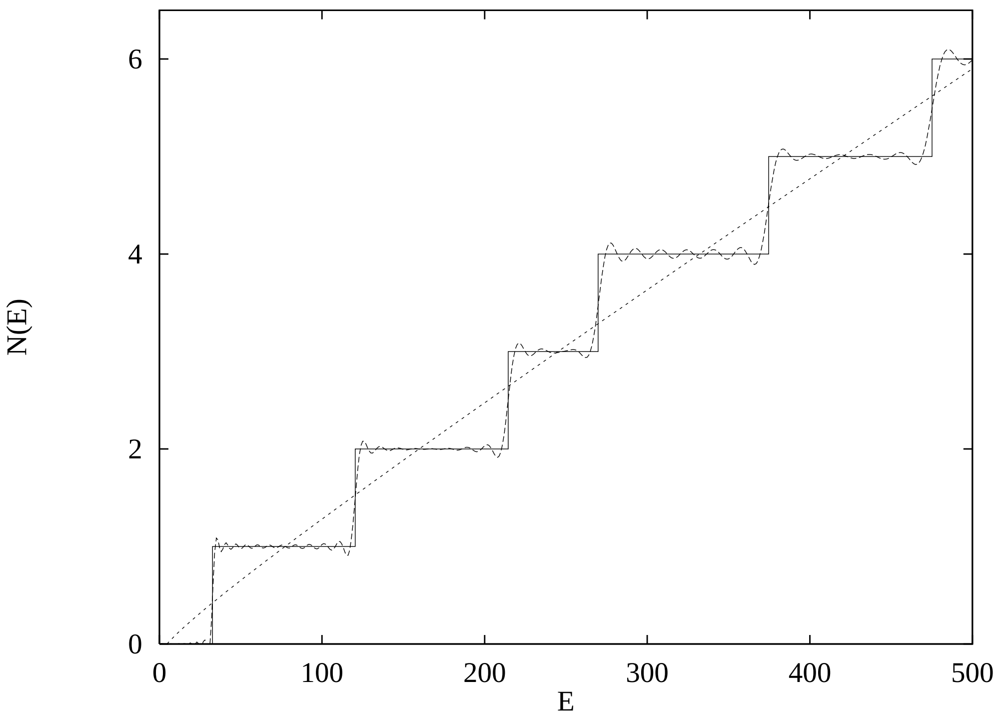

Figure 25: The spectral staircase $\mathcal{N}(E)$ of $T^*(2,3,8)$ with boundary conditions "dnn" (solid curve) is compared with the approximation obtained from (4.86) (dashed curve). The dotted straight line indicates Weyl's law (4.87).

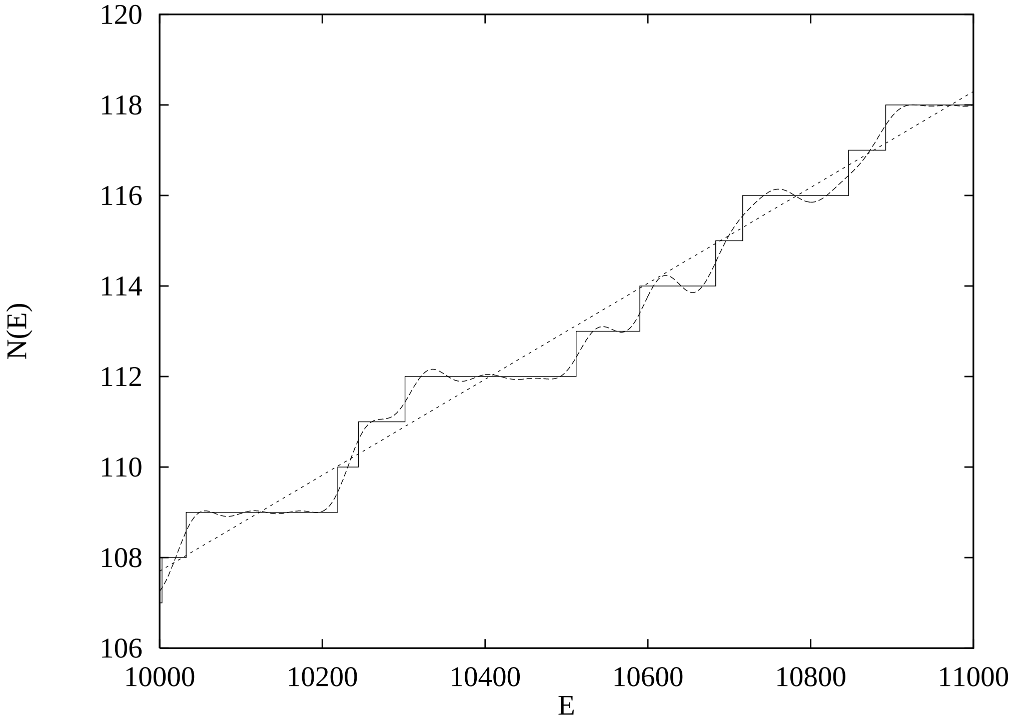

Figure 26: The same curves as in fig. 25 are shown above the 108th energy eigenvalue.

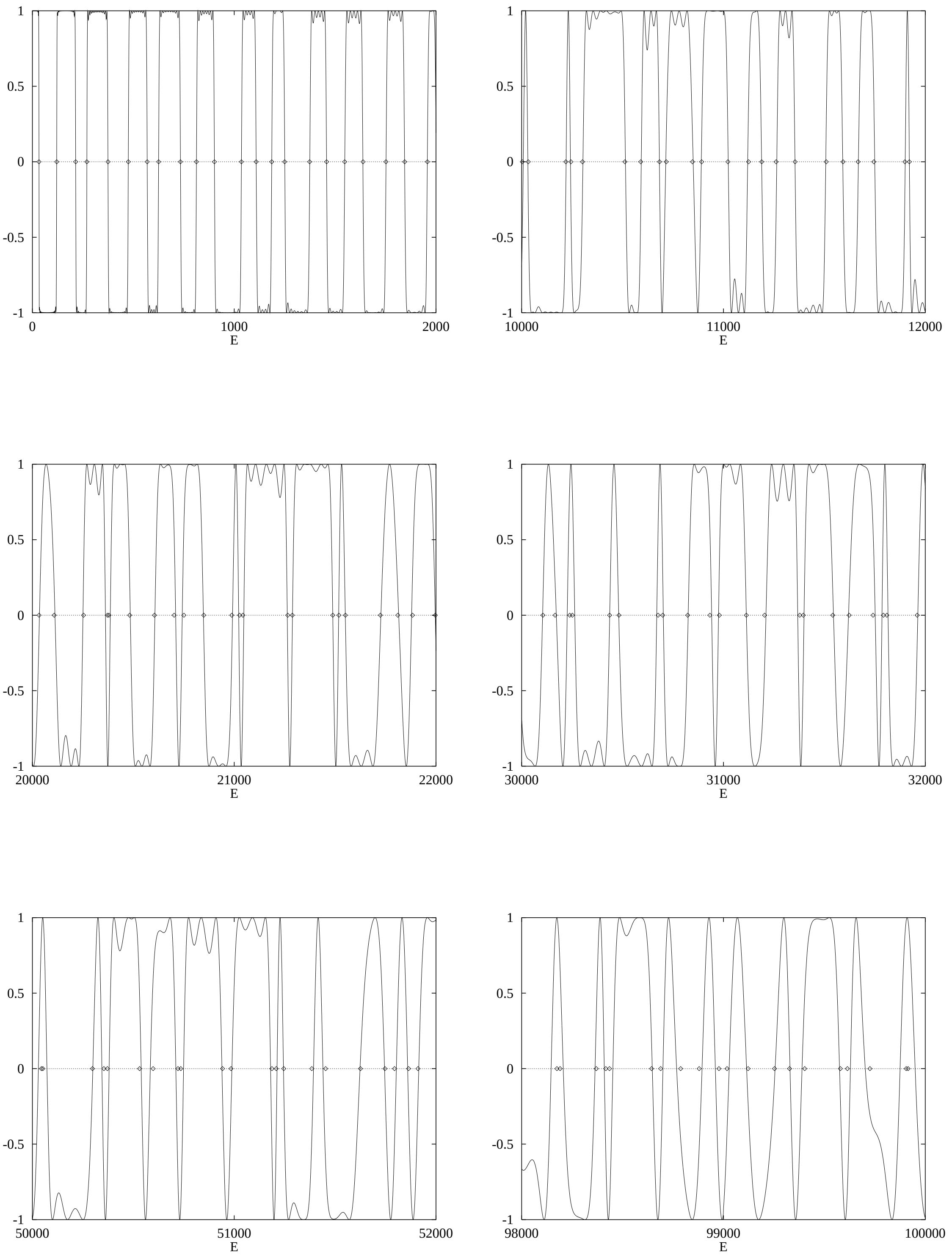

Figure 27: The quantization function $\xi(E) := \cos(\pi\mathcal{N}(E))$ of $T^*(2,3,8)$ with boundary conditions "dnn" is compared with the energy eigenvalues obtained from numerically solving Schrödinger's equation for different energy ranges.

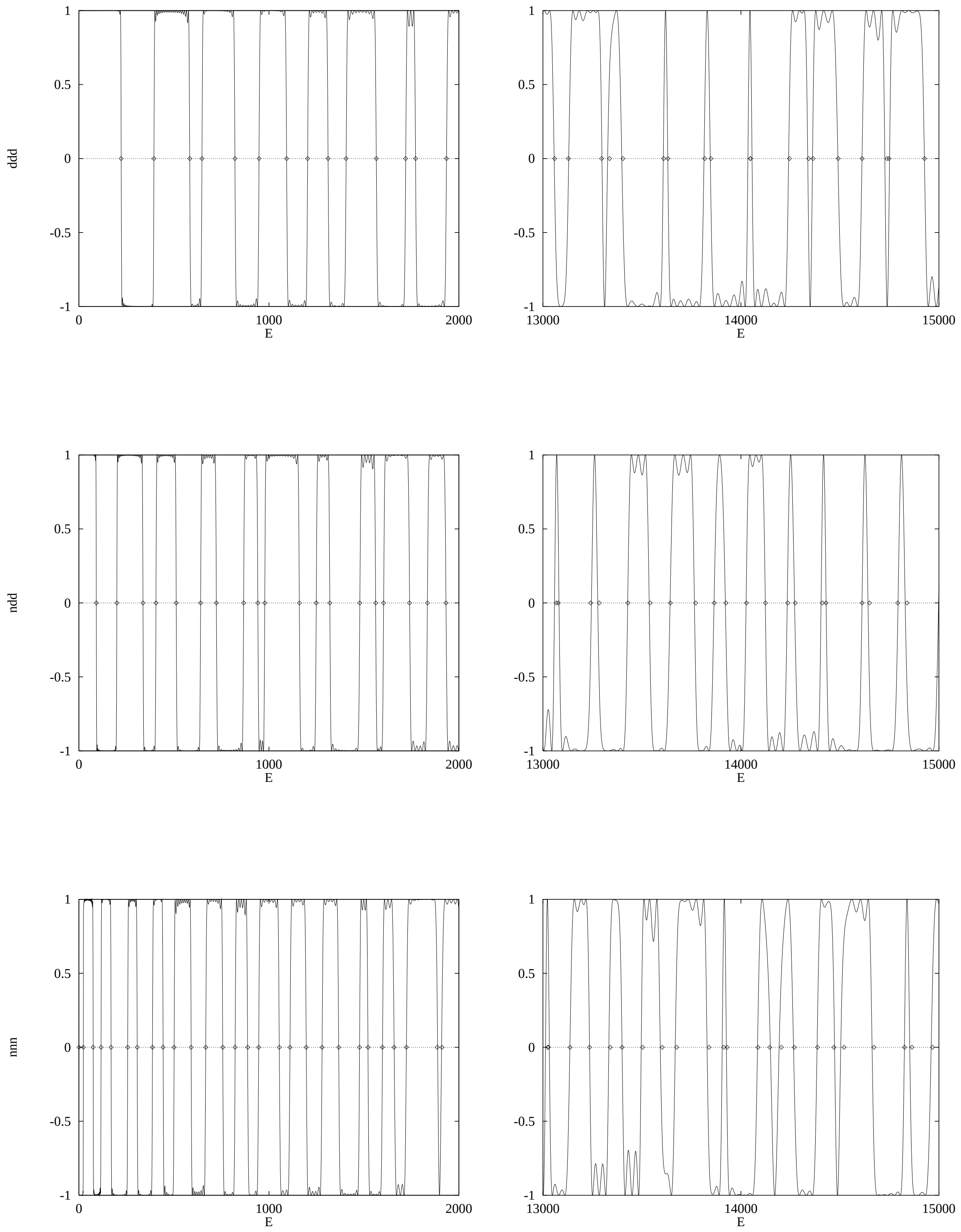

Figure 28: The quantization function $\xi(E) := \cos(\pi\mathcal{N}(E))$ of $T^*(2,3,8)$ with boundary conditions, which allow one-dimensional unitary representations χ, is compared with the energy eigenvalues obtained by the method of finite elements.

From the Selberg trace formula for polygonal hyperbolic billiards Selberg's zeta function

$$
\begin{aligned}
Z(s) &= \prod_{\{\gamma_I\}} \prod_{n=0}^{\infty} \left(1 - \chi(\gamma_I)\, e^{-(s+2n+\frac{1}{2}[1-\chi(I)])\, l_{\gamma_I}}\right) \\
&\quad \times \prod_{\{\gamma_{\mathrm{hyp}}\}} \prod_{n=0}^{\infty} \left(1 - \chi(\gamma)\, \sigma^n(\gamma)\, e^{-(s+n)\, l_\gamma}\right), \qquad \operatorname{Re} s > \tau. \qquad (4.88)
\end{aligned}
$$

can be derived (cf. appendix C). As described in section 3.3, the non-trivial zeros of $Z(s)$ are related to the quantal energies of the dynamical system under consideration, and thus can be used to establish a quantization rule. The corresponding Ruelle-type zeta function

$$
R(s) := \prod_{\{\gamma_{\mathrm{hyp}}\}} \left(1 - \chi(\gamma)\, e^{-s l_\gamma}\right), \qquad \operatorname{Re} s > \tau \qquad (4.89)
$$

can be rewritten as a Dirichlet series to be summed over D-orbits L_ρ

$$
R(s) = \sum_\rho A_\rho\, e^{-sL_\rho}, \qquad \operatorname{Re} s > \tau, \qquad (4.90)
$$

which converge conditionally in right half-planes $\operatorname{Re} s > \sigma_c$, and converge absolutely in right half-planes $\operatorname{Re} s > \sigma_a = \tau$. The Dirichlet coefficients $A_\rho := \prod_{\gamma\in\rho}[-\chi(\gamma)]$ are determined by the characters of the primitive closed geodesics constituting a D-orbit L_ρ. Arranging the D-orbits in ascending order $L_1 \leq L_2 \leq L_3 \leq \cdots$ allows to calculate the abscissae of convergence by

$$
\begin{aligned}
\sigma_a &= \limsup_{N\to\infty} \frac{1}{L_N} \log \sum_{n=1}^{N} |A_n|\,, \\
\sigma_c &= \limsup_{N\to\infty} \frac{1}{L_N} \log \left|\sum_{n=1}^{N} A_n\right|.
\end{aligned} \qquad (4.91)
$$

Introducing effective D-multiplicities

$$
g_D(L) = \sum_{\substack{\rho \\ L_\rho = L}} A_\rho \qquad (4.92)
$$

turns the Ruelle-type zeta function into

$$
R(s) = \sum_{n=1}^{\infty} g_D(L_n)\, e^{-sL_n}, \qquad \operatorname{Re} s > \tau. \qquad (4.93)
$$

A fit to the absolute value of the average effective D-multiplicities

$$
|< g_D(L) >| \sim d e^{\alpha L}, \qquad L \to \infty \qquad (4.94)
$$

then allows to derive a prediction (3.89) for σ_c, based on a random walk model, which assumes, that the signs of $g_D(L_n)$ are randomly distributed.

Due to the presence of comparatively short geodesic lengths $l_1 \simeq 0.632974, \ldots$ in the case of the hyperbolic triangle group $T^*(2,3,8)$, the number of different D-lengths grows very rapidly, soon reaching the limits of computational power. Already the first 8241 geodesic lengths, covering the range $l_1 \leq l \leq 15$, result in 2287989 D-orbits of 524642 different D-lengths. A fit to $| < g_D(L) > |$ according to (4.94) yields $d = 0.3641\ldots$ and $\alpha = 0.1765$ for all combination of boundary conditions, which are compatible with Selberg's trace formula (cf. fig. 29 for the dnn-case). Thus the statistical model leads to the prediction $\sigma_c = 0.5883\ldots$ by (3.89). Evaluation of the sequences (4.91), however, seems to indicate a value of $\sigma_c < \frac{1}{2}$, which allows to use the representation (4.93) of the Ruelle-type zeta function $R(s)$ on the critical line $s = \frac{1}{2} - ip$, $p \in \mathbb{R}$ (see figs. 30 and 32). The assumption of the signs of $g_D(L_n)$ to be randomly distributed can be observed to be much better realized than for Gutzwiller's group (figs. 31 and 32).

In figs. 33 to 35 the absolute value of the Ruelle-type zeta function $|R(s)|$ is evaluated on the critical line as a function of $E = s(s-1)$, $E \in \mathbb{R}$. A comparison with the numerical solutions of Schrödinger's equation shows a reasonably good agreement. In comparison to the quantization rule based on $\xi(E)$ as defined in (3.74), however, the investigation of $|R(s)|$ on the critical line has two drawbacks.

On the one hand, if short geodesics are present, the number of different D-lengths grows very rapidly. For the numerical values given above, more than 60 times as much terms have to be used to evaluate $R(s)$, than for the calculation of $\xi(E)$. This relation becomes even worse, as can be seen from the value of α, suggesting that the degeneracy of the D-orbit spectrum grows much weaker, than the average multiplicity (4.31) of the geodesic length spectrum.

On the other hand, the search for zeroes of the complex valued function $R(s)$ actually becomes a search for minima, due to the finite number of D-lengths taken into account. Thus towards higher energies the resolution of energy levels, which are very closed to each other, tends to be difficult. Even the decision of *how much* quantal energies are associated to a minimum becomes impossible, as opposed to the quantization rule based on $\xi(E)$. Based on Selberg's zeta function, however, a quantization rule can be derived, which amounts to the search of zeroes of a real valued function [7]. But rewriting (4.88) into a Dirichlet series, turns out to require the spectrum of pseudo-lengths, which proliferates even faster than the spectrum of D-lengths.

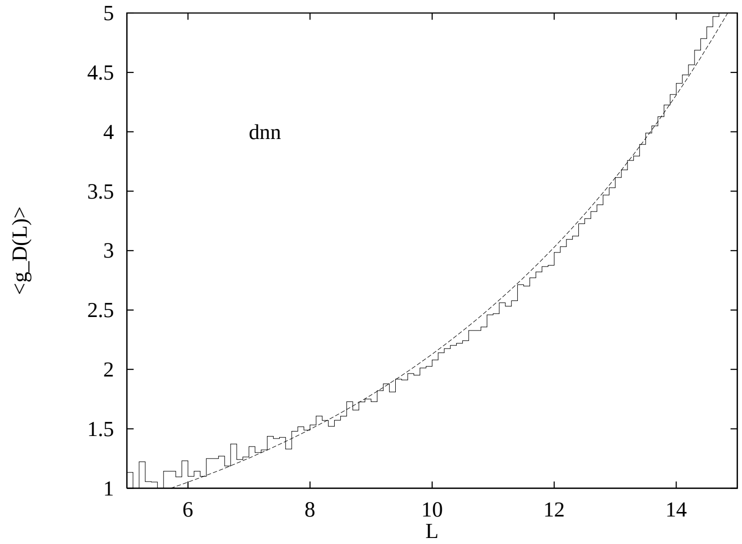

Figure 29: The average D-multiplicity $| < g_D(L) > |$ of $T^*(2,3,8)$ with boundary conditions "dnn" is shown together with the fit curve $de^{\alpha L}$.

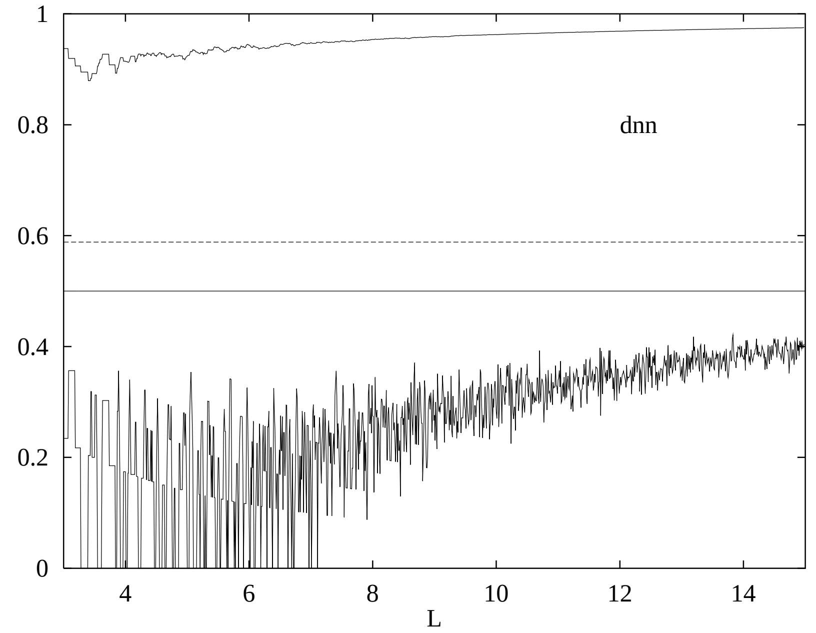

Figure 30: The numerical evaluations of the partial sums (4.91) for $T^*(2,3,8)$ with boundary conditions "dnn" are plotted as functions of the D-length L_N. The upper curve corresponds to σ_a, the lower one to σ_c. The critical line is indicated by the full horizontal line at $s = \frac{1}{2}$, whereas the prediction (3.89) from the statistical model is shown as a dashed line at $\sigma_c = 0.5883\ldots$.

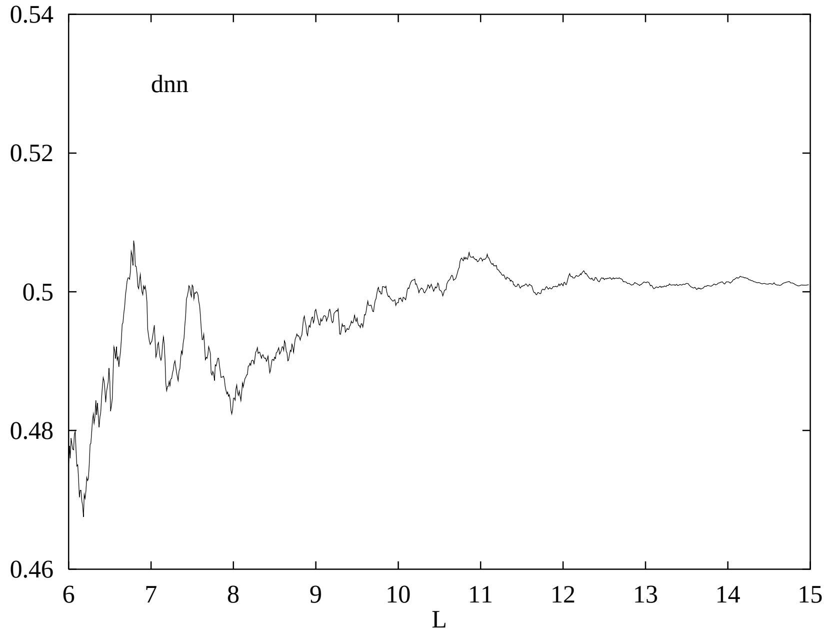

Figure 31: The probability of the effective multiplicity $g_D(L_{n+1})$ to have the same sign as $g_D(L_n)$ is shown for $T^*(2,3,8)$ with boundary conditions "dnn".

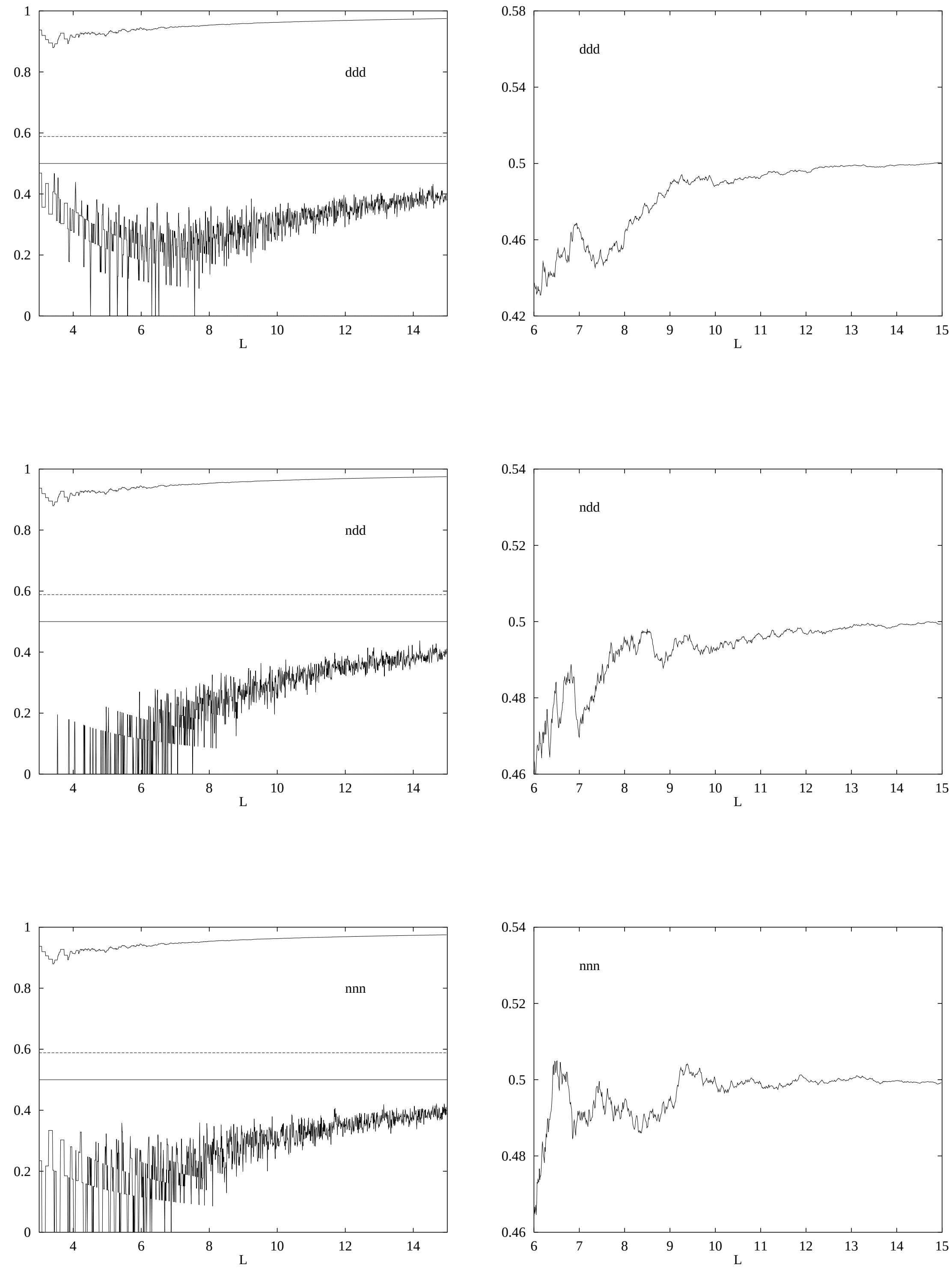

Figure 32: The same curves as in figs. 30 and 31 are shown for the remaining three combinations of boundary conditions obeying $\chi(M) = \chi(N)$.

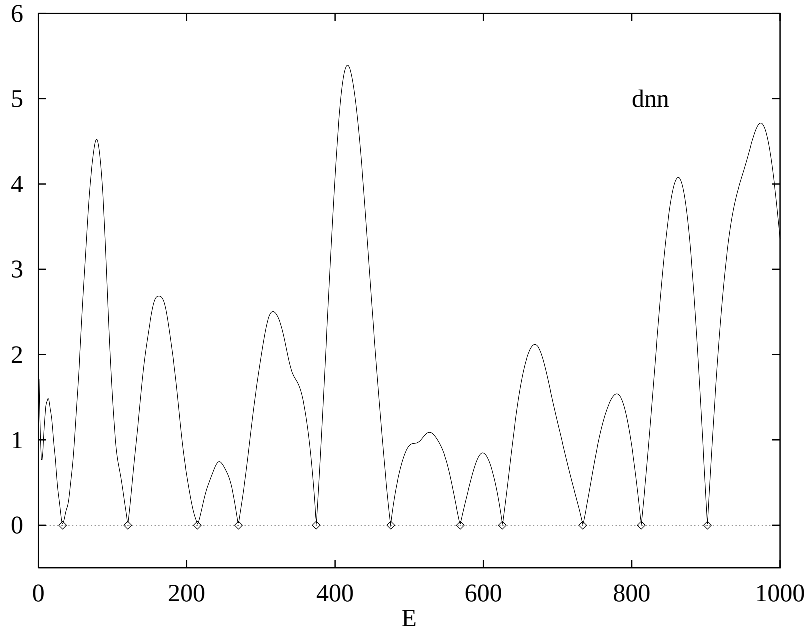

Figure 33: The absolute value of the Ruelle-type zeta function $|R(s)|$ for $T^*(2,3,8)$ with boundary conditions "dnn" is evaluated on the critical line as a function of $E = s(s-1)$, $E \in \mathbb{R}$, and compared with the energy eigenvalues obtained by the method of boundary elements.

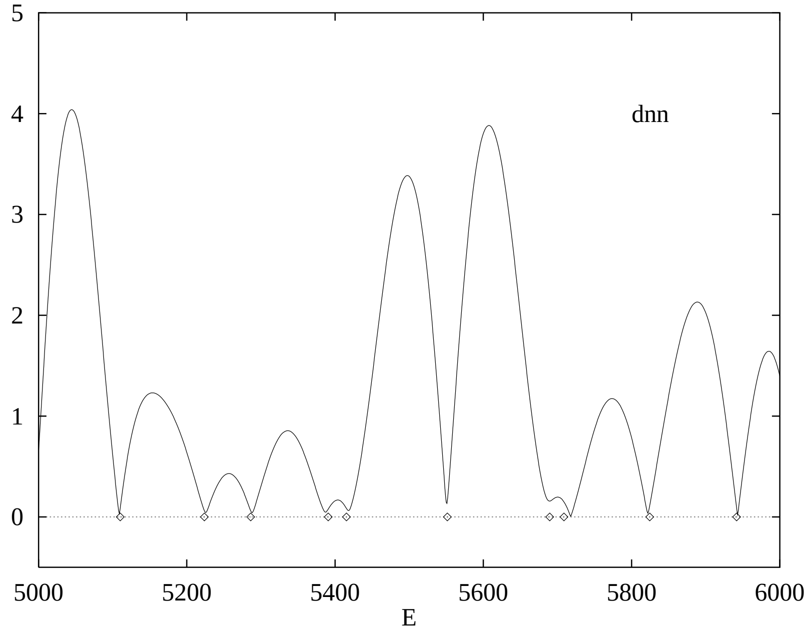

Figure 34: The same curve as in fig. 33 is shown above the 56th eigenvalue.

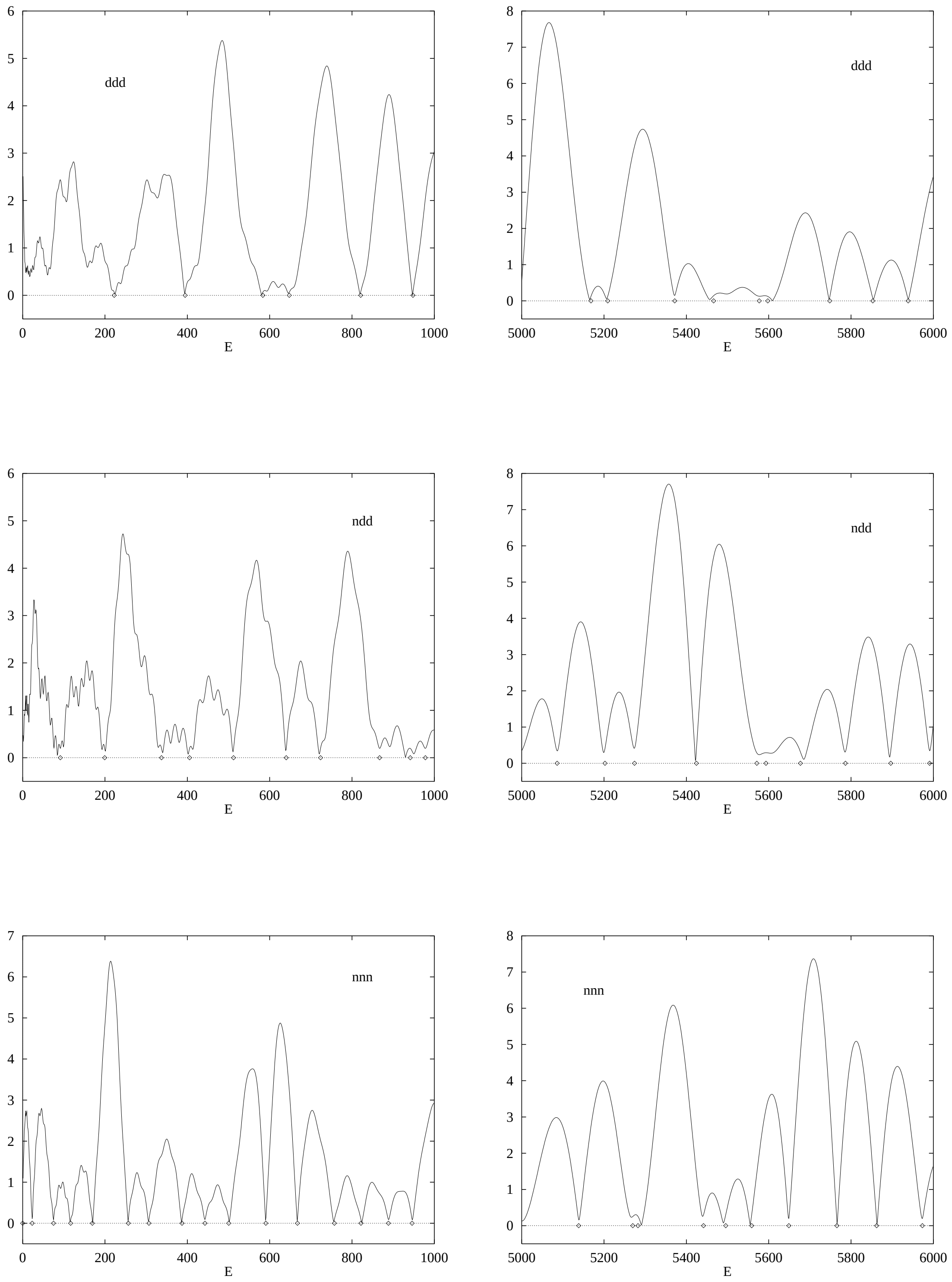

Figure 35: The same curves as in figs. 33 and 34 are shown for the remaining three combinations of boundary conditions.

4.5 Inverse Quantum Chaology

Substituting the smearing function $h(p)$ as defined in (3.90) into Selberg's trace formula (4.68) yields the trace of the cosine-modulated heat kernel for $T^*(2,3,8)$

$$
\begin{aligned}
&\sum_{n=0}^{\infty} \cos(p_n L)\, e^{-\left(p_n^2+\frac{1}{4}\right)t} \\
&\quad = e^{-\frac{t}{4}} \int_0^{\infty} \mathrm{d}p\, \cos(pL)\, e^{-p^2 t} \left\{ \frac{A}{2\pi}\, p\, \tanh(\pi p) + \frac{1}{4\pi} \sum_{\{I\}} \chi(I)\, l_{[I]} \right. \\
&\qquad\qquad \left. + \sum_{\{r\}} \sum_{k=1}^{m_r-1} \frac{\chi^k(r)}{4 m_r \sin\frac{\pi k}{m_r}}\, \frac{\cosh\left[\left(\frac{2k}{m_r}-1\right)\pi p\right]}{\cosh \pi p} \right\} \\
&\quad + \frac{e^{-\frac{t}{4}}}{16\sqrt{\pi t}} \sum_{\{\gamma_I\}} \sum_{k=1}^{\infty} \frac{\chi^k(\gamma_I)\, l_{\gamma_I}}{4} \left\{ \frac{1}{\sinh\frac{k l_{\gamma_I}}{2}} + \frac{\chi(I)}{\cosh\frac{k l_{\gamma_I}}{2}} \right\} \left\{ e^{-\frac{(L-kl_\gamma)^2}{4t}} + e^{-\frac{(L+kl_\gamma)^2}{4t}} \right\} \\
&\quad + \frac{e^{-\frac{t}{4}}}{4\sqrt{\pi t}} \sum_{\{\gamma_{\text{hyp}}\}} \sum_{k=1}^{\infty} \frac{\chi^k(\gamma)\, l_\gamma}{\exp\left(\frac{k l_\gamma}{2}\right) - \sigma^k(\gamma)\exp\left(-\frac{k l_\gamma}{2}\right)} \left\{ e^{-\frac{(L-kl_\gamma)^2}{4t}} + e^{-\frac{(L+kl_\gamma)^2}{4t}} \right\}. \qquad (4.95)
\end{aligned}
$$

Since the sums over hyperbolic conjugacy classes produce Gaussian peaks at the lengths l_γ of the closed geodesics on $T^*(2,3,8)\backslash\mathcal{D}$, relation (4.95) can be used as a consistency check for the numerically determined geodesic length spectrum of $T^*(2,3,8)$. Remember, that using a finite number of energy levels on the left-hand side of (4.95) has to be accounted for by adjusting the upper limit of integration (see the discussion in section 3.4).

Using geodesic lengths in the range $l_1 \le l_\gamma \le 18$ and the numerical solutions of Schrödinger's equation as mentioned in the previous section, both sides of (4.95) totally agree for boundary conditions subject to $\chi(M) = \chi(N)$. Since no differences can be observed graphically, fig. 36 only shows the sums over hyperbolic conjugacy classes in (4.95), calculated by the energy spectrum, for boundary conditions "dnn".

Due to the presence of inverse hyperbolic conjugacy classes, which introduce the quantity $\sigma^k(\gamma)$ in the periodic orbit sum, it is not possible to derive an expression for $N(l)$ from (4.95) along the lines described in the context of Gutzwiller's group.

4.6 Pseudoarithmetical Triangles

Since the equivalence of the boundary conditions along edges M and N of the fundamental domain of $T^*(2,3,8)$ essentially entered the derivation of Selberg's trace formula, the latter cannot be expected to hold for the pseudoarithmetical case, i.e., $\chi(M) \neq \chi(N)$. However, the Selberg trace formula can then be conjectured to be part of a semiclassical approximation, since the zero-length term and the periodic orbit sums in (4.68) are present in Gutzwiller's trace formula, too. Evaluating the trace of the cosine-modulated heat kernel for boundary conditions subject to $\chi(M) \neq \chi(N)$ shows, that quantum mechanical and classical side of (4.95) disagree (fig. 37). Thus additional terms are missing, which will be investigated in the following.

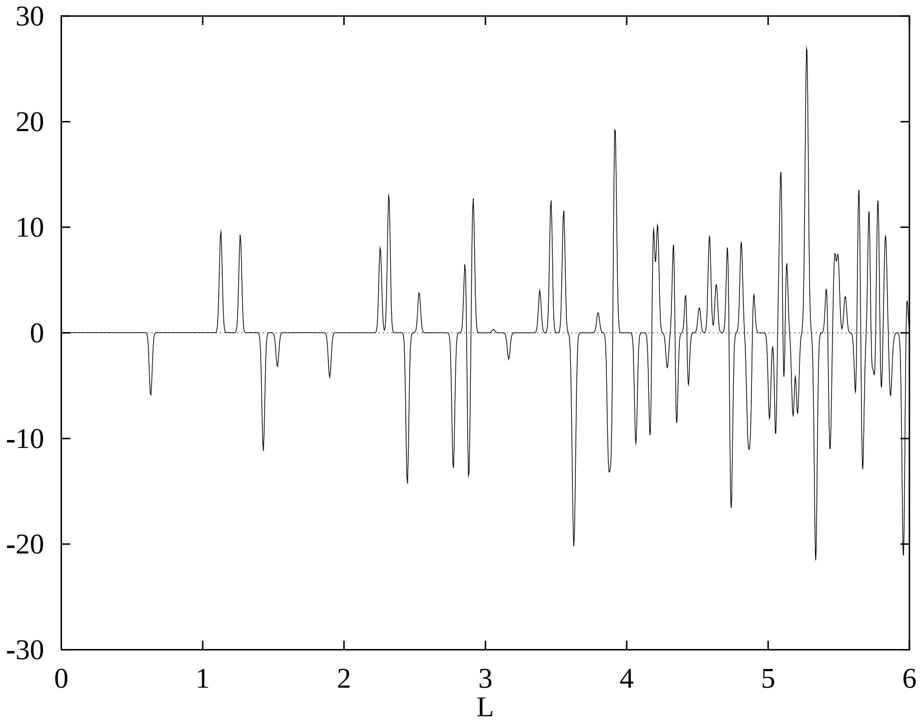

Figure 36: The sums over hyperbolic conjugacy classes of the trace of the cosine-modulated heat kernel for $T^*(2,3,8)$ with boundary conditions "dnn" is calculated by using the energy spectrum in the range $0 \le E_n \le 100000$. The parameter t has been chosen as $t = 0.00005$.

The first term of Selberg's trace formula, which is based on the assumption $\chi(M) = \chi(N)$, is the sum over inversion conjugacy classes. Here the fact, that M and N belong to the same conjugacy class led to the introduction of lengths $l_{[I]}$ of boundary segments, which are delimited by even vertices. One may, however, turn the sum over inversion *conjugacy classes* into a sum over the inversions itself

$$\sum_I \frac{\chi(I)\, l_I}{4}\, \hat{h}(0). \tag{4.96}$$

If the characters $\chi(I)$ are defined to be $+1$ or -1 according to Neumann or Dirichlet boundary conditions along the edge associated to I, and the l_I are the lengths of this edge, substituting into (4.86) reproduces the boundary contribution in Weyl's law for general billiards, which is in the special case of the hyperbolic billiard $T^*(2,3,8)$

$$\mathcal{N}(E) = \cdots + \frac{\chi(L)\, l_L + \chi(M)\, l_M + \chi(N)\, l_N}{4\pi}\sqrt{E} + \cdots \quad . \tag{4.97}$$

The next term, which has to be adjusted, is the sum over elliptic conjugacy classes. It has been observed [10], that using $\mathcal{N}(E)$ as derived from Selberg's trace formula in (4.86), leads to a constant contribution in Weyl's law, which does not agree with the value obtained from fitting the numerical solutions of Schrödingers equation. Thus one is pointed to the contribution of the vertex with angle $\frac{\pi}{3}$, which is associated to the elliptic element MN not allowing a unique definition of the character χ.

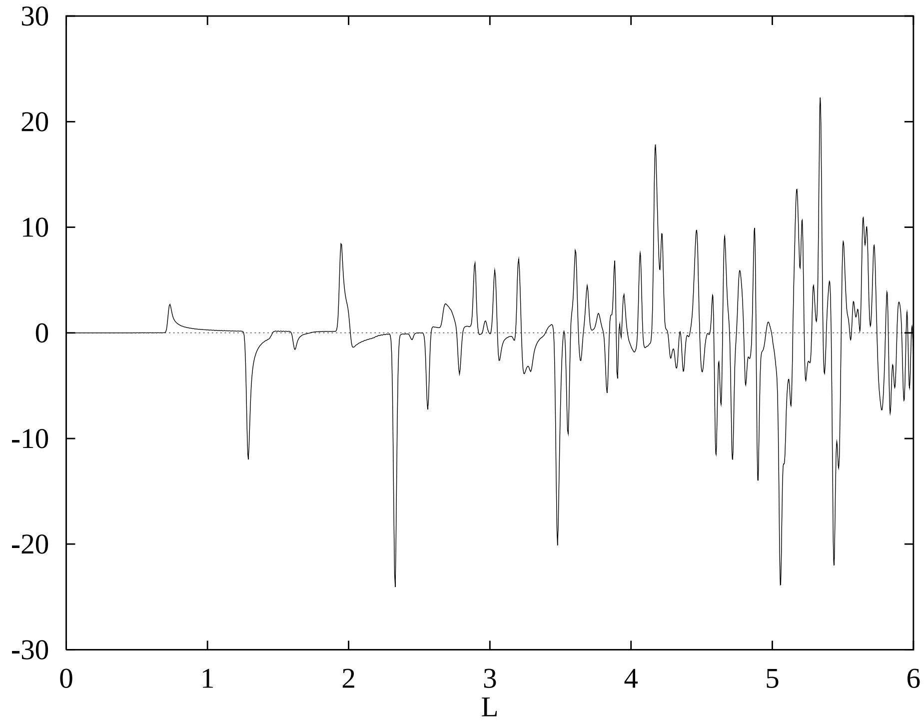

Figure 37: The difference between quantum mechanical side and classical side of the trace of the cosine-modulated heat kernel (4.95) is shown for $T^*(2,3,8)$ with boundary conditions "nnd", which do *not* obey $\chi(M) = \chi(N)$. The parameter t has been chosen as $t = 0.00005$.

Denoting the constant contribution of the elliptic term corresponding to a vertex of angle $\varphi = \frac{2\pi}{m_r}$ as E_φ, it can be shown from Selberg's trace formula, that [17]

$$E_\varphi = \frac{1}{24}\left(m_r - \frac{1}{m_r}\right), \qquad m_r \in \mathbb{N}, \tag{4.98}$$

if the boundary conditions along the edges adjacent to the vertex under consideration are chosen to be equivalent. It is, moreover, known that (4.98) even holds for possibly nonintegral m_r [18]. Assuming, that the contribution E_φ is additively composed by contributions $E_{\frac{\varphi}{n}}$ from fractional parts of the inner angle of the vertex [51], relation (4.98) may be used to determine $E_{\frac{\pi}{3}}$ for $T^*(2,3,8)$ in the pseudoarithmetical case. For this purpose consider a vertex with angle $\frac{2\pi}{3}$, where the boundary conditions along the adjacent edges are chosen to be Neumann. This vertex is composed by two vertices of angle $\frac{\pi}{3}$, but for the latter only the boundary condition along *one* edge is fixed (cf. fig. 38). The boundary condition along the inner edge may be chosen to be Dirichlet *or* Neumann, thus one is led to

$$E^{\mathrm{nn}}_{\frac{2\pi}{3}} = E^{\mathrm{nn}}_{\frac{\pi}{3}} + E^{\mathrm{dn}}_{\frac{\pi}{3}}. \tag{4.99}$$

Using relation (4.98) then reveals

$$E^{\mathrm{dn}}_{\frac{\pi}{3}} = -\frac{11}{144}. \tag{4.100}$$

Replacing the constant contribution of the elliptic conjugacy class $[MN]$ in (4.86) by $E^{\mathrm{dn}}_{\frac{\pi}{3}}$ and taking into account the modified inversion term (4.96) leads to the asymptotic behavior

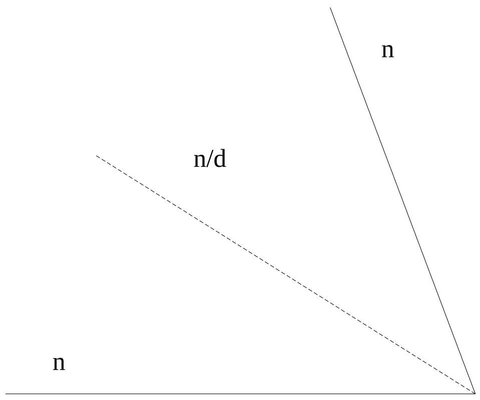

Figure 38: A vertex with fixed boundary conditions along the adjacent edges allows two choices of boundary conditions for the two composing sectors.

of the spectral staircase $\mathcal{N}(E)$ in the limit $E \to \infty$ for $T^*(2,3,8)$ with boundary conditions subject to $\chi(M) \neq \chi(N)$

$$\mathcal{N}(E) = \frac{A}{4\pi} E + \frac{\chi(L)\, l_L + \chi(M)\, l_M + \chi(N)\, l_N}{4\pi} \sqrt{E} - \frac{1 + 108\, \chi(LM)}{576} + \cdots . \tag{4.101}$$

Comparing the constant contributions for all pseudoarithmetical combinations of boundary conditions with the values obtained by fitting the numerical solutions of Schrödinger's equation along the same lines as in section 4.4 yields a reasonably good agreement (table 6). It must be pointed out again, that the fit value corresponding to boundary conditions "nnd" is the most reliable one, since it is based on five times as much of energy eigenvalues than the values for the remaining combinations of boundary conditions.

boundary condition	dnd	ndn	ddn	nnd
$\sigma_{\text{theor.}}$	+0.1857	+0.1857	-0.1892	-0.1892
σ_{fit}	+0.231	+0.229	-0.146	-0.188

Table 6: Constant in Weyl's law (pseudoarithmetic case).

However, additional contributions must be present in a semiclassical trace formula for $T^*(2,3,8)$ with boundary conditions subject to $\chi(M) \neq \chi(N)$, since despite adjusting Selberg's trace formula as described above, both sides of the trace of the cosine-modulated heat kernel (4.95) still disagree. This disagreement may be understood by a contribution arising as follows. Assume, a periodic orbit hits an even vertex, say Q in fig. 18. Then all those orbits just missing to hit Q are either reflected first at the edge M and afterwards at the edge L or in reverse order, as can be seen from the tessellation picture fig. 19. Since $\chi(LM) = \chi(ML)$, even in the pseudoarithmetical case, possibly different boundary conditions along the edges adjacent to Q do not introduce a discontinuous behavior at Q. The situation changes, however, for an orbit hitting an odd vertex, say P in fig. 18. Then the neighbored trajectories either bounce at the edges M, N and M or at N, M and N, thus introducing a discontinuous behavior by $\chi(MNM) \neq \chi(NMN)$. One may now suspect, that this peculiarity causes the stationary phase argument in the derivation of Gutzwiller's trace formula [33] to break down. The stationary phase argument selects those orbits to contribute, which are periodic in *phase space*, as opposed to those, which are just closed in the *configuration space*.

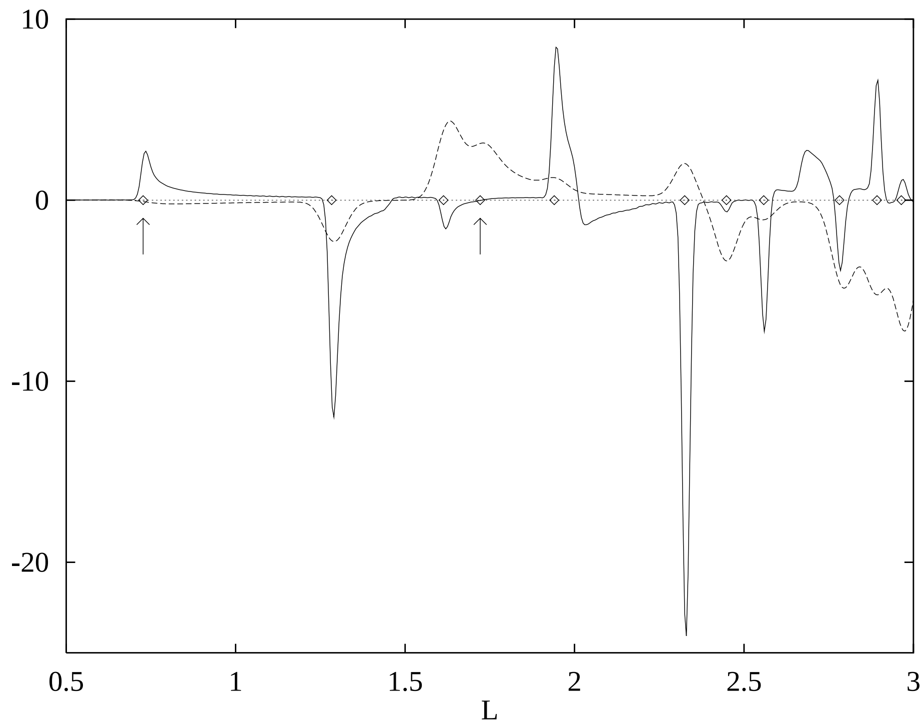

Figure 39: The differences of both sides of (4.95) are shown for boundary conditions "nnd" (solid) and "ndn" (dashed). The dots indicate geodesic lengths of non-periodic orbits passing the corner with angle $\frac{\pi}{3}$ of the fundamental domain of $T^*(2,3,8)$.

Thus in the case of $T^*(2,3,8)$, closed, but non-periodic orbits, which pass the vertex with angle $\frac{\pi}{3}$ may contribute to a semiclassical trace formula if the boundary conditions are subject to $\chi(M) \neq \chi(N)$. In fig. 39 the difference between quantum mechanical side and classical side of the trace of the cosine-modulated heat kernel (4.95) as derived from Selberg's trace formula is plotted for two combinations of boundary conditions, namely "nnd" and "ndn", together with the geodesic lengths of the non-periodic orbits described above. The latter can be easily generated by calculating the geodesic distance $d(z_Q, \gamma z_Q)$ between the vertex Q and its images under the operation of all group elements $\gamma \in T^*(2,3,8)$. The positions of the peaks coincide quite well with this set of lengths. The two marked lengths correspond to double traversals of the edges M and N, which are *no* periodic orbits (compare the discussion of boundary orbits in section 4.3). Whereas the orbit along edge M only contributes for boundary conditions "nnd", the orbit along edge N only does for the case "ndn". Thus, contributions of non-periodic boundary orbits along edges with Dirichlet boundary conditions seem to vanish. This behavior can be compared with "true" boundary orbits associated to an edge with Dirichlet boundary condition, for which the contribution to Selberg's trace formula is exponentially small (cf. (4.68)). Extending Gutzwiller's trace formula in order to explain the contribution of non-periodic orbits *quantitatively*, however, seems to be impossible analytically, due to the complicated structure of the hyperbolic distance $d(z_Q, \gamma z_Q)$ (cf. (2.7)), as compared with geodesic lengths related to traces of group matrices.

5 Summary

Two objectives have been attacked in this paper. The first one was the numerical investigation of quantization rules based on the Selberg trace formula with respect to their accuracy and applicability to particular chaotic systems. In the more general context, it is Gutzwiller's trace formula, which establishes a semiclassical relation between the quantal energy spectrum and the spectrum of classical periodic orbits of a given chaotic system. Thus Gutzwiller's trace formula can be considered to be a substitute for the semiclassical EBK quantization rule, which applies to integrable systems only. For a special class of dynamical systems, namely, the geodesic flow on surfaces of constant negative curvature, Gutzwiller's trace formula turns into an exact identity, known as the Selberg trace formula. Within the class of chaotic systems, those obeying Selberg's trace formula are the prototype examples for studying quantization rules, since they do not suffer from unknown contributions in higher orders of Planck's constant $\hbar$.

Two particular dynamical systems were investigated in this work. One of them is the free motion of a point-particle on the Riemann surface of genus $g = 2$, which is generated by Gutzwiller's group. The other dynamical system is the hyperbolic triangle billiard $T^*(2,3,8)$. Since it is generated by a reflection group, the influence of the boundary and of the vertices on the quantization procedure has to be treated carefully. The hyperbolic triangle group $T^*(2,3,8)$ already arose in the context of the investigation of the regular octagon group, and it has been pointed out before [5], that according to different choices of boundary conditions the quantal energy statistics may differ completely. This fact led to the second aim of this paper, which was the examination of the different behavior of quantized systems arising from *one* classical dynamical system from the point of view of classical quantities entering semiclassical quantization rules.

In detail the content of this work can be summarized as follows. After briefly reviewing the relevant aspects of classical and quantum mechanics of dynamical systems associated to hyperbolic surfaces, Gutzwiller's octagon was investigated in chapter 3 as the first model. It was found to be the fundamental domain of a particular compact Riemann surface of genus $g = 2$. According to the choice of identifications of the edges, however, different fundamental domains result, each representing the same Riemann surface. Due to the arithmetical nature of Gutzwiller's group Γ_{GW}, the group elements have been specified explicitly as 2×2 matrices with entries, which are algebraic numbers obeying particular restrictions. Subsequently, this property has been used to derive the average multiplicity of the geodesic length spectrum. Moreover, the explicit knowledge of the group matrices was the main ingredient to an algorithm, which allows to calculate the multiplicities of the geodesic length spectrum up to some cutoff length $\mathcal{L}$ completely. Numerically, the geodesic length spectrum has been determined up to $\mathcal{L} \simeq 18$, covering more than 4 million closed geodesics on $\Gamma_{\mathrm{GW}} \backslash \mathcal{D}$.

Two quantization rules based on Selberg's trace formula have then been investigated by using the numerically determined geodesic length spectrum as input data. The first one results from an approximation of the spectral staircase $\mathcal{N}(E)$. For a given cutoff length $\mathcal{L}$ of the geodesic length spectrum, the accuracy of the obtained quantal energy eigenvalues is mainly limited by the area of the dynamical system under consideration. The second method relies on the examination of Selberg's zeta function $Z(s)$, whose nontrivial zeroes on the critical line $\mathrm{Re}\, s = \frac{1}{2}$ are related to the quantal energies. Since the Euler product representation of $Z(s)$ does not converge on the critical line, it is rearranged into a Dirichlet series, which may improve the convergence properties. The price to be paid, however, is a combinatorial effort, since then pseudo-orbits enter the classical side of a quantization rule, instead of the geodesic length spectrum itself. The combinatorial effort can be somewhat reduced by considering the Ruelle-type zeta function, which possesses the same zeroes as $Z(s)$ on the critical line, and can be calculated by use of D-orbits. For the particular case of the Gutzwiller group, however, no convergence is achieved on the critical line, thus this quantization rule fails to apply.

Concluding the treatment of Gutzwiller's octagon, Selberg's trace formula has been used to extract information about the geodesic length spectrum by the spectrum of quantal energies, which has been calculated by numerically solving Schrödinger's equation using the method of finite elements [4]. Two methods have been used, one relying on the trace of the cosine-modulated heat kernel, the other on the calculation of the classical staircase function $N(l)$. Within the limits of numerical errors, no discrepancies were observed, confirming the geodesic length spectrum calculated before.

The triangular billiard $T^*(2,3,8)$ was investigated as the second model in chapter 4. Whereas the "boundary" of the fundamental domain of a strictly hyperbolic Fuchsian group is merely of artificial nature, vanishing by the identification of the edges according to *periodic* boundary conditions, the fundamental domain of a reflection group possesses a true boundary. Due to this property, in reflection groups several classes of group elements arise in addition to hyperbolic ones. Inversions are associated to reflections at the edges, elliptic elements correspond to rotations around a vertex of the fundamental domain, and hyperbolic elements have to be distinguished according to the number of reflections at the boundary. Studying the properties of the hyperbolic triangle group $T^*(2,3,8)$, the arithmeticity can be used to derive an explicit representation of the group elements as 2×2 matrices with algebraic entries along the same lines as for Γ_{GW}. However, the algebraic restrictions for group elements of $T^*(2,3,8)$ seem to be more intricate than for the case of Gutzwiller's group.

For this reason the geodesic length spectrum of $T^*(2,3,8)$ has been calculated by building group elements as products of an efficient set of generators and properly separating a unique representative for each conjugacy class. Due to the presence of edges of the fundamental domain, a quantization procedure requires the specification of boundary conditions along the edges. Thus the classical triangular billiard $T^*(2,3,8)$ gives rise to eight different quantized systems. The boundary conditions are incorporated in the transformation behavior of the wave functions by introducing characters $\chi(\gamma)$. However, two situations may arise. Either the choice of boundary conditions is compatible with the group structure, thus allowing $\chi(\gamma)$ to be a one-dimensional unitary representation of $T^*(2,3,8)$. In that case, the so-called arithmetical case, the characters are invariants of conjugacy classes and can be easily determined. Otherwise, in the "pseudoarithmetical" case, the representatives of the conjugacy classes have to be used to construct the corresponding periodic orbits as a set of geodesic segments inside the previously fixed fundamental domain. The characters can then be derived from the actual "physical" reflections at the boundary of the domain of motion, i.e., in the same way they are defined for generic systems obeying Gutzwiller's trace formula.

Subsequently, a generalized Selberg trace formula was derived, which applies to polygonal hyperbolic billiards with mixed boundary conditions. The existence of a one-dimensional unitary representation compatible with the chosen set of boundary conditions essentially entered the proof, thus for the case of $T^*(2,3,8)$ only those quantized systems are subject to Selberg's trace formula, which result from the desymmetrization procedure of the regular octagon group. For this class of systems, afterwards, the same quantization rules were investigated as for Gutzwiller's group Γ_{GW}. Due to the small area of the fundamental domain of $T^*(2,3,8)$ a much larger range of energy eigenvalues has been resolved with a high degree of accuracy by the method relying on the spectral staircase $\mathcal{N}(E)$. In contrast to the case of $\Gamma_{\rm GW}$, the quantization rule based on examining the zeroes of the Ruelle-type zeta function $R(s)$ applies for $T^*(2,3,8)$. However, the combinatorial effort in order to determine the spectrum of D-orbits increases much more rapidly, due to the presence of comparatively short geodesic lengths. Moreover, the zeta function quantization using $R(s)$ suffers from the impossibility to resolve energy eigenvalues which are very close to each other.

Finally, the trace of the cosine-modulated heat kernel has been used to check the consistency between the numerically determined geodesic length spectrum and the quantal energy spectrum [5, 48]. For the four choices of boundary conditions leading to arithmetical systems, no discrepancies could be observed. In the pseudoarithmetical case, the Selberg trace formula was not expected to apply. But interpreting Selberg's trace formula as part of a generalized Gutzwiller trace formula, the difference between quantum mechanical and classical side of the trace of the cosine-modulated heat kernel has been investigated to obtain hints for the nature of the additional contributions. The terms corresponding to edges and vertices of the fundamental domain arising in Selberg's trace formula have been adjusted to agree with the behavior predicted by Weyl's asymptotic law for the spectral staircase $\mathcal{N}(E)$. The remaining contributions seem to originate from non-periodic orbits, which are however not incorporated in the form of Gutzwiller's trace formula known so far. A similar observation has been made recently for the truncated hyperbola billiard, which has a finite area [38]. Thus the difference between the spectral statistics of the two classes of quantized systems associated to $T^*(2,3,8)$ can be understood from the classical point of view by the applicability of Selberg's trace formula. In the arithmetical case Selberg's trace formula applies, being a special case of Gutzwiller's trace formula. In the pseudoarithmetical case, however, a new class of orbits arises, which contribute due to the subtle combination of boundary conditions.

Acknowledgements

It is a pleasure to thank Professor Frank Steiner for many valuable discussions and for his continuous encouragement throughout the time I have been his student.

I also like to thank Ralf Aurich, Guido Beneke, Jens Bolte, Matthias Schmidt and Martin Sieber for many useful discussions. Furthermore I am grateful to Ralf Aurich and Frank Scheffler, who generously supplied me with their numerical data.

I acknowledge financial support by the University of Hamburg, the Studienstiftung des deutschen Volkes and the Deutsche Forschungsgemeinschaft DFG.

A General Structure of Group Matrices in Γ_{GW}

In order to prove the relations (3.21sqq) characterizing the matrix entries of an arbitrary element $\gamma \in \Gamma_{\mathrm{GW}}$ of Gutzwiller's group one proceeds in three steps.

At first, note that the generators $a_\nu, b_\nu \in \Gamma_{\mathrm{GW}}$ of Gutzwiller's group are related to the generators $g_k^{\pm 1} \in \Gamma_{\mathrm{reg}}$ of the regular octagon group by

$$\begin{aligned} a_1 &= R_{\frac{\pi}{2}}\, g_0^{-1} = g_2^{-1} R_{\frac{\pi}{2}}, \\ b_1 &= R_{-\frac{\pi}{2}}\, g_3 = g_1\, R_{-\frac{\pi}{2}}, \\ a_2 &= R_{\frac{\pi}{2}}\, g_0 = g_2\, R_{\frac{\pi}{2}}, \\ b_2 &= R_{-\frac{\pi}{2}}\, g_3^{-1} = g_1^{-1} R_{-\frac{\pi}{2}}, \end{aligned} \tag{A.1}$$

and similarly for their inverses. Thus the rotations $R_{\pm\frac{\pi}{2}}$ "commute" with the generators of the regular octagon group in the sense, that for any $R_{\pm\frac{\pi}{2}}\, g_k^{\pm 1}$ a $g_l^{\pm 1}$ can be found, such that $R_{\pm\frac{\pi}{2}}\, g_k^{\pm 1} = g_l^{\pm 1} R_{\pm\frac{\pi}{2}}$. Furthermore, also the rotations $R_{\pm\pi}$ "commute" with the generators of the regular octagon group

$$R_{\pm\pi}\, g_k^{\pm 1} = g_k^{\mp 1}\, R_{\pm\pi}, \tag{A.2}$$

and obviously with the rotations $R_{\pm\frac{\pi}{2}}$ too. Therefore any element $\gamma_{\mathrm{GW}} \in \Gamma_{\mathrm{GW}}$ may be written as a product of generators $g_k^{\pm 1}$ of the regular octagon group and a number of rotations $R_{\frac{\pi}{2}}$, all commuted to the right (cf. 3.20)

$$\gamma_{\mathrm{GW}} = \gamma_{\mathrm{reg}}\, R_{\frac{k\pi}{2}}, \qquad k = 0, 1, 2, 3. \tag{A.3}$$

According to this relation, matrices $\gamma_1 \in \Gamma_{\mathrm{GW}}$ composed of an even number of generators are either of the form

$$\gamma_1 = \gamma_{\mathrm{reg}} \tag{A.4}$$

or

$$\gamma_1 = \gamma_{\mathrm{reg}}\, R_\pi = \begin{pmatrix} -u_I + iu_R & (v_I - iv_R)\alpha \\ (v_I + iv_R)\alpha & -u_I - iu_R \end{pmatrix}. \tag{A.5}$$

In the first case $\gamma_1 \in \Gamma_{\mathrm{GW}}$ obeys the same restrictions (3.12) and (3.13) as group matrices of the regular octagon group Γ_{reg}, whereas in the second case the roles of real and imaginary part are reversed. Thus even group matrices $\gamma_1 \in \Gamma_{\mathrm{GW}}$ share the same algebraic decomposition of their entries (3.23) as elements $\gamma_{\mathrm{reg}} \in \Gamma_{\mathrm{reg}}$ and are subject to

$$\pi(m_{1,I}) \neq \pi(m_{1,R}), \quad \pi(p_{1,R}) = \pi(p_{1,I}). \tag{A.6}$$

Elements $\gamma_2 \in \Gamma_{\mathrm{GW}}$ being a product of an odd number of generators can be written as

$$\gamma_2 = \gamma_{\mathrm{reg}}\, R_{\pm\frac{\pi}{2}} = \begin{pmatrix} u_R + iu_I & (v_R + iv_I)\alpha \\ (v_R - iv_I)\alpha & u_R - iu_I \end{pmatrix} \begin{pmatrix} (1 \pm i)\frac{\sqrt{2}}{2} & 0 \\ 0 & (1 \mp i)\frac{\sqrt{2}}{2} \end{pmatrix} \tag{A.7}$$

leading to

$$\begin{aligned} u_{2,R} &= (u_R \mp u_I)\tfrac{\sqrt{2}}{2} = n_R \mp n_I + (m_R \mp m_I)\tfrac{\sqrt{2}}{2}, \\ u_{2,I} &= (u_I \pm u_R)\tfrac{\sqrt{2}}{2} = n_I \pm n_R + (m_I \pm m_R)\tfrac{\sqrt{2}}{2}, \\ v_{2,R} &= (v_R \pm v_I)\tfrac{\sqrt{2}}{2} = q_R \pm q_I + (p_R \pm p_I)\tfrac{\sqrt{2}}{2}, \\ v_{2,I} &= (v_I \mp v_R)\tfrac{\sqrt{2}}{2} = q_I \mp q_R + (p_I \mp p_R)\tfrac{\sqrt{2}}{2}. \end{aligned} \tag{A.8}$$

Since matrices of the regular octagon group $\Gamma_{\rm reg}$ obey

$$\pi(m_R) \neq \pi(m_I), \quad \pi(p_R) = \pi(p_I), \tag{A.9}$$

the algebraic decomposition (3.25) follows from (A.8), and the entries of odd group matrices $\gamma_2 \in \Gamma_{\rm GW}$ are restricted by

$$\begin{aligned} \pi(m_{2,R}) &= \pi(m_{2,I}), \\ \pi(n_{2,R}) &= 1 = \pi(n_{2,I}), \\ \pi(p_{2,R}) &= \pi(p_{2,I}). \end{aligned} \tag{A.10}$$

The second step consists in forming all possible products of general group matrices $\gamma_k \in \Gamma_{\rm GW}$ and generators $a_\nu^{\pm 1}, b_\nu^{\pm 1} \in \Gamma_{\rm GW}$ of Gutzwiller's group in the proper algebraically decomposed form. For the investigation of the resulting expressions the following relations, valid for arbitrary integers $x, y \in \mathbb{Z}$, will be useful

$$\pi(x) = \pi(y) = \left\{ \begin{array}{c} 0 \\ 1 \end{array} \right. \;\Rightarrow\; \pi\left[\tfrac{1}{2}(x+y)\right] \left\{ \begin{array}{c} = \\ \neq \end{array} \right\} \pi\left[\tfrac{1}{2}(x-y)\right] \;, \tag{A.11}$$

$$\pi(x) = \pi(y) = \left\{ \begin{array}{c} 0 \\ 1 \end{array} \right. \;\Rightarrow\; \pi\left[\tfrac{1}{2}(x^2+y^2)\right] = \left\{ \begin{array}{c} 0 \\ 1 \end{array} \right. \;, \tag{A.12}$$

$$\pi(x) \left\{ \begin{array}{c} = \\ \neq \end{array} \right\} \pi(y) \;\Rightarrow\; \pi(x^2+y^2) = \left\{ \begin{array}{c} 0 \\ 1 \end{array} \right. \;, \tag{A.13}$$

$$\pi(x) \neq \pi(y) \;\Rightarrow\; \pi\left[\tfrac{1}{2}(1-x^2-y^2)\right] = 0 \;. \tag{A.14}$$

Since from (3.15) it follows, that

$$\gamma_k\, a_2^{\pm 1} = \gamma_k\, R_\pi\, a_1^{\pm 1} R_{-\pi} = R_\pi\, \gamma_k'\, a_1^{\pm 1} R_{-\pi}, \tag{A.15}$$

where γ_k' denotes an element of $\Gamma_{\rm GW}$ usually different from γ_k, and a analogous relation holds for $\gamma_k\, b_2^{\pm 1}$, only products $\gamma_k\, a_1^{\pm 1}$ and $\gamma_k\, b_1^{\pm 1}$ need to be considered explicitly. The remaining products $\gamma_k\, a_2^{\pm 1}$ and $\gamma_k\, b_2^{\pm 1}$ only differ by a conjugation by R_π, i.e., by the signs of the off-diagonal elements, thus yielding no further information. Using

$$\begin{pmatrix} a & b \\ c & d \end{pmatrix}^{-1} = \frac{1}{ad-bc} \begin{pmatrix} d & -b \\ -c & a \end{pmatrix}^{-1} \tag{A.16}$$

the generators $a_1^{\pm 1}, b_1^{\pm 1} \in \Gamma_{\rm GW}$ of Gutzwiller's group can be written as

$$\begin{aligned} a_1^{\pm 1} &= \begin{pmatrix} \left(1+\frac{\sqrt{2}}{2}\right)(1 \pm i) & \mp(1+\sqrt{2})(1+i)\,\alpha \\ \mp(1+\sqrt{2})(1-i)\,\alpha & \left(1+\frac{\sqrt{2}}{2}\right)(1 \mp i) \end{pmatrix}, \\ b_1^{\pm 1} &= \begin{pmatrix} \left(1+\frac{\sqrt{2}}{2}\right)(1 \mp i) & \pm(2+\sqrt{2})\,\alpha i \\ \mp(2+\sqrt{2})\,\alpha i & \left(1+\frac{\sqrt{2}}{2}\right)(1 \pm i) \end{pmatrix}. \end{aligned} \tag{A.17}$$

Now, four kinds of products have to be investigated:

(i) $\gamma_1 = \gamma_2\, a_1^{\pm 1}$, yielding

$$u_{1,R} + iu_{1,I} = (u_{2,R} + iu_{2,I})(1 \pm i)\left(1 + \tfrac{\sqrt{2}}{2}\right) \mp (v_{2,R} + iv_{2,I})(1 - i)(1 + \sqrt{2})\,\alpha^2, \tag{A.18}$$

thus

$$\begin{aligned} u_{1,R} &= m_{1,R} + n_{1,R}\sqrt{2} = (u_{2,R} \mp u_{2,I})\left(1 + \tfrac{\sqrt{2}}{2}\right) \mp (v_{2,R} + v_{2,I}), \\ u_{1,I} &= m_{1,I} + n_{1,I}\sqrt{2} = (u_{2,I} \pm u_{2,R})\left(1 + \tfrac{\sqrt{2}}{2}\right) \mp (v_{2,I} - v_{2,R}), \end{aligned} \tag{A.19}$$

and

$$\begin{aligned} n_{1,R} &= \tfrac{1}{2}(m_{2,R} \mp m_{2,I}) + \tfrac{1}{2}(n_{2,R} \mp n_{2,I}) \mp (q_{2,R} + q_{2,I}), \\ n_{1,I} &= \tfrac{1}{2}(m_{2,I} \pm m_{2,R}) + \tfrac{1}{2}(n_{2,I} \pm n_{2,R}) \mp (q_{2,I} - q_{2,R}). \end{aligned} \tag{A.20}$$

Since $\pi(n_{2,R}) = 1 = \pi(n_{2,I})$ relation (A.11) results in

$$\pi\left[\tfrac{1}{2}(n_{2,R} \mp n_{2,I})\right] \neq \pi\left[\tfrac{1}{2}(n_{2,R} \pm n_{2,I})\right], \tag{A.21}$$

therefore (A.20) forces

$$\pi(m_{2,R}) = \pi(m_{2,I}) = \left\{ \begin{array}{c} 0 \\ 1 \end{array} \right. \quad \Leftrightarrow \quad \pi(n_{1,R}) \left\{ \begin{array}{c} \neq \\ = \end{array} \right\} \pi(n_{1,I}) \ . \tag{A.22}$$

(ii) $\gamma_1 = \gamma_2\, b_1^{\pm 1}$, yielding

$$u_{1,R} + iu_{1,I} = (u_{2,R} + iu_{2,I})(1 \mp i)\left(1 + \tfrac{\sqrt{2}}{2}\right) \mp (v_{2,R} + iv_{2,I})\, i(2 + \sqrt{2})\,\alpha^2, \tag{A.23}$$

thus

$$\begin{aligned} u_{1,R} &= m_{1,R} + n_{1,R}\sqrt{2} = (u_{2,R} \mp u_{2,I})\left(1 + \tfrac{\sqrt{2}}{2}\right) \pm v_{2,I}\sqrt{2}, \\ u_{1,I} &= m_{1,I} + n_{1,I}\sqrt{2} = (u_{2,I} \mp u_{2,R})\left(1 + \tfrac{\sqrt{2}}{2}\right) \mp v_{2,R}\sqrt{2}, \end{aligned} \tag{A.24}$$

and

$$\begin{aligned} n_{1,R} &= \tfrac{1}{2}(m_{2,R} \pm m_{2,I}) + \tfrac{1}{2}(n_{2,R} \pm n_{2,I}) \pm p_{2,I}, \\ n_{1,I} &= \tfrac{1}{2}(m_{2,I} \mp m_{2,R}) + \tfrac{1}{2}(n_{2,I} \mp n_{2,R}) \mp p_{2,R}, \end{aligned} \tag{A.25}$$

also leading to (A.22) by use of $\pi(p_{2,R}) = \pi(p_{2,I})$.

(iii) $\gamma_2 = \gamma_1\, a_1^{\pm 1}$, yielding

$$u_{2,R} + iu_{2,I} = (u_{1,R} + iu_{1,I})(1 \pm i)\left(1 + \tfrac{\sqrt{2}}{2}\right) \mp (v_{1,R} + iv_{1,I})(1 - i)(1 + \sqrt{2})\,\alpha^2, \tag{A.26}$$

thus

$$\begin{aligned} u_{2,R} &= m_{2,R} + n_{2,R}\tfrac{\sqrt{2}}{2} = (u_{1,R} \mp u_{1,I})\left(1 + \tfrac{\sqrt{2}}{2}\right) \mp (v_{1,R} + v_{1,I}), \\ u_{2,I} &= m_{2,I} + n_{2,I}\tfrac{\sqrt{2}}{2} = (u_{1,I} \pm u_{1,R})\left(1 + \tfrac{\sqrt{2}}{2}\right) \pm (v_{2,R} - v_{1,I}), \end{aligned} \tag{A.27}$$

and

$$\begin{aligned} m_{2,R} &= (m_{1,R} \mp m_{1,I}) + (n_{1,R} \mp n_{1,I}) \mp (p_{1,R} + p_{1,I}), \\ m_{2,I} &= (m_{1,I} \pm m_{1,R}) + (n_{1,I} \pm n_{1,R}) \pm (p_{1,R} - p_{1,I}), \end{aligned} \tag{A.28}$$

again leading to (A.22) by (A.6).

(iv) $\gamma_2 = \gamma_1 \, b_1^{\pm 1}$, yielding

$$u_{2,R} + i u_{2,I} = (u_{1,R} + i u_{1,I})(1 \mp i) \left(1 + \tfrac{\sqrt{2}}{2}\right) \mp (v_{1,R} + i v_{1,I}) \, i (2 + \sqrt{2}) \, \alpha^2, \qquad \text{(A.29)}$$

thus

$$\begin{aligned} u_{2,R} &= m_{2,R} + n_{2,R} \tfrac{\sqrt{2}}{2} = (u_{1,R} \pm u_{1,I}) \left(1 + \tfrac{\sqrt{2}}{2}\right) \pm v_{1,I} \sqrt{2}, \\ u_{2,I} &= m_{2,I} + n_{2,I} \tfrac{\sqrt{2}}{2} = (u_{1,I} \mp u_{1,R}) \left(1 + \tfrac{\sqrt{2}}{2}\right) \mp v_{1,R} \sqrt{2}, \end{aligned} \qquad \text{(A.30)}$$

and

$$\begin{aligned} m_{2,R} &= (m_{1,R} \pm m_{1,I}) + (n_{1,R} \pm n_{1,I}) \pm 2 q_{1,I}, \\ m_{2,I} &= (m_{1,I} \mp m_{1,R}) + (n_{1,I} \mp n_{1,R}) \mp 2 q_{1,R}. \end{aligned} \qquad \text{(A.31)}$$

This case again yields (A.22), since $\pi(m_{1,R}) \neq \pi(m_{1,R})$.

Putting all together, incrementing the wordlength of an arbitrary $\gamma \in \Gamma_{\mathrm{GW}}$ is always subject to the relation (A.22). Since, however, all generators $a_1, b_1, a_2, b_2 \in \Gamma_{\mathrm{GW}}$ and their inverses fulfill $\pi(m_{2,R}) = 1$, general group matrices $\gamma_k \in \Gamma_{\mathrm{GW}}$ obey

$$\begin{aligned} \pi(m_{2,R}) &= 1, \\ \pi(n_{1,R}) &= \pi(n_{1,I}). \end{aligned} \qquad \text{(A.32)}$$

The final step takes advantage of the determinant condition

$$\det \gamma_k = 1, \qquad \forall \gamma_k \in \Gamma_{\mathrm{GW}}, \qquad \text{(A.33)}$$

or explicitly

$$u_{k,R}^2 + u_{k,I}^2 - (\sqrt{2} - 1)(v_{k,R}^2 + v_{k,I}^2) = 1. \qquad \text{(A.34)}$$

Applying an algebraic conjugation results in

$$\tilde{u}_{k,R}^2 + \tilde{u}_{k,I}^2 + (\sqrt{2} + 1)(\tilde{v}_{k,R}^2 + \tilde{v}_{k,I}^2) = 1, \qquad \text{(A.35)}$$

leading to

$$\begin{aligned} |\tilde{u}_{k,R}| &< 1, \quad |\tilde{u}_{k,I}| < 1, \\ |\tilde{v}_{k,R}| &< \alpha, \quad |\tilde{v}_{k,I}| < \alpha. \end{aligned} \qquad \text{(A.36)}$$

Inserting the algebraic decompositions of group matrices (3.23) and (3.25) into (A.34) yields two independent relations, an integer and an irrational part.

In the case of group elements $\gamma_1 \in \Gamma_{\mathrm{GW}}$ being the product of an even number of generators the integer part turns out to be

$$2(n_{1,R}^2 + n_{1,I}^2) + p_{1,R}^2 + p_{1,I}^2 + 2(q_{1,R}^2 + q_{1,I}^2) - 4(p_{1,R}\, q_{1,R} + p_{1,I}\, q_{1,I}) = 1 - m_{1,R}^2 - m_{1,I}^2. \qquad \text{(A.37)}$$

By $\pi(p_{1,R}) = \pi(p_{1,I})$ and (A.13) one finds

$$\pi(p_{1,R}^2 + p_{1,I}^2) = 0, \qquad \text{(A.38)}$$

thus (A.37) can be multiplied by $\frac{1}{2}$. Since $\pi(m_{1,R}) \neq \pi(m_{1,I})$ relation (A.14) leads to

$$\pi \left[\tfrac{1}{2}(1 - m_{1,R}^2 - m_{1,I}^2) \right] = 0, \qquad \text{(A.39)}$$

therefore

$$\pi\left[n_{1,R}^2+n_{1,I}^2+\tfrac{1}{2}(p_{1,R}^2+p_{1,I}^2)+q_{1,R}^2+q_{1,I}^2\right]=0. \tag{A.40}$$

However, $\pi(n_{1,R})=\pi(n_{1,I})$ yields $\pi(n_{1,R}^2+n_{1,I}^2)=0$ by (A.13), leading to

$$\pi\left[\tfrac{1}{2}(p_{1,R}^2+p_{1,I}^2)\right]=\pi(q_{1,R}^2+q_{1,I}^2), \tag{A.41}$$

which can be rewritten as

$$\pi(p_{1,R})=\pi(p_{1,I})=\begin{cases}0 & \Rightarrow \quad \pi(q_{1,R})=\pi(q_{1,I})\\ 1 & \Rightarrow \quad \pi(q_{1,R})\neq\pi(q_{1,I})\end{cases} \tag{A.42}$$

by using (A.12) and (A.13). From (A.40) and (A.41) one finds

$$\pi(n_{1,R}^2+n_{1,I}^2)=\pi\left[\tfrac{1}{2}(p_{1,R}^2+p_{1,I}^2)+q_{1,R}^2+q_{1,I}^2\right]=\pi(p_{1,R}^2+p_{1,I}^2)=0. \tag{A.43}$$

Multiplying by $\frac{1}{2}$ yields

$$\pi\left[\tfrac{1}{2}(n_{1,R}^2+n_{1,I}^2)\right]=\pi\left[\tfrac{1}{2}(p_{1,R}^2+p_{1,I}^2)\right], \tag{A.44}$$

unraveling

$$\pi(p_{1,R})=\pi(n_{1,R}) \tag{A.45}$$

by use of (A.12).

Turning to the case of odd group elements $\gamma_2\in\Gamma_{\mathrm{GW}}$, the integer part of the determinant condition (A.34) can be found to be

$$m_{2,R}^2+m_{2,I}^2+p_{2,R}^2+p_{2,I}^2+2(q_{2,R}^2+q_{2,I}^2)-4(p_{2,R}\,q_{2,R}+p_{2,I}\,q_{2,I})=1-\tfrac{1}{2}(n_{2,R}^2+n_{2,I}^2). \tag{A.46}$$

Since $\pi(n_{2,R})=\pi(n_{2,I})=1$ the right-hand side is even by (A.12), i.e., (A.46) can be multiplied by $\frac{1}{2}$ yielding

$$\pi\left[\tfrac{1}{2}(m_{2,R}^2+m_{2,I}^2)+\tfrac{1}{2}(p_{2,R}^2+p_{2,I}^2)+q_{2,R}^2+q_{2,I}^2\right]=0, \tag{A.47}$$

which can be rewritten as

$$\pi\left[\tfrac{1}{2}(p_{2,R}^2+p_{2,I}^2)\right]\neq\pi(q_{2,R}^2+q_{2,I}), \tag{A.48}$$

by using

$$\pi\left[\tfrac{1}{2}(m_{2,R}^2+m_{2,I}^2)\right]=1, \tag{A.49}$$

resulting from $\pi(m_{2,R})=1=\pi(m_{2,I})$ and (A.12). Finally, by use of (A.12) and (A.13) one finds

$$\pi(p_{2,R})=\pi(p_{2,I})=\begin{cases}0 & \Rightarrow \quad \pi(q_{2,R})\neq\pi(q_{2,I})\\ 1 & \Rightarrow \quad \pi(q_{2,R})=\pi(q_{2,I})\end{cases} \tag{A.50}$$

from (A.48).

B General Structure of Group Matrices in $T^*(2,3,8)$

The outline of the proof of the relations (4.15sqq), which characterize arbitrary group elements $\gamma \in T^*(2,3,8)$ is follows. At first, the structure (4.15) of the two different kinds of matrices $\gamma_k \in T^*(2,3,8)$ is assumed to be true. Then the determinant condition

$$\det \gamma_k = 1, \qquad \forall \gamma_k \in T^*(2,3,8), \tag{B.1}$$

will be inspected to derive parity restrictions on the matrix entries of γ_k, which in turn will be used to show, that the structure (4.15) of matrices is conserved under multiplication with a generator of $T^*(2,3,8)$.

Throughout the calculations, the following two statements will be of some use.

Let $x_1, x_2, y_1, y_2 \in \mathbb{Z}$ be integer numbers subject to

$$\pi(x_1) = \pi(x_2). \tag{B.2}$$

(i) If the x_i are connected to y_i by

$$\pi(x_1) = \left\{ \begin{array}{c} 0 \\ 1 \end{array} \right. \Rightarrow \quad \pi(y_1) \left\{ \begin{array}{c} \neq \\ = \end{array} \right\} \pi(y_2)\ , \tag{B.3}$$

it follows, that

$$\pi(x_1\, y_1 + x_2\, y_2) = 0. \tag{B.4}$$

(ii) If on the other hand

$$\pi(x_1) = \left\{ \begin{array}{c} 0 \\ 1 \end{array} \right. \Rightarrow \quad \pi(y_1) \left\{ \begin{array}{c} = \\ \neq \end{array} \right\} \pi(y_2)\ , \tag{B.5}$$

one finds

$$\pi(x_1\, y_1 + x_2\, y_2) = \pi(x_1). \tag{B.6}$$

Starting with the case of $k = 1$, equation (B.1) explicitly yields

$$u_{1,R}^2 + u_{1,I}^2 - (\sqrt{2} - 1)(v_{1,R}^2 + v_{1,I}^2) = 4. \tag{B.7}$$

Applying an algebraic conjugation results in

$$\tilde{u}_{1,R}^2 + \tilde{u}_{1,I}^2 + (\sqrt{2} + 1)(\tilde{v}_{1,R}^2 + \tilde{v}_{1,I}^2) = 4, \tag{B.8}$$

thus

$$\begin{array}{ll} |\tilde{u}_{1,R}| < 2, & |\tilde{u}_{1,I}| < 2, \\ |\tilde{v}_{1,R}| < 2\alpha, & |\tilde{v}_{1,I}| < 2\alpha. \end{array} \tag{B.9}$$

The proper algebraic decomposition yields the two relations

$$\begin{aligned} &\tfrac{1}{4}(m_{1,R}^2 + m_{1,I}^2) + \tfrac{1}{2}(n_{1,R}^2 + n_{1,I}^2) + \tfrac{1}{4}(p_{1,R}^2 + p_{1,I}^2) \\ &\qquad + \tfrac{1}{2}(q_{1,R}^2 + q_{1,I}^2) - (p_{1,R}\, q_{1,R} + p_{1,I}\, p_{1,I}) = 1 \end{aligned} \tag{B.10}$$

and

$$
\begin{aligned}
&\tfrac{1}{2}(m_{1,R}\,m_{1,R} + m_{1,I}\,m_{1,I}) - \tfrac{1}{4}(p_{1,R}^2 + p_{1,I}^2) \\
&\qquad - \tfrac{1}{2}(q_{1,R}^2 + q_{1,I}^2) + \tfrac{1}{2}(p_{1,R}\,q_{1,R} + p_{1,I}\,q_{1,I}) = 0.
\end{aligned}
\tag{B.11}
$$

Multiplying (B.11) by four, immediately results in

$$
\pi(p_{1,R}^2 + p_{1,I}^2) = 0 \qquad \Rightarrow \qquad \pi(p_{1,R}) = \pi(p_{1,I}), \tag{B.12}
$$

by use of (A.13). Thus, multiplying (B.10) by four, one can draw the analogous conclusion

$$
\pi(m_{1,R}) = \pi(m_{1,I}). \tag{B.13}
$$

Now multiply (B.10) by two. The resulting expression

$$
\pi\left\{\tfrac{1}{2}(m_{1,R}^2 + m_{1,I}^2) + (n_{1,R}^2 + n_{1,I}^2)\right\} = \pi\left\{\tfrac{1}{2}(p_{1,R}^2 + p_{1,I}^2) + (q_{1,R}^2 + q_{1,I}^2)\right\} \tag{B.14}
$$

can be rewritten by (A.12), (B.12) and (B.13) to yield

$$
\pi(m_{1,R}) + \pi(n_{1,R}^2 + n_{1,I}^2) = \pi(p_{1,R}) + \pi(q_{1,R}^2 + q_{1,I}^2). \tag{B.15}
$$

The value of the latter expression can be determined as follows. At first, assume it to be one. Then (A.13) would lead to

$$
\begin{aligned}
\pi(m_{1,R}) &= \begin{cases} 0 & \Rightarrow \quad \pi(n_{1,R}) \neq \pi(n_{1,I}) \\ 1 & \Rightarrow \quad \pi(n_{1,R}) = \pi(n_{1,I}) \end{cases}, \\
\pi(p_{1,R}) &= \begin{cases} 0 & \Rightarrow \quad \pi(q_{1,R}) \neq \pi(q_{1,I}) \\ 1 & \Rightarrow \quad \pi(q_{1,R}) = \pi(q_{1,I}) \end{cases}.
\end{aligned}
\tag{B.16}
$$

Multiplying (B.11) by two and inserting

$$
\pi\left\{\tfrac{1}{2}(p_{1,R}^2 + p_{1,I}^2) + (q_{1,R}^2 + q_{1,I}^2)\right\} = 1 \tag{B.17}
$$

offers

$$
\pi\left\{(m_{1,R}\,n_{1,R} + m_{1,I}\,n_{1,I}) + (p_{1,R}\,q_{1,R} + p_{1,I}\,p_{1,I})\right\} = 1. \tag{B.18}
$$

Using (B.3sqq), however, leads to a contradiction. Thus the assumption (B.16) must have been wrong, i.e., the value of the expression (B.15) is zero, resulting to

$$
\begin{aligned}
\pi(m_{1,R}) &= \begin{cases} 0 & \Rightarrow \quad \pi(n_{1,R}) = \pi(n_{1,I}) \\ 1 & \Rightarrow \quad \pi(n_{1,R}) \neq \pi(n_{1,I}) \end{cases}, \\
\pi(p_{1,R}) &= \begin{cases} 0 & \Rightarrow \quad \pi(q_{1,R}) = \pi(q_{1,I}) \\ 1 & \Rightarrow \quad \pi(q_{1,R}) \neq \pi(q_{1,I}) \end{cases}.
\end{aligned}
\tag{B.19}
$$

Since (B.18) turns into

$$
\pi\left\{(m_{1,R}\,n_{1,R} + m_{1,I}\,n_{1,I}) + (p_{1,R}\,q_{1,R} + p_{1,I}\,p_{1,I})\right\} = 0, \tag{B.20}
$$

applying (B.5sqq) yields

$$
\pi(m_{1,R}) = \pi(p_{1,R}). \tag{B.21}
$$

Investigating the second type of matrices ($k = 2$), the determinant condition (B.1) yields

$$(2 - \sqrt{2})(u_{2,R}^2 + u_{2,I}^2) - \sqrt{2}(v_{2,R}^2 + v_{2,I}^2) = 4, \tag{B.22}$$

which transforms into

$$(2 - \sqrt{2})(\tilde{u}_{2,R}^2 + \tilde{u}_{2,I}^2) - \sqrt{2}(\tilde{v}_{2,R}^2 + \tilde{v}_{2,I}^2) = 4 \tag{B.23}$$

under algebraic conjugation, i.e.,

$$\begin{array}{ll} |\tilde{u}_{2,R}| < \sqrt{2}\,\gamma, & |\tilde{u}_{2,I}| < \sqrt{2}\,\gamma, \\ |\tilde{v}_{2,R}| < \sqrt{2}\,\beta, & |\tilde{v}_{2,I}| < \sqrt{2}\,\beta. \end{array} \tag{B.24}$$

Decomposing (B.22) algebraically, yields

$$\begin{aligned} &\tfrac{1}{2}(m_{2,R}^2 + m_{2,I}^2) + (n_{2,R}^2 + n_{2,I}^2) \\ &\qquad - (m_{2,R}\, n_{2,R} + m_{2,I}\, n_{2,I}) - (p_{2,R}\, q_{2,R} + p_{2,I}\, p_{2,I}) = 1 \end{aligned} \tag{B.25}$$

and

$$\begin{aligned} &(m_{2,R}\, n_{2,R} + m_{2,I}\, n_{2,I}) - \tfrac{1}{4}(m_{2,R}^2 + m_{2,I}^2) - \tfrac{1}{4}(n_{2,R}^2 + n_{2,I}^2) \\ &\qquad - \tfrac{1}{2}(n_{2,R}^2 + n_{2,I}^2) - \tfrac{1}{2}(q_{2,R}^2 + q_{2,I}^2) = 0. \end{aligned} \tag{B.26}$$

Multiplying (B.25) by two, leads to

$$\pi(m_{2,R}^2 + m_{2,I}^2) = 0 \qquad \Rightarrow \qquad \pi(m_{2,R}) = \pi(m_{2,I}), \tag{B.27}$$

by relation (A.13), finally revealing

$$\pi(p_{2,R}) = \pi(p_{2,I}) \tag{B.28}$$

from equation (B.26).

Finally, it must be checked, if the algebraic structure of the matrices γ_1 and γ_2, defined in (4.15) is compatible with the multiplication in $T^*(2,3,8)$. This can be accomplished by an induction argument. On the one hand, the group generators L, M, N obviously fit into the structure (4.15). For arbitrary group elements, on the other hand, all kinds of product of generators L, M, N and matrices γ_1, γ_2 have to be investigated. Since, however, multiplication by L does not affect the algebraic structure of a group matrix, only four different kinds of products need to be considered explicitly.

(i) $\gamma_2 = M\gamma_1$, yielding after algebraic decomposition

$$\begin{array}{ll} m_{2,R} = m_{1,I} + n_{1,I} + q_{1,I}, & p_{2,R} = n_{1,I} + q_{1,I}, \\ n_{2,R} = n_{1,I} + \tfrac{1}{2}(m_{1,I} + p_{1,I}), & q_{2,R} = \tfrac{1}{2}(m_{1,I} + p_{1,I}), \\ m_{2,I} = m_{1,R} + n_{1,R} - q_{1,R}, & p_{2,I} = q_{1,R} - n_{1,R}, \\ n_{2,I} = n_{1,R} + \tfrac{1}{2}(m_{1,R} - p_{1,R}), & q_{2,I} = \tfrac{1}{2}(p_{1,R} - m_{1,R}). \end{array} \tag{B.29}$$

All of the right-hand sides result to integer numbers, as can be derived from (B.12), (B.13) and (B.21).

(ii) $\gamma_2 = N\gamma_1$, yielding

$$
\begin{aligned}
m_{2,R} &= \tfrac{1}{2}(m_{1,R} + m_{1,I}) + n_{1,R}, & p_{2,R} &= q_{1,I} + \tfrac{1}{2}(p_{1,R} - p_{1,I}),\\
n_{2,R} &= \tfrac{1}{2}(m_{1,R} + n_{1,R} + n_{1,I}), & q_{2,R} &= \tfrac{1}{2}(p_{1,I} + q_{1,R} - q_{1,I}),\\
m_{2,I} &= \tfrac{1}{2}(m_{1,R} - m_{1,I}) - n_{1,I}, & p_{2,I} &= q_{1,R} - \tfrac{1}{2}(p_{1,R} + p_{1,I}),\\
n_{2,I} &= \tfrac{1}{2}(n_{1,R} - m_{1,I} - n_{1,I}), & q_{2,I} &= \tfrac{1}{2}(p_{1,R} - q_{1,R} - q_{1,I}).
\end{aligned}
\tag{B.30}
$$

Using in addition (B.19), here the right-hand sides result to integer numbers, too.

(iii) $\gamma_1 = M\gamma_2$, yielding

$$
\begin{aligned}
m_{1,R} &= m_{2,I} + p_{2,I}, & p_{1,R} &= m_{2,I} + p_{2,I} + 2q_{2,I},\\
n_{1,R} &= n_{2,I} + q_{2,I}, & q_{1,R} &= n_{2,I} + p_{2,I} + q_{2,I},\\
m_{1,I} &= m_{2,R} - p_{2,R}, & p_{1,I} &= p_{2,R} - m_{2,R} + 2q_{2,R},\\
n_{1,I} &= n_{2,R} - q_{2,R}, & q_{1,I} &= p_{2,R} - n_{2,R} + q_{2,R},
\end{aligned}
\tag{B.31}
$$

which are obviously integer expressions.

(iv) $\gamma_1 = N\gamma_2$, yielding

$$
\begin{aligned}
m_{1,R} &= m_{2,I} + n_{2,R} - n_{2,I}, & p_{1,R} &= q_{2,R} + q_{2,I} + p_{2,R},\\
n_{1,R} &= n_{2,I} + \tfrac{1}{2}(m_{2,R} - m_{2,I}), & q_{1,R} &= q_{2,R} + \tfrac{1}{2}(p_{2,R} + p_{2,I}),\\
m_{1,I} &= m_{2,R} - n_{2,R} - n_{2,I}, & p_{1,I} &= q_{2,R} - p_{2,I} - q_{2,I},\\
n_{1,I} &= n_{2,R} - \tfrac{1}{2}(m_{2,R} + m_{2,R}), & q_{1,I} &= \tfrac{1}{2}(p_{2,R} - p_{2,I}) - q_{2,I}.
\end{aligned}
\tag{B.32}
$$

Taking into account relations (B.27) and (B.28), in this case also all expressions are integer valued.

Thus any product of the group generators L, M, N possesses the structure (4.15), thereby concluding the proof.

C Selberg's Zeta Function for Polygonal Hyperbolic Billiards

In this appendix the Selberg zeta function for polygonal hyperbolic billiards is derived from the generalized Selberg trace formula (4.68). The calculation proceeds along the same lines as in the strictly hyperbolic case. However, a slight modification due to the presence of boundary orbits arises.

Using Selberg's trace formula to calculate the trace of the regularized resolvent, the sums over hyperbolic conjugacy classes can be expressed as the logarithmic derivative of Selberg's zeta function. Thus one is led to the smearing function

$$h(p) = \frac{1}{p^2 + (s-\frac{1}{2})^2} - \frac{1}{p^2 + (\sigma - \frac{1}{2})^2}, \tag{C.1}$$

which is a valid choice for $\operatorname{Re} s > 1$, $\operatorname{Re} \sigma > 1$. Inserting the first term of the Fourier transform

$$\hat{h}(q) = \frac{1}{2s-1}\, e^{-(s-\frac{1}{2})\,|q|} - \frac{1}{2\sigma - 1}\, e^{-(\sigma-\frac{1}{2})\,|q|} \tag{C.2}$$

into the sum over hyperbolic conjugacy classes in (4.68), which is associated to closed geodesics *inside* the fundamental domain, yields

$$\begin{aligned}
&\frac{1}{2s-1} \sum_{\{\gamma_{\text{hyp}}\}} \sum_{k=1}^{\infty} \frac{\chi^k(\gamma)\, l_\gamma}{\exp\left(\frac{kl_\gamma}{2}\right) - \sigma^k(\gamma)\, \exp\left(-\frac{kl_\gamma}{2}\right)}\, e^{-(s-\frac{1}{2})\, kl_\gamma} \\
&= \frac{1}{2s-1} \sum_{\{\gamma_{\text{hyp}}\}} \sum_{k=1}^{\infty} \frac{\chi^k(\gamma)\, l_\gamma}{1 - \sigma^k(\gamma)\, e^{-kl_\gamma}}\, e^{-skl_\gamma} \\
&= \frac{1}{2s-1} \sum_{\{\gamma_{\text{hyp}}\}} \sum_{k=1}^{\infty} \sum_{n=0}^{\infty} \chi^k(\gamma)\, l_\gamma\, \sigma^{kn}(\gamma)\, e^{-(s+n)kl_\gamma} \\
&= \frac{1}{2s-1} \sum_{\{\gamma_{\text{hyp}}\}} \sum_{n=0}^{\infty} \frac{\chi(\gamma)\, l_\gamma\, \sigma^n(\gamma)\, e^{-(s+n)l_\gamma}}{1 - \chi(\gamma)\, \sigma^n(\gamma)\, e^{-(s+n)l_\gamma}} \\
&= \frac{1}{2s-1} \frac{\mathrm{d}}{\mathrm{d}s} \log Z_{\text{hyp}}(s),
\end{aligned} \tag{C.3}$$

where

$$Z_{\text{hyp}}(s) := \prod_{\{\gamma_{\text{hyp}}\}} \prod_{n=0}^{\infty} \left(1 - \chi(\gamma)\, \sigma^n(\gamma)\, e^{-(s+n)\, l_\gamma}\right). \tag{C.4}$$

The contribution of boundary orbits can be found to be

$$\begin{aligned}
&\frac{1}{2s-1} \sum_{\{\gamma_I\}} \sum_{k=1}^{\infty} \frac{\chi^k(\gamma_I)\, l_{\gamma_I}}{4} \left\{ \frac{1}{\sinh \frac{kl_{\gamma_I}}{2}} + \frac{\chi(I)}{\cosh \frac{kl_{\gamma_I}}{2}} \right\} e^{-(s-\frac{1}{2})\, kl_{\gamma_I}} \\
&= \frac{1}{2(2s-1)} \sum_{\{\gamma_I\}} \sum_{k=1}^{\infty} \chi^k(\gamma_I)\, l_{\gamma_I} \left\{ \frac{e^{-skl_{\gamma_I}}}{1 - e^{-kl_{\gamma_I}}} + \frac{\chi(I)\, e^{-skl_{\gamma_I}}}{1 + e^{-kl_{\gamma_I}}} \right\}
\end{aligned}$$

$$
\begin{aligned}
&= \frac{1}{2(2s-1)} \sum_{\{\gamma_I\}} \sum_{k=1}^{\infty} \sum_{n=0}^{\infty} \chi^k(\gamma_I)\, l_{\gamma_I} \left[1+\chi(I)\,(-1)^n\right] \, e^{-(s+n)\, k l_{\gamma_I}} \\
&= \frac{1}{2s-1} \sum_{\{\gamma_I\}} \sum_{k=1}^{\infty} \sum_{n=0}^{\infty} \chi^k(\gamma_I)\, l_{\gamma_I}\, e^{-(s+2n+\frac{1}{2}[1-\chi(I)])\, k l_{\gamma_I}} \\
&= \frac{1}{2s-1} \sum_{\{\gamma_I\}} \sum_{n=0}^{\infty} \frac{\chi(\gamma_I)\, l_{\gamma_I}\, e^{-(s+2n+\frac{1}{2}[1-\chi(I)])\, l_{\gamma_I}}}{1-\chi(\gamma_I)\, e^{-(s+2n+\frac{1}{2}[1-\chi(I)])\, l_{\gamma_I}}} \\
&= \frac{1}{2s-1} \frac{\mathrm{d}}{\mathrm{d}s} \log Z_{\mathrm{b.o.}}(s),
\end{aligned}
\tag{C.5}
$$

where

$$
Z_{\mathrm{b.o.}}(s) := \prod_{\{\gamma_I\}} \prod_{n=0}^{\infty} \left(1-\chi(\gamma_I)\, e^{-(s+2n+\frac{1}{2}[1-\chi(I)])\, l_{\gamma_I}}\right). \tag{C.6}
$$

Thus the Selberg zeta function turns out to be

$$
\begin{aligned}
Z(s) &= \prod_{\{\gamma_I\}} \prod_{n=0}^{\infty} \left(1-\chi(\gamma_I)\, e^{-(s+2n+\frac{1}{2}[1-\chi(I)])\, l_{\gamma_I}}\right) \\
&\quad \times \prod_{\{\gamma_{\mathrm{hyp}}\}} \prod_{n=0}^{\infty} \left(1-\chi(\gamma)\, \sigma^n(\gamma)\, e^{-(s+n)\, l_\gamma}\right), \qquad \mathrm{Re}\, s > 1.
\end{aligned}
\tag{C.7}
$$

Since the Euler product representation of the corresponding Ruelle-type zeta function

$$
\begin{aligned}
\hat{R}(s) &= \prod_{\{\gamma_I\}} \left(1-\chi(\gamma_I)\, e^{-(s+\frac{1}{2}[1-\chi(I)])\, l_{\gamma_I}}\right) \\
&\quad \times \prod_{\{\gamma_{\mathrm{hyp}}\}} \left(1-\chi(\gamma)\, e^{-s l_\gamma}\right)
\end{aligned}
\tag{C.8}
$$

is absolutely convergent for $\mathrm{Re}\, s > 1$, and

$$
Z(s) = \prod_{n=0}^{\infty} \hat{R}(s+n), \qquad \mathrm{Re}\, s > 1, \tag{C.9}
$$

$\hat{R}(s)$ and $Z(s)$ have the same zeroes on the critical line $\mathrm{Re}\, s = \frac{1}{2}$. Moreover the first term in (C.8) is a product over a *finite* number of boundary orbits, which can be evaluated directly on the critical line. For $\mathrm{Re}\, s = \frac{1}{2}$, however, it never vanishes, thus it cannot contribute to the zeroes of $\hat{R}(s)$ on the critical line. Therefore one finally arrives at

$$
R(s) = \prod_{\{\gamma_{\mathrm{hyp}}\}} \left(1-\chi(\gamma)\, e^{-s l_\gamma}\right), \qquad \mathrm{Re}\, s > 1, \tag{C.10}
$$

which has the same zeroes on the critical line as the Selberg zeta function $Z(s)$.

References

[1] M. Abramowitz and I.A. Stegun: Handbook of Mathematical Functions. *Dover Publications, New York*, 1972

[2] V.I. Arnold and A. Avez: Ergodic Problems of Classical Mechanics. *Benjamin, NewYork*, 1968

[3] E. Artin: Ein mechanisches System mit quasiergodischen Bahnen. *Abh. Math. Sem. Univ. Hamburg* **3** (1924) 170-175

[4] R. Aurich: private communication

[5] R. Aurich: Studium eines chaotischen Quantenbillards: das Hadamard-Gutzwiller-Modell. *PhD Thesis, Univ. Hamburg*, 1990

[6] R. Aurich, E.B. Bogomolny and F. Steiner: Periodic Orbits on the Regular Hyperbolic Octagon. *Physica* **D48** (1991) 91-101

[7] R. Aurich and J. Bolte: Quantization Rules for Strongly Chaotic Systems. *Mod. Phys. Lett.* **B6** (1992) 1691-1719

[8] R. Aurich, J. Bolte, C. Matthies, M. Sieber and F. Steiner: Crossing the Entropy Barrier of Dynamical Zeta Functions. *Physica* **D63** (1993) 71-86

[9] R. Aurich, C. Matthies, M. Sieber and F. Steiner: Novel Rule for Quantizing Chaos. *Phys. Rev. Lett.* **68** (1992) 1629-1632

[10] R. Aurich, F. Scheffler and F. Steiner: On the Subtleties of Arithmetical Quantum Chaos. *DESY-report*, DESY 94-152, 1994 (submitted to *Phys. Rev.* **E**)

[11] R. Aurich and F. Steiner: On the Periodic Orbits of a Strongly Chaotic System. *Physica* **D32** (1988) 451-460

[12] R. Aurich and F. Steiner: Periodic-Orbit Sum Rules for the Hadamard-Gutzwiller Model. *Physica* **D39** (1989) 169-193

[13] R. Aurich and F. Steiner: From Classical Periodic Orbits to the Quantization of Chaos. *Proc. Roy. Soc. London* **A437** (1992) 693-714

[14] R. Aurich and F. Steiner: Staircase Functions, Spectral Rigidity and a Rule for Quantizing Chaos. *Phys. Rev.* **A45** (1992) 583-592

[15] R. Aurich and F. Steiner: Asymptotic Distribution of the Pseudo-Orbits and the Generalized Euler Constant γ_Δ for a Family of Strongly Chaotic Systems. *Phys. Rev.* **A46** (1992) 771-781

[16] R. Aurich and F. Steiner: Statistical Properties of Highly Excited Quantum Eigenstates of a Strongly Chaotic System. *Physica* **D64** (1993) 185-214

[17] N.L. Balazs and A. Voros: Chaos on the Pseudosphere. *Phys. Rep.* **148** (1986) 109-240

[18] H.P. Baltes and E.R. Hilf: Spectra of Finite Systems. *Bibliographisches Institut, Mannheim*, 1976

[19] R. Berndt and F. Steiner: Hyperbolische Geometrie und Anwendungen in der Physik. *Hamburger Beiträge zur Mathematik aus dem Mathematischen Seminar*, Heft 8, 1988

[20] M.V. Berry and J.P Keating: A Rule for Quantizing Chaos? *J. Phys.* **A23** (1990) 4839-4849

[21] M.V. Berry and M. Tabor: Level Clustering in the Regular Spectrum. *Proc. Roy. Soc. London* **A356** (1977) 375-394

[22] E.B. Bogomolny and M. Carioli: Quantum Maps from Transfer Operators. *Physica* **D67** (1993) 88-112

[23] O. Bohigas, M.-J. Giannoni and C. Schmit: Characterization of Chaotic Quantum Spectra and Universality of Level Fluctuation Laws. *Phys. Rev. Lett.* **52** (1984) 1-4

[24] J. Bolte: Some Studies on Arithmetical Chaos in Classical and Quantum Mechanics. PhD Thesis, Univ. Hamburg, 1993. *Int. J. Mod. Phys.* **B7** (1993) 4451-4553

[25] J. Bolte: Periodic Orbits in Arithmetical Chaos on Hyperbolic Surfaces. *Nonlinearity* **6** (1993) 935-951

[26] I.P. Cornfeld, S.V. Fomin and Ya.G. Sinai: Ergodic Theory. *Springer, Berlin · Heidelberg · New York*, 1982

[27] F.J. Dyson and M.L. Mehta: Statistical Theory of the Energy Levels of Complex Systems. IV. *J. Math. Phys.* **4** (1963) 701-719

[28] A. Erdélyi (ed.): Higher Transcendental Functions, Vol. II. *McGraw-Hill, New York*, 1953

[29] I.S. Gradshteyn and I.M. Ryzhik: Table of Integrals, Series, and Products. *Academic Press, San Diego*, 1965

[30] M.C. Gutzwiller: Phase-Integral Approximation in Momentum Space and the Bound States of an Atom. *J. Math. Phys.* **8** (1967) 1979-2000; Phase-Integral Approximation in Momentum Space and the Bound States of an Atom II. *J. Math. Phys.* **10** (1969) 1004-1020; Energy Spectrum According to Classical Mechanics. *J. Math. Phys.* **11** (1970) 1791-1806; Periodic Orbits and Classical Quantization Conditions. *J. Math. Phys.* **12** (1971) 343-358

[31] M.C. Gutzwiller: Classical Quantization with Ergodic Behavior. *Phys. Rev. Lett.* **45** (1980) 150-153

[32] M.C. Gutzwiller: A Practical Guide Through the Chaos on the Double Torus. *Preprint*, 1990

[33] M.C. Gutzwiller: Chaos in Classical and Quantum Mechanics. *Springer, Berlin · Heidelberg · New York*, 1990

[34] J. Hadamard: Les surfaces à courbures opposées et leurs lignes géodésiques. *J. Math. Pures et Appl.* **4** (1898) 27-73

[35] E.R. Hansen: A Table of Series and Products. *Prentice-Hall, London*, 1975

[36] G.H. Hardy and E.M. Wright: An Introduction to the Theory of Numbers, 5th ed. *Oxford Univ. Press, Oxford*, 1979

[37] D.A. Hejhal: The Selberg Trace Formula for $\mathrm{PSL}(2,\mathbb{R})$, Vol. I and II. *Springer Lecture Notes in Mathematics*, **548**(1976) and **1001**(1983)

[38] T. Hesse: Die spektrale Stufenfunktion des abgeschnittenen Hyperbelbilliards. *Diploma Thesis, Univ. Hamburg*, 1994

[39] H. Huber: Zur analytischen Theorie hyperbolischer Raumformen und Bewegungsgruppen. *Math. Annalen* **138** (1959) 1-26

[40] C. Jacquemin and C. Schmit: Classical Quantization of a Compact Billiard on the Pseudo-Sphere. *Orsay-preprint*, IPNO/TH 91-65, 1991

[41] J.P. Keating: Periodic Orbit Resummation and the Quantization of Chaos. *Proc. Roy. Soc. London* **A436** (1991) 99-108

[42] W. Magnus: Noneuclidean Tesselations and Their Groups. *Academic Press, New York · London*, 1974

[43] W. Magnus, A. Karrass and D. Solitar: Combinatorial Group Theory. *Interscience, New York*, 1966

[44] W. Magnus, F. Oberhettinger and R.P. Soni: Formulas and Theorems for the Special Functions of Mathematical Physics. *Grundlehren der mathematischen Wissenschaften,* Band 52. *Springer, Berlin · Heidelberg · New York*, 1966

[45] H.P. McKean: Selberg's Trace Formula as Applied to a Compact Riemann Surface. *Commun. Pure and Appl. Math.* **25** (1972) 225-246

[46] M.L. Mehta: Random Matrices and the Statistical Theory of Energy Levels. *Academic Press, New York*, 1967

[47] T. Pignataro: Hausdorff Dimension, Spectral Theory and Applications to the Quantization of Geodesic Flows on Surfaces of Constant Negative Curvature. *PhD Thesis, Princeton Univ.*, 1984

[48] F. Scheffler: Zu den spektralen Statistiken eines stark chaotischen Dreiecksbillards. *Diploma Thesis, Univ. Hamburg*, 1994

[49] D. Schleicher: Bestimmung des Energiespektrums in einem chaotischen System mit Hilfe der Selbergschen Spurformel. *Diploma Thesis, Univ. Hamburg*, 1991

[50] A. Selberg: Harmonic Analysis and Discontinuous Groups in Weakly Symmetric Riemannian Spaces with Applications to Dirichlet Series. *J. Indian Math. Soc.* **20** (1956) 47-87

[51] M. Sieber: private communication

[52] M. Sieber: The Hyperbola Billiard: A Model for the Semiclassical Quantization of Chaotic Systems. *PhD Thesis, Univ. Hamburg*, 1991

[53] F. Steiner: On Selberg's Zeta Function for Compact Riemann Surfaces. *Phys. Lett.* **B188** (1987) 447-454

[54] K. Takeuchi: Arithmetic Triangle Groups. *J. Math. Soc. Japan* **29** (1977) 91-106